NASA-CR-204473

NASA Contractor Report

COMPUTATIONAL NOISE STUDY OF A SUPERSONIC SHORT CONICAL PLUG-NOZZLE JET

Indu S. Das
The Pennsylvania State University
Sharon, Pennsylvania

Abbas Khavaran
Lewis Research Center Group
NYMA, Cleveland, Ohio

and

A. P. Das
Graduate Student
Youngstown State University, Ohio

September 1996

Final Report Prepared for:
Lewis Research Center
Under Grant No. NAG3-1708

NASA
National Aeronautics & Space Administration

TABLE OF CONTENTS

Section		Page
1.	SUMMARY	3
2.	INTRODUCTION	4
3.	PLUG-NOZZLE CONFIGURATION	8
4.	METHOD OF SOLUTION	9
5.	COMPUTATIONAL DOMAIN & SCOPE OF DATA	18
6.	RESULTS & DISCUSSION	20
7.	CONCLUSIONS & RECOMMENDATIONS	34
8.	NOMENCLATURE	36
9.	REFERENCES	37
10.	LIST OF FIGURES	41

FIGURES

APPENDICES:

APPENDIX A - Co-ordinates of the Conical Plug-Nozzle

APPENDIX B - Tables of Acoustic Data

REPORT DOCUMENTATION PAGE

1. SUMMARY

A computational noise study of a scale model of a simple-geometry short conical plug-nozzle (PN) is presented. The short conical PN has an exit diameter of 45 mm and a design pressure ratio of 3.62. The geometrical configuration closely approximates that of an ideally contoured PN having a shockless jet flow at a pressure ratio of 3.62. The gasdynamics of the jet flows has been predicted using the NPARC Computational Fluid Dynamics code with k-ε turbulence model. The gasdynamics data are then used to perform the noise computations based on the modified General Electric MGB code. The study covers a range of pressure ratios, $2.0 \leq \xi \leq 5.0$. The agreement of the computational aeroacoustic results with the reported experimental data is favorable. At the design pressure ratio, the codes predict overall sound pressure levels within 4.0 dB of the experimental data. At the off-design pressure ratios, the modeling, in general, predicts noise levels within 5.0 dB except at very high frequencies when deviations up to 10 dB are noted. At the design pressure ratio, noise levels of the short conical PN are comparable to those of the equivalent convergent-divergent (CD) nozzle and the ideally contoured PN; but, at the off-design conditions, the noise levels of the short conical PN are noted to be significantly lower. The mechanism of shock formations in the short conical PN jet flows is noted to be basically different from those in the convergent and CD nozzle jet flows. The modified GE/MGB noise code in conjunction with the CFD code, NPARC with k-ε turbulence model, is noted to be a satisfactory prediction tool for assessment of jet noise suppression schemes; however, the noise code needs to be further modified to accommodate for shock formations in cases involving the presence of center-bodies in propulsion nozzles.

2. INTRODUCTION

A need for development of a high speed cruise aircraft has lately been felt by the commercial aircraft industry and the problem of supersonic jet noise suppression must be addressed to meet this need. The magnitude of the challenge could be appreciated by noting that the four Olympus engines of the Concorde produce noise levels of 12, 18, and 13 EPNdB above the Federal Aviation Administration FAR 36 Stage III noise regulations for sideline, cutback and approach, respectively. The earlier jet noise suppression researches could achieve noise reductions of the order of only 2 EPNdB per percent thrust loss whereas the FAR Stage III regulations would require a noise reduction of the order of 4 EPNdB per percent thrust loss [1, 2].

In perfectly expanded (shock-free) supersonic jet flows, the noise mechanism is primarily due to turbulent mixing which depends upon the mean flow speed, the flow velocity gradients downstream of the nozzle exit, and the turbulence characteristics [3]. Imperfectly expanded supersonic jet flows contain repetitive shocks which interact with turbulence related fluctuations generating: (a) harmonically related discrete tones of noise often termed "screech" [4], and (b) broadband but strongly peaked shock-associated noise [5-9]. The shock structure and its interaction with the convecting turbulence structure may also change the turbulence structure which then affects the strength of the mixing noise sources. It is generally recognized that the shock-associated noise is dominant at off-design supercritical pressure ratios, at lower temperatures and at higher angles to the downstream jet axis. The intensity of the shock-associated noise is known to be dependent upon (i) the strength and the spacing of the repetitive shock cells, and (ii) the strength and coherence of the flow fluctuations convected through the shock fronts. Therefore, to suppress the dominant shock-related noise component, the characteristics of the shock structure need to be modified such that the contributing noise sources and the effectiveness of their noise generating mechanism are both reduced.

The use of a contoured convergent-divergent (CD) nozzle is often considered as a design option for attenuating the shock-associated noise component generated by the exhaust flow of a modern high specific thrust jet engine. The shock-associated noise

component is eliminated if the exhaust flow of a contoured CD nozzle, operated at its design pressure ratio, is shock free. However, in practice, such exhaust nozzles are of necessity operated over an extended range of pressure ratio, where at the off-design pressure ratios in either the over- or the underexpanded mode, the repetitive shock structure is formed in the exhaust flows. At low supercritical pressure ratios, the shock structure may even be present in the diverging part of the contoured CD nozzle. The overall sound pressure level as a function of the fully expanded jet Mach number M_j of the moderately over- and underexpanded CD nozzle jet has been shown to be significantly lower than those of an equivalent (i.e., of the same mass flow rate, operating pressure ratio, and the exhaust area) round convergent nozzle [5, 10].

Some recent experimental acoustic studies of supersonic jet flows from plug-nozzles have also shown appreciable shock noise suppression effects [11-15]. In some of these plug-nozzle studies, the plugs were rather long cylindrical center-bodies [11-12] and in others [13-14] the plug surface was uncontoured with pointed or truncated termination. The repetitive cellular shock structure is necessarily formed in the supersonic jet flows from such nozzles. Moreover, long plugs are likely to have the related aerodynamic and weight penalties. Therefore, to circumvent some of these disadvantages and to eliminate or to weaken the repetitive shock structure in supersonic jet flows, the use of a short ideally contoured externally expanded plug with a pointed termination suggests itself as an attractive alternative. The plug surface of such *a minimum length* supersonic plug-nozzle cancels all the incident expansion waves and the exhaust flow is shockless at the design condition. The preliminary experimental noise study of an ideally *contoured* plug-nozzle with a *pointed* termination [15] reported substantial reductions in the noise levels relative to an equivalent convergent nozzle; these reductions were noted at all observation angles and at all off-design and design pressure ratios. The ideally contoured PN jet flows were found to considerably inhibit the growth and the strength of shock structure when operated at off-design supercritical pressure ratios, thereby reducing the intensity of the shock-associated noise component. The noise suppression effectiveness of the contoured PN was observed to be of the same order as that of an equivalent contoured CD nozzle at the same design pressure ratio (shockless flows). But,

at the off-design pressure ratios (flows with shocks), the noise suppression effectiveness of the contoured PN was reported to be better than that of the equivalent CD nozzle. It is thus clear that the presence of a suitable plug results in significant jet noise suppression through weakening/elimination of repetitive shock cells.

A simple single-stream plug-nozzle may not be able to meet the demands of the FAR 36 Stage III noise regulations. However, a plug of suitable geometry could be accommodated inside single- or multi-stream nozzle schemes such as co-axial nozzle [16, 17], rectangular geometry supersonic nozzle [18], elliptical geometry supersonic nozzle [19-20] and ejector-mixer nozzle [21] which have been recently considered for supersonic jet noise suppression. The placement of suitable plug(s) could add to the noise suppression effectiveness of these nozzles without plugs.

The evaluation of the role of an ideally contoured plug in a supersonic jet is an important step towards use of suitable plug(s) in future nozzle schemes to achieve satisfactory jet noise suppression. The only reported experimental study of a contoured PN jet noise is a preliminary investigation [15] which focused upon the far-field noise measurements and no flow-field measurements other than the shadowgraph records are available. A detailed computational study of the gasdynamics and the far-field noise characteristics of the jet flows of the ideally contoured PN in the over-, the fully-, and the underexpanded modes of operation over a range of supercritical pressure ratios appropriate for practical jet engine applications has been recently reported [22]. The theoretical study, in general, confirmed the experimental results.

A plug having an ideal contour (isentropic profile and an extremely pointed tip) may not be a practical choice. Is there then a more practical plug profile with simpler un-contoured geometry as an alternative to the ideally contoured-plug which could result in comparable mixing noise and reduced shock-associated noise? It is imperative that the geometry of a non-contoured plug closely agree with the overall geometry of the ideally contoured plug in order to achieve the maximum possible noise reduction benefit and minimum thrust penalty. An experimental jet noise study of such a short conical plug plug-nozzle [23] reported promising noise suppression effectiveness. The far-field noise levels of the short solid conical plug were noted to be within 3 dB of those of an

equivalent ideally contoured plug. It is important to note that the aeroacoustic performance of the short conical plug was observed to approach that of the ideally contoured plug when the conical plug surface was provided with simple perforations. This indicates that there is further scope of improving the noise suppression effectiveness of a short conical plug.

The present investigation aims at a detailed computational study of the gasdynamics and the far-field noise radiation of jets issuing from a short solid (non-perforated) conical plug-nozzle which closely approximates the geometry of an ideal contoured plug-nozzle. A short plug of simple geometry may be a preferable aerodynamic choice for incorporation into propulsion nozzle schemes if this results in comparable jet noise suppression. It is hoped that the computational study will help in further evaluation of the role of a plug in supersonic jet noise suppression.

3. PLUG-NOZZLE CONFIGURATION

The computational study is carried for the short conical plug-nozzle geometry of the Syracuse experimental study [14] (see Fig. 1 for nomenclature). This would enable comparison of the predicted data with the measurements. A complete geometry of the annular flow boundaries (plug-stem surface is the inner boundary and inner nozzle surface is the outer boundary) is presented in Table A. The reference point ($X = 0$, $R = 0$) is located on the jet axis (an axis of symmetry) at the start of the converging section of the nozzle; X-axis is directed along the downstream jet axis, and the radial R-axis is perpendicular to the jet axis. The nominal design Mach number of this short conical plug-nozzle is 1.5 for which the jet flow from an equivalent ideal contoured plug-nozzle is shock-free. The overall geometrical parameters of the short conical PN annulus radius ratio, K, the lip angle, α, the plug-surface angle at the sonic point, Ψ, and ratio of the maximum length to the lip radius, (L_{max}/R_N), are, respectively, 0.43, 11.91°, 23.9° and 0.97. The corresponding values of the parameters for the ideal contoured plug-nozzle are, respectively, 0.43, 11.91°, 28.4°, and 1.37. Thus, for the same lip radius R_N, the short conical plug-nozzle has the same annulus radius ratio K, the same lip angle α and the same throat area as those of the ideally contoured plug-nozzle. When operated at the same pressure ratio as that of the ideal contoured PN, such a short conical PN therefore has the same mass flow rate and nearly the same specific thrust. The choice of the solid conical plug semi-angle of 23.9° results in a surface area of the conical plug equal to that of the ideally contoured plug which yields a conical plug of maximum length (L_{max}) even less (about 30% shorter) than that of the ideally contoured plug. The plug-nozzle has a lip of radius, $R_N = 22.5$ mm and a lip thickness of 0.25 mm, which are the same as those for the ideally contoured plug-nozzle. The ratio of the converging nozzle inlet to exit area is 46 which again is the same for both the short conical and ideal contoured PN's. It was reported that the ideal contoured plug-nozzle jet was shockless at the design pressure ratio of $\xi_d = 3.62$ and the jet screech noise was absent. A complete profile of the short conical plug-nozzle geometry is presented as Fig. A in Appendix A. For further details of the experimental setup, see Ref. 23.

4. METHOD OF SOLUTION

It is generally accepted that the direct numerical simulation based on the full, unsteady, compressible Navier-Stokes equations govern both the generation and the propagation of sound. Current efforts in this area of study, usually labeled as the computational aeroacoustics (CAA), are directed towards resolving various computational issues, such as grid resolution for frequencies of interest, computational domain, boundary conditions, finite difference scheme, shock noise formulation and so on. A unified aerodynamic/acoustic code (the MGB code) was developed at the General Electric [24]. In the GE methodology, the aerodynamic predictions were carried out by applying an extension of the Reichardt's model. The components of turbulent shear stress are computed based upon contour integrals around the nozzle exit geometry and utilized in deriving an expression for the source strength. The Reichardt's solution neglects the radial mean flow and swirl, and the effect of shock structure, if present, on mixing and turbulence. The closed-form nature of this solution results in a relatively fast numerical scheme, but the predictions for complex geometry are found to be unsatisfactory. The MGB code was subsequently modified by the NASA Lewis researchers [25, 26] by applying a two-stage algorithm. The Reichardt's model was replaced by a CFD Navier-Stokes solver and the aerodynamic calculations were carried out independently. The resulting plume data were then used for the noise computation. The two-stage algorithm has the following advantages: (i) start of the aerodynamics calculations from within the nozzle giving a more realistic model of the exit conditions, (ii) independent grid selection for aerodynamic and acoustic purposes; and (iii) proper prediction of shock-cell structure as well as shock intensity essential for prediction of the shock-associated noise. For full details of the NASA Lewis methodology see, Refs. 25 and 26.

The flow field computation in the present study is based on the axisymmetric version of the NPARC code [27] with Chien's k-ε turbulence model [28]. This CFD code is an evolution of the PARC code developed by the Arnold Engineering Development Center, which in turn was based upon the NASA Ames ARC code. The

extensively validated code solves the complete Reynolds-averaged Navier-Stokes equations in conservative law form. The Beam and Warming approximate factorization algorithm [29] is used for forming the implicit central-difference scheme. The viscous coefficients are determined based on the Sutherland's law, the Stokes's hypothesis, and constant Prandtl number assumptions. A Baldwin and Lomax type turbulence model is utilized to compute the boundary values and initial conditions for k and ε.

The solution technique for noise prediction in the present study is based upon the NASA Lewis methodology. In what follows, only an overview of the methodology is presented. The first section briefly describes the application of the NPARC code with k-ε turbulence model for computation of the source strength and its spectrum, and explains the empirical constants used in the computation of the characteristic Strouhal number and the supersonic convection factor. In the second section, the effect of the surrounding medium (velocities and temperature gradients) on the noise radiated from the convecting quadrupole sources is discussed. The third section presents an outline of the shock-associated noise prediction scheme.

4.1 Source Spectrum Model

It is generally recognized that at subsonic and low supersonic speeds, small scale turbulence is the primary source of the mixing noise. Each finite volume of turbulence may be described as a multipole source that convects downstream and emits sound that is refracted by mean flow gradients. As the jet becomes highly supersonic, large-scale structures or instability waves of the flow become increasingly active. The prediction scheme assumes the dominance of fine-scale turbulence. In a fine-scale turbulence, it is assumed that the turbulence length scale is small. Lilley's equation suggests that, at subsonic convection Mach numbers, the radiation field arriving from each source volume element is independent of that due to any other region of the flow. As such, the mean square pressure at any point in the sound field is simply the sum of the mean square pressures produced by independent correlation volume elements that make up the jet. The compactness condition is not that restrictive and may hold true even at moderate supersonic Mach numbers. With the compact eddy approximation, the solution is

expressed as a Fourier transform of space-time correlation function to be integrated over the entire jet volume. This requires modeling of the space-time correlation function.

Following the Lighthill's acoustic analogy approach, the mean square acoustic pressure in the far-field in absence of convection and refraction may be written as,

$$\overline{p^2}(R,\ \theta,\ \phi) = \frac{R_i R_j R_k R_l}{16\pi^2 C_\infty^4 R^6} \int\int_{\vec{y}\,\vec{\xi}} \frac{\partial^4}{\partial \tau^4} \overline{(T_{ij} T'_{kl})}\, d\vec{\xi}\, d\vec{y} \tag{1}$$

The source strength is assumed to be dominated by the unsteady momentum flux, i.e., $T_{ij} \sim \rho V_i V_j$. The vector $\vec{\xi}$ is the separation vector between locations $\vec{y}$ and $\vec{y}+\vec{\xi}$ having correlations $\rho V_i V_j$, and $\rho V_k V_l'$, respectively, and τ is the time-delay of correlation. The corresponding spectrum in terms of the Fourier transform of the autocorrelation function is,

$$\overline{p_\omega^2} = \frac{1}{2\pi} \int_{-\infty}^{\infty} \overline{p^2} e^{i\omega\tau} d\tau \tag{2}$$

As such, for a quasi-incompressible turbulence, the source strength is characterized by a two-point time-delayed fourth-order velocity correlation tensor. For a nearly parallel mean flow, contributions of the self-noise terms may be shown to be independent of the mean flow. Assuming a normal joint probability for turbulent velocity components and following the Batchelor's model for isotropic turbulence, the fourth-order correlation is a linear combination of the second-order correlations,

$$\overline{v_i v_j v'_k v'_l} = \overline{(v_i v'_k)}\,\overline{(v_j v'_l)} + \overline{(v_i v'_l)}\,\overline{(v_j v'_k)} + \overline{(v_i v'_j)}\,\overline{(v_k v'_l)} \tag{3}$$

By assuming the two-point velocity correlation to be separable in space/time factors,

$$\overline{v_i v'_j} = R_{ij}(\vec{\xi}) g(\tau), \tag{4}$$

the integration can be carried out in closed form. The space factor may be written as,

$$R_{ij}(\vec{\xi}) = T\left[\left(f + \frac{1}{2}\xi f'\right)\delta_{ij} - \frac{1}{2} f' \xi_i \xi_j / \xi\right] \tag{5}$$

where $T = [(\overline{v_i v_i}) / 3]$ is the intensity of turbulence replacing the axial turbulence in the Reichardt's model and $f' = \partial f / \partial \xi$ and $f(\xi) = \exp[-\pi\xi^2/L^2]$, L being longitudinal macroscale of turbulence. The time factor of correlation may be expressed as,

$g(\tau) = \exp[-(\tau/\tau_0)^2]$, where τ_0 is the characteristic time delay in moving reference frame. For axisymmetric jets, it has been shown that τ_0 is proportional to the inverse of mean shear. The eddy length scale L_ε is related to the kinetic energy of turbulence, $k=(\overline{v_i v_i})/2$, and its dissipation rate ε as $L_\varepsilon = k^{3/2}/\varepsilon$,. Assuming $L \sim L_\varepsilon$, it can be shown that $1/\tau_0 \sim \varepsilon/k$. The first component of source/ spectrum correlation tensor is given by [25],

$$I_{1111}(\Omega) = (3/8\sqrt{\pi})\rho^2 k^{7/2}(\Omega\tau_0)^4 \exp[-(\Omega\tau_0)^2/8] \tag{6}$$

which is used to compute the noise field in conjunction with the refraction effect of the mean flow. The Doppler effect relating the source frequency Ω and the observer frequency f is given by, $\Omega = 2\pi f\overline{C}$, where the eddy convection factor, $\overline{C} = (1\text{-}M_c\cos\theta)$. In the modified computational approach, the eddy convection factor is taken as,

$$\overline{C} = \sqrt{(1 - M_c \cos\theta)^2 + (\alpha_c\sqrt{k}/C_\infty)^2} \tag{7}$$

The empirical constant α_c has been assumed to be 0.5. An average value of the convection Mach number M_c in the initial mixing region of the jet is $0.62M_j$. Experimental measurements [30] show that the convection velocity may vary across the jet. Variation of the convection Mach number with the source location may be taken as a weighted average of the exit Mach number and the local Mach number,

$$M_c = 0.5M + \beta_c M_j \tag{8}$$

The convection constant β_c in the range of 0.25 to 0.3 appears to yield the best results and a value of 0.3 has been selected.

4.2 Sound / Flow Interaction

The effect of the surrounding mean flow on acoustic radiations caused by convecting multipole sources, which is not accounted for by the acoustic analogy approach, needs to be incorporated. Many investigators have studied the radiation field of the multipole sources in parallel sheared flows. Mani studied the mean flow interaction of round jets for slug flow profiles assuming quadrupole sources convecting along the centerline of the jet [31]. The analysis was extended to arbitrary velocity profiles in the high-frequency and low-frequency limits and then generalized for arbitrarily located

sources in continuously varying monotonic profiles [32, 33]. It has been proposed that the high-frequency solution provides an adequate approximation for supersonic jets [34, 35].

The non-linear terms in the Lighthill's analysis are entirely contained in the source term $T_{ij} = (\rho + \rho')v_i v_j + \delta_{ij}(p - C_\infty^2 \rho') - e_{ij}$, where ρ and ρ' denote the mean and fluctuating density, p is the acoustic pressure, C_∞ is the ambient sound speed and e_{ij} is the viscous stress tensor. This source term can be approximated as $T_{ij} \sim \rho v_i v_j$ by assuming small entropy change and neglecting e_{ij} compared with much larger Reynolds stress term $\rho v_i v_j$ [36].

Other variations of the Lighthill's equation, such as Lilley's or Phillips' formulations have the advantage of separating fluids effects from the sound generating term. For example, in Lilley's formulation, the terms corresponding to source convection and sound refraction appear in the operator part of the equation. Apart from the added complexity, the other disadvantage of the Lilley's equation is the nonlinearity. But the turbulence velocities in the jet are fairly small compared to the mean velocity (see figures 5(b), 8(b) and 11(b)). Hence, for many practical cases of interest, assuming that the jet is not highly supersonic, it is reasonable to neglect terms on the operator side of the equation involving product of the fluctuating quantities and to replace the velocity and sound speed by their mean values. Physically, this linearization process amounts to ignoring effects such as scattering of sound by turbulence.

The sound/flow interaction effect consideration is primarily based on the axisymmetric solution of the Lilley's equation developed by Mani and Balsa [24]. The mean square acoustic pressure in the far field is given by,

$$\overline{p^2}(R,\ \theta,\ \Omega) = \int_{\bar{y}} \Lambda(a_{xx} + 4a_{xy} + 2a_{yy} + 2a_{yz})\, d\bar{y} \qquad (9)$$

where $a_{xx},\ldots,a_{yz}$ are the directivity factors which describe the noise field due to each of the quadrupole contained within a turbulent eddy volume element. The weighting factors are those derived by Ribner. Factor Λ, related to the source intensity and frequency, is:

$$\Lambda \approx \frac{\left(\frac{\rho_\infty}{\rho}-1\right)^2 I_{1111}(\Omega)}{(4\pi R C_\infty C)^2 (1-M\cos\theta)^2 (1-M_c\cos\theta)^2} \tag{10}$$

The directivity factors are functions of the shielding function g^2 given by,

$$g^2(r) = \frac{(1-M\cos\theta)^2\left(\frac{C_\infty}{C}\right)^2 - (\cos\theta)^2}{(1-M_c\cos\theta)^2} \tag{11}$$

The mean flow variables obtained from the CFD computation are used to estimate $g^2(r)$ and hence the directivity factors. The location where $g^2(r)$ changes sign is known as the turning point. A negative value of $g^2(r)$ between the source and the observer indicates the possibility of fluid shielding. The position of source with respect to the turning points of $g^2(r)$ contributes to the amount of shielding by a factor of

$$\exp\left[-2K\int_{r_1}^{r_2}\sqrt{|g^2(r)|}\,dr\right],$$

where the limits are determined by the source location with respect to the turning points, and $K = \Omega/C_\infty$ is the wave number.

A correction of one Doppler factor has been utilized for the source volume effects [37]. The correction for flight speed has been included using the flight dynamic factor, $(1 + M_\infty \cos\theta)^{-1}$, where M_∞ is the flight number.

4.3 Shock-Associated Noise Prediction

The mechanism of the generation of the shock-associated noise is not clearly understood and a general theoretical modeling effort is yet to reach a satisfactory stage. The distinctive features of the shock-associated noise for choked convergent nozzle jet flows were identified by Harper-Bourne and Fisher experimental study [6] and these were later confirmed by Tanna [9] for a wide range of operating conditions. It was observed that, for low supersonic Mach numbers, the shock-associated noise intensity I scaled as the fourth-power of a shock strength parameter $\beta = (M_j^2-1)^{1/2}$. For high supersonic Mach numbers, the scaling breaks down because of the Mach disk formation. By extending Powell's model for the jet screech tones [4], Harper-Bourne and Fisher proposed a point

source array model where the acoustic energy source is located at the end of each shock cell and the relative phasing between the sources is correlated by the spacing and the convection speed of the turbulent eddies between them. In a later formulation, Tam and Tanna considered that the shock-associated noise is generated by weak interaction between the quasi-periodic shock cells and the downstream propagating large scale turbulence structures in the mixing layer of the jet [10]. The Harper-Bourne and Fisher results for the choked convergent nozzle follow from the Tam and Tanna formulation for the CD nozzle when the design Mach number is set to unity. This agreement appears to be due to the fact that both models describe generation of noise by the coherent scattering of sound sources.

The shock-associated noise formulation of Tam and Tanna [10] is based on the vortex sheet shock cell model of Pack [38] which assumes that the mixing layer is thin and thus can be treated as a vortex sheet. This approximation is valid only close to the exit of the jet and it breaks down as the jet spreads downstream. A later development considers multiple scales shock cell model which accounts for spreading of the mean flow, and the shock cell structure is represented by a superposition of the wave guide modes of the jet flow [39]. The mechanism is further elaborated in Tam's stochastic model theory in which the large turbulence structures are represented by a superposition of the intrinsic instability waves of the mean jet flow [40, 41]. Combined with the multiple-scales shock cell model, the stochastic model theory predicts both the near and far field spectra. The predicted results appear to be in better agreement with the experimental results.

The shock-associated noise prediction methodology incorporated in the code follows the formulations of Tam and his associates. The shock-associated noise power spectral density at a point (r, θ) is given by,

$$S(r,\theta,f)=\frac{\Gamma L_w^2 A_j \bar{A}^2\left(\dfrac{\rho_\infty^2 C_\infty^4 M_j^2}{f(fD_j/U_j)}\right)}{(1+\dfrac{\gamma-1}{2}M_d^2)r^2} \tag{12}$$

$$\times \sum_{m=1}^{\infty}\frac{1}{\sigma_m^2 J_1^2(\sigma_m)}\exp\left\{-\left(\frac{(f_m-f)(1+M_c\cos\theta)L_W}{f(U_c/U_j)}\right)^2\frac{1}{2\ln 2}\right\}$$

where Γ is an unknown empirical constant and L_w is the half-width of Tam's "similarity source model" and is related to the core length of the jet. Both parameters need to be determined by fitting the prediction formula to the experimental data. The fully-expanded jet diameter D_j is related to the nozzle exit diameter D through the mass conservation equation as,

$$\frac{D_j}{D}=\left[\frac{1+\dfrac{\gamma-1}{2}M_j^2}{1+\dfrac{\gamma-1}{2}M_d^2}\right]^{\frac{\gamma+1}{4(\gamma-1)}}\left(\frac{M_d}{M_j}\right)^{1/2} \tag{13}$$

The parameter σ_m is the m^{th} root of the zeroth order Bessel function and f_m is defined as,

$$f_m=\frac{U_c k_m}{2\pi(1+M_c\cos\theta)} \tag{14}$$

where k_m corresponds to the wave number of the m^{th} wave-guide mode of the shock cell structure at maximum wave amplitude. J_1 is the Bessel function of order one. The quantity $\bar{A}^2$ which characterizes the shock cell strength (to be determined semi-empirically to improve the prediction) is given by,

$$\bar{A}^2=\left[\left(\frac{M_j^2-M_d^2}{1+\dfrac{\gamma-1}{2}M_d^2}\right)^2\left(\frac{D}{D_j}\right)^2\right]\div\left[1+n_1\left(\frac{M_j^2-M_d^2}{1+\dfrac{\gamma-1}{2}M_d^2}\right)^{n_2}\right] \tag{15}$$

where $n_1 = 3.0$, $n_2 = 3.0$ for underexpanded flows and $n_1 = 6.0$, $n_2 = 5.0$ for overexpanded flows. These values in Tam's model are based upon the measurements of the convergent-divergent nozzle jet flows so that a better match between the prediction and the experimental data for such flows could be attained.

It should be noted that the shock noise prediction scheme as incorporated in the code is independent of the CFD data. The prediction incorporates the hot jet effect and it has been further modified to accommodate the forward flight effect [42].

The empirical parameters used as inputs to the codes for the short conical plug-nozzle computational studies are the same as those used in the earlier computational studies of the CD nozzle [25, 26] and ideal contoured plug-nozzle [22]; this would enable a proper basis for comparisons of the computed data of the two cold PN jet noise studies.

5. COMPUTATIONAL DOMAIN AND SCOPE OF DATA

The axisymmetric flow-field is represented by a computational domain consisting of a 151 x 351 grid (Fig. 2), which is highly clustered along all the solid surfaces and along the plug-nozzle lip line in the jet exit region. The domain starts at the beginning of the converging inlet of the plug-nozzle and extends to an axial length of $33D$ and has an outer radius of $11D$ (the plug-nozzle exit diameter D = 45 mm and the aspect ratio = 3). That is, the domain is contained within $X = 0, X = 33D$ and $Y = 0, Y = 11D$.

The computational flow boundary conditions are as follows. All solid surfaces are assigned as no-slip, adiabatic wall conditions; all velocity components and the normal gradients of pressure and temperature are set to zero on boundary segments using this option. The jet axis downstream from the plug tip is prescribed as an *axis of symmetry*; this is very similar in function to the slip-surface boundary condition. The upper bounding surface ($Y = 11D$) of the domain is set as a slip-surface; all flow gradients normal to this boundary segment along with the component of velocity normal to this surface are taken to be zero. The conditions at the inlet ($X = 0$) and the exit ($X = 33D$) are assumed to be *free stream* boundary conditions; on these external far-field boundary segments, imposition of the correct subsonic or supersonic, inflow or outflow state is taken care of automatically. The assumed ambient conditions are: Mach number = 0.05 and static temperature (also the reference) = 294°K. The noise data are computed at far-field stations located on an arc of radius 3.05 m centered at a point on the jet axis in the exit plane of the plug-nozzle at the lip.

The gasdynamics and far-field noise of the flow field have been computed at pressure ratios, ξ = 2.0, 2.5, 3.0, 3.62 (design), 4.0, 4.5 and 5.0. For the first pressure ratio ξ = 3.62, a run time of about 5 hours on the Cray Y-MP supercomputer was needed to attain satisfactory convergence for the CFD computations. The result of computations at the first pressure ratio is used as the starting condition for calculations at the next adjacent pressure ratio, and the run times for subsequent computations from one adjacent pressure ratio to another are of the order of only four hours. A complete set of the acoustic data at the one-third octave band center frequencies were obtained at angles,

measured from the downstream jet axis θ, in multiples of 10° from 20° to 160°. The computed results for the mixing noise, the shock-associated noise and the total noise levels are included in Appendix B.

6. RESULTS & DISCUSSIONS

A complete set of the gasdynamics data is available. The gasdynamics data consist of the predicted numerical outputs of the flow variables at the grid points and the associated contour plots. Only some typical gasdynamics and far-field noise results which help assess the role of a short conical PN as a supersonic jet noise suppressor are presented as part of the discussion that follows.

6.1 Some Gasdynamic Features

Some typical color contour plots of the turbulence intensity and the Mach number for the short conical PN jet flow at the design pressure ratio (ξ_d = 3.62) are presented in Fig. 3 and Fig. 4, respectively, and the radial distributions at selected axial locations are provided in Fig. 5. Similar plots for pressure ratios ξ = 2.50 and ξ = 4.50 are shown in Figs. 6-8 and Figs. 9-11, respectively. The turbulence intensity level shown is normalized with respect to the acoustic speed at 294°K and is defined as $[(1/3)v_i v_i]^{1/2}/C_\infty$ except on the color contour plots where the levels indicate values of $[(1/2)v_i v_i]/C_\infty^2$.

The turbulence intensity levels for the short conical PN at the design condition are found to be nearly uniform in the supersonic core of the jet, the values ranging from 10% to 15%. For the off-design conditions, the intensity levels are low in the supersonic region and thus the mixing region of the short conical PN jet is dominant only in a region near the free jet boundary adjacent to the supersonic core of the jet. The ideal contoured PN theoretical study indicated high values of turbulence intensity levels confined within a very narrow region along the nozzle lip line at all pressure ratios [22]. The maximum turbulence intensity levels for the ideal contoured and the short conical plug-nozzles are noted to be of the same order. The trends and magnitudes of the predicted turbulence intensity levels of the short conical PN jet at off-design conditions are nearly the same as those predicted for (i) the ideal contoured PN of the same design pressure ratio ξ_d = 3.62 [22] and (ii) the ideal CD nozzle jet of *lower* design pressure ratio ξ_d = 3.18 [25, 26]. Hence, the theoretical studies indicate that, in respect of the turbulence intensity

distributions of the jet under imperfectly-expanded flow conditions, the short conical plug nozzle may be comparable to the ideal contoured plug-nozzle or the ideal contoured CD nozzle. Note that the turbulence intensity is primarily responsible for generation of the mixing noise.

The predicted short conical PN jet flow at the design condition is noted be fairly uniform at the exit plane in the vicinity of the plug tip, the exit Mach number being of the order of 1.4. The presence of a fine subsonic wake flow is observed just near the plug tip, but this subsonic pocket rapidly vanishes and the jet flow is fully supersonic slightly beyond the plug tip at about five jet diameters from the inlet. This subsonic wake is due to the non-contoured nature of the conical plug. The supersonic core of the short conical PN jet at the design pressure ratio $\xi_d = 3.62$ is noted to extend about twelve diameters downstream from the plug-nozzle lip. This is nearly the same as the reported value for the convergent nozzle [43] and significantly different from the corresponding values of about sixteen diameters for the ideal contoured plug-nozzle ($\xi_d = 3.62$) and the contoured CD nozzle of *lower* design pressure ratio ($\xi_d = 3.18$) [25].

The predicted data indicate only a weak shock structure in the short conical PN jet at the design condition as was seen to be the case in the experimental study (see shadowgraph in Fig. 12). As compared to the convergent nozzle, and even convergent-divergent nozzle, relatively weak cellular shock structures are observed in the short conical PN jet at all off-design pressure ratios (both less than or greater than the design pressure ratio). Close to the design pressure ratio, at imperfectly expanded jet pressure ratio $\xi = 3.0$ or $\xi = 4.0$, it is observed that the first few shock cells are too weak to repeat themselves farther downstream. The formations of the first shock cell in the short conical PN jet flows occur relatively farther downstream, and the strength of the shock cells and their extents decay rapidly. These observations of the short conical PN jet flows at the design and off-design conditions are in general agreement with the reported shadowgraph records of the conical plug-nozzle jet flow which are reproduced from an earlier study in Fig. 12 [23]. The Mach number contour plot at the design condition indicates the presence of a small narrow subsonic pocket embedded in the supersonic core of the jet

near its axis beyond the plug tip. This is explained by the presence of a thin separated flow region starting from the plug tip (wake flow on account of a finite plug tip dimension). A similar thin wake flow is also visible in the shadowgraph of the short conical PN jet flow (see Fig. 12 labeled as ξ = 3.62). A significant wake flow is necessarily accompanied by a recompression shock which, if strong enough, could lead to formation of its own repetitive shock structure. An ideally pointed plug, of course, will not generate a wake but this is not a practical proposition. Also, the computed data exhibit no evidence of formation of wake shock or Mach disc even at the highest jet pressure ratio (ξ = 5.0) which was also found to be the case in the earlier experimental study of the short conical PN [14]. At such high off-design supercritical pressure ratios, the Mach disc formations always occur in the convergent and the CD nozzle jet flows.

In the present two-stage algorithm for the jet noise prediction, as mentioned earlier, the relevant CFD data are used as inputs for the noise computation. The CFD related errors would thus pass on to the prediction of the jet noise. At this stage, it is not possible to identify the sources of such errors as no experimental gasdynamics data (turbulence intensity, static pressure, velocity, Mach number, etc.) for a plug-nozzle jet are available in the literature to enable a satisfactory validation of the use of NPARC code for prediction of such jet flows. In particular, the computation of the turbulence intensity which plays a key role in generation of the mixing noise needs to be further interpreted and validated. Also, it is important to further validate the estimation of the cellular shock structure characteristics of the short conical PN jet flows which are responsible for generation of the often dominant shock-associated noise in imperfectly expanded jets.

6.2 Mechanism Of Shock Formation

The shock cell formations in a short conical PN jet flow is basically different from those in an ideal contoured PN, the convergent nozzle and the CD nozzle jets. In a convergent nozzle, the supersonic jet is always underexpanded and as such strong shock structures are present at supercritical pressure ratios. In the CD nozzle, the supersonic jet is shockless at the design condition and has only weak shock structures for imperfectly

expanded condition close to the design; but, for all other off-design conditions, the CD nozzle jet flows have shock structures comparable in strength to those for the equivalent convergent nozzle jet. In an ideally contoured PN jet flow, since the contoured plug surface quenches all of the expansion waves incident on the plug surface, the shock structures are absent at the design condition and, relative to the equivalent CD nozzle, are weak at all pressure ratios less than or greater than the design pressure ratio.

The short conical plug-nozzle is about 25% less longer than the equivalent ideally contoured plug and the plug surface is conical downstream from the sonic throat (the overall geometry of the conical plug is, however, very close to that of the ideally contoured plug). The leading expansion wave (of the fan centered at and originating from the nozzle lip) that meets the conical plug tip has a Mach number $M_{tip} = 1.27$ approximately. Note that, unlike an ideally contoured plug surface which provide continuous suitable compression turnings, the solid straight plug surface would reflect any expansion wave that is incident upon it as an expansion wave or generate expansion waves of its own. There are thus three distinct flow regimes in such short conical plug-nozzle jet flows having three different types of shock cell formations: (i) regime I for fully-expanded jet Mach number $M_j < M_{tip}$, (ii) regime II for $M_j \cong M_{tip}$ and (iii) regime III for $M_j > M_{tip}$. In regime I, the flow field near the plug region is widely interspersed with expansion waves consisting of the expansion waves reflected by the plug surface and the expansion waves generated by the surface farther downstream up to the plug tip (see the shadowgraph Fig. 12(a) and the flow sketch Fig. 13(a)). All these scattered expansion waves get reflected from the free jet flow boundary as widely dispersed compression waves which finally coalesce together to form the first conical shock cell in the jet farther downstream from the plug tip; subsequent series of reflections from the jet boundary then lead to the development of a single set of rapidly decaying repetitive shock cells. Shock cell structures in short conical plug-nozzle jets under such conditions ($M_j < M_{tip}$) are relatively weak and are comparable in strength to those of the corresponding ideal contoured plug-nozzle jets; thus, one would expect comparable shock noise levels in short conical plug-nozzle and ideal contoured plug-nozzle. In regime II, the plug surface intercepts and reflects nearly all of the expansion waves emanating from the nozzle lip

and subsequent reflections from the free jet boundary generate, again, a single set of repetitive shock cell structure; whereas, the ideal contoured plug-nozzle, under such operating conditions, has shock structure which are either vanishingly weak ($M_j \cong M_{tip}$) or totally absent (corresponding to design condition $M_j = M_d = 1.49$). In regime II, therefore, one would expect the short conical plug-nozzle jet flow to have some shock-associated noise component as compared to the ideal contoured plug-nozzle. In regime III, the shock formation mechanism is qualitatively different from those for regimes I & II (see Figs. 12 and 13). In such jet flows ($M_j > M_{tip}$), two distinct families of repetitive shock cell structures would be present. One family of the repetitive shock cell structure is on account of the reflections of the incident expansion waves from the solid plug surface which are reflected as compressions from the jet flow boundary (see shock labeled S_1 in Fig. 13(b)). The second family of shock structures originates because the centered expansion fan from the nozzle lip is not completely intercepted by the conical plug, and the escaping expansion fronts reflect as compressions from the opposite jet flow boundary (see shock labeled S_2 in Fig. 13(b)). In an ideally contoured plug-nozzle jet, all the expansion waves pertaining to the pressure ratios up to the design pressure ratio incident on the plug surface are canceled, and thus in the underexpanded mode of operation one would expect only a weak repetitive shock cell structure formed by reflections of the expansion waves, which escape beyond the plug tip, from the free jet boundary. The presence of two weak families of repetitive shock cell structures instead of a very strong single family of shock cell structure to accommodate the same jet pressure ratio may have favorable impact on shock noise radiation. For operating conditions of $M_j > M_{tip}$, the noise levels of a short conical plug-nozzle jet may be comparable or lesser than those for the ideally contoured plug-nozzle jet. From the gasdynamics of the short conical PN jet flows, the short conical plug-nozzle jet noise may thus be comparable to the ideal contoured plug-nozzle jet noise except at operating conditions very close to the design.

6.3 Computational Noise Prediction

Some typical predicted one-third octave SPL spectra of the short conical PN jet flows for the design pressure ratio, ξ_d = 3.62, are compared with the short conical PN measurements [14] in Fig. 14. The figure shows spectra at four typical angles, *measured from the downstream jet axis,* θ = 30°, 60°, 90° & 120°. The corresponding OASPL's of the plug-nozzle are presented in Fig. 15. For typical off-design pressure ratios, ξ = 3.0 (less than the design pressure ratio) and ξ = 4.5 (greater than the design pressure ratio), the comparisons of the SPL's are shown in Figs. 16-17; the corresponding OASPL's comparisons are included in Fig. 18. Experimental data for the short conical plug-nozzle have been reported only for a limited range of pressure ratio and only at some selected angles to the downstream jet axis.

Noise Prediction at Design Pressure Ratio

At the design pressure ratio (ξ_d = 3.62, Fig. 14), the agreement of the predicted SPL'S with the measurements may be considered to be, in general, very good, the maximum deviation being of the order of 3 dB. The agreement is excellent for most of the frequencies at higher angles θ to the downstream jet axis. But, for higher frequencies at smaller angles θ, deviations up to 8 dB are observed, the discrepancies increasing with decreasing angle θ. As compared to the ideal contoured plug-nozzle computational data, the short conical plug-nozzle noise levels are slightly higher at very high band center frequencies; the levels being identical for both the plug-nozzles at lower frequencies. This is explained by the absence of the shock-associated in the ideal contoured plug-nozzle jet at the design condition of shockless flow whereas the short conical plug-nozzle jet has a weak shock which generates some high frequency shock-associated noise. A comparison of the computed mixing noise level spectra for the short conical PN (Table B-10, Appendix B) and for the equivalent ideal contoured PN [22] shows that the two are nearly identical. The CFD data for the short conical PN indicate that, at the design pressure ratio, the jet flow has very weak shock structure and the dominant component of the noise generating mechanism should thus be due to mixing alone. But, this observation is not supported by a comparison of the predicted data of the mixing noise and the shock-

associated noise for the short conical PN (see Tables B-10 and B-11) which shows that the shock-associated noise levels are significantly higher than the mixing noise levels. The predicted noise levels for the short conical PN are the same as those for the ideal contoured PN for the one-third band center frequencies less than 5 kHz, but considerably higher for frequencies greater than 5 kHz. Such large departures in the levels for very high frequencies are in contradiction with the computed CFD data for the jet flows. The reason for the anomaly may be explained by usage of the value of the input parameter $\bar{A}$ in the shock-associated noise prediction part of the modified GE/MGB code incorporating Tam's formulation (see equation 15, page 16). The shock-associated noise computation uses a value of the design Mach number for which the jet is shockless which is true for the ideal contoured PN at the design condition of $M_d = 1.49$, but not for the short conical PN. The use of this value of M_d for noise computations of the short conical PN results in shock-associated noise levels which are identical with those of the contoured PN, and this is not acceptable in light of the physics of the short conical PN - the short conical PN can never be fully-expanded at any supersonic Mach number except in the limit of $M = 1$. In the present computational scheme of the shock-associated noise prediction for the short conical PN, the value of the "design Mach number" in the code has been set to unity for which the short conical PN jet flow is truly shockless. However, the code, the way it is formulated, senses the true design pressure ratio as an imperfectly expanded flow condition (treating it as an under-expanded type of the jet flow), and, thus, overly predicts the shock noise. This is one of the shortcomings of the present shock-associated noise formulation of the code based primarily on the CD nozzle but used for nozzles with center bodies.

The computational scheme predicts a peak Strouhal number of the order of 0.3 ($f_{peak}D / U_j \cong 0.3$), which is nearly the same at all angles. The predicted values of the peak Strouhal number are nearly the same as that of the contoured plug-nozzle at the design pressure ratio [22]. However, the experimental data for the short conical plug-nozzle show that the peak Strouhal number increases with increasing angle up to $\theta = 60°$ and then levels off to a nearly constant value [14]. It may be noted that the same trend was also exhibited by the ideal contoured plug-nozzle computational studies. For the short

conical plug-nozzle, a slight shift in the predicted peak frequency to a lower value, as compared to the measurements, is observed at almost all higher angles θ. The agreement of predictions with the measurements in the present conical plug-nozzle study is generally of the same order as that reported in earlier computational studies of the convergent-divergent nozzle [25] and the contoured plug-nozzle [22]. Once again, in interpreting Strouhal number predictions, one should take into account the code-related overprediction of the shock-associated noise in the short conical plug-nozzle jet flows when the physics of the jet flows and the computed gasdynamics data indicate otherwise.

The OASPL's vs θ comparison at the design pressure ratio (see Fig. 15), when the jet flow has weak shock structures and the dominant noise is due to turbulent mixing, shows that the agreement of the computational noise data with the measurements are quite fair, deviations being within 3 dB in the higher range of angles θ and much less in the lower range of angles. The predicted maximum OASPL is noted to be about 119 dB at $\theta = 40°$ as compared to the measurement of 118 dB at $\theta = 30°$. The codes tend to overpredict the OASPL's but the trend of variation seems to be well represented. Earlier measurements have shown that, at lower angles to the downstream jet axis, where the mixing noise is known to be dominant, the OASPL's of a short conical plug-nozzle (M_d = 1.49, present case) are significantly lower than those of a contoured CD nozzle (M_d = 1.48). This trend is also confirmed by the present computational study. At higher angles to the downstream jet axis, the computed OASPL's for the short conical plug-nozzle is some 5 dB higher than those of the contoured CD nozzle. This may be attributed to the complete absence of shock at design condition for ideal nozzles and to the problem associated with the code-related overprediction of the shock-associated noise, as noted before.

It appears that the combination of the NPARC CFD code and the modified GE/MGB noise code reasonably predicts the CPN jet noise at its design condition except in situations of very high frequencies and in regard to the peak Strouhal number. The computational short conical PN data indicate that, at the design pressure ratio, the jet flow has a very weak shock structure. Therefore, the reasons for the discrepancies may be

traced to (a) the noise modeling and (b) the application of the code to a flow with a center-body.

The present prediction methodology assumes that the jet noise is dominated by small-scale turbulence. Until recently, it was generally believed that large-scale turbulence structures or instability waves of the flow became active as a noise source only at very high supersonic numbers. A more recent investigation of the noise spectra for both subsonic and supersonic jets indicates that both scales of turbulence structures may influence the turbulence mixing noise at all jet Mach numbers [44]. Prediction of the mixing noise due to large-scale turbulence is usually done using a linear inviscid stability analysis [45]. This noise component is dominant inside the zone of silence of fine-scale turbulence, which is formed near the downstream jet axis. It has been suggested that the dominant part of radiated noise due to large scale turbulence is in a downstream direction for angles $\theta < 55°$ with a peak Strouhal number decreasing with the angle [46]. These observations may partly explain the lack of a proper shift in the predicted spectra of the short conical PN at the design condition. The reason for discrepancy at very high frequencies is partly because of the code-related shock-associated noise overprediction. Also, it may be possibly attributed to the breakdown of modeling associated with the sound-flow interaction. Present modeling is based primarily on round jet studies which ignore the presence of a solid center-body. It appears that in plug-nozzle situations, the high-frequency solution [34, 35] may provide an adequate approximation for prediction of the jet noise over the most energetic portion of the spectrum. This issue needs to be examined further.

The errors in the mixing noise prediction may also be due to source description and propagation modeling. Validations of the source intensity formulation in the code have often reported a discrepancy of the order of 10% for simple round nozzle situations. In order to use the Lighthill's equation to predict the sound intensity, it is necessary to develop an approximate model of turbulence which will allow an analytical integration of the two-point space-time correlations. Ribner's assumption of isotropic turbulence leads to an exact analytical evaluation of the correlation volume integrals. Admittedly, the turbulence in a jet is not isotropic. For example, it has been reported that the

measurements of the fourth-order velocity correlation in the direction of the flow are different from the transverse components [47]. Other models of turbulence such as axisymmetric turbulence [48] have been documented in the literature. Clearly, new computational challenges, including development of CFD codes with non-isotropic turbulence model need to be addressed.

Several issues need to be noted in regard to the application of the present codes for predicting the jet mixing noise for plug-nozzle situations, i.e., flows with center-bodies. A number of empirical parameters (α, α_c, β_c, etc.) need to be used as inputs to the codes and these parameters are to be chosen based on the available experimental data as guide. In the present study, the choice of these parameters was primarily based upon the experimental data of the convergent nozzle and the CD nozzle jet flows. No experimental data on contoured plug-nozzle jet flows are available to help determine a suitable set of values for the empirical constants. Second, the underlying mechanism of the mixing noise radiation used in the computational modeling is supported primarily by the studies on round convergent nozzle and the CD nozzle jet flows. These studies are silent as to the effect of a center body on an otherwise free jet flow. A solid body such as a well-contoured plug immersed in an unbounded flow may influence the turbulence-related characteristics.

Noise Prediction at Off-Design Pressure Ratios

At pressure ratio close to and less than the design pressure ratio, $\xi = 3.0$ (Fig. 16), the agreement of the predictions with the measurements are excellent in the entire range of frequencies at all angles to the jet flow except at the lowest angle where a deviation of up to 8 dB are observed. Based on examination of the detailed numerical acoustic data (Appendix B), it may be concluded that, for all smaller angles to the jet axis, the mixing noise levels are comparable to the shock-associated levels when pressure ratios are less than the design pressure ratio; however, the shock noise component is noted to be dominant at very high frequencies and at larger angles θ. The data shows that the predicted one-third octave band SPL's for the mixing noise component are close to the total noise measurements of the short conical PN [14] as well as to the total noise level

measurements for the ideal contoured PN jet flows [15]. The short conical PN and the ideal contoured PN have the same predicted noise levels at ξ = 2.0, farthest from the design pressure ratio, except at very high frequencies. It is interesting to note that for the pressure ratio farthest from the design, the predicted noise levels in the high frequency range are *lower* for the short conical PN than for the *ideal* contoured PN. This indicates that for such conditions, contribution of the shock-associated is more pronounced for the ideal contoured PN than for the short conical PN. The computational noise levels of the short conical PN and the ideal contoured PN, for the entire range of the one-third band center frequencies and at all angles to the jet axis, are almost identical at pressure ratio ξ = 2.5 and not significantly different at pressure ratio ξ = 3.0.

The OASPL's vs θ variations for the short conical PN theory and measurements are compared in Fig. 18 for a typical case of pressure ratio less than the design pressure ratio. The predicted noise radiation exhibits a lack of significant directivity pattern which gradually emerges with increasing supercritical pressure ratio (being almost absent at ξ = 2.0). Such a directivity pattern is not indicated by the measurements. At off-design pressure ratios less than the design, the trend of the predicted noise directivity appears to be basically different; the measurements consistently indicate a tapering off of the OASPL's from its highest value at the lowest angle θ, to a gradual leveling off with increasing θ. Another peculiarity of the modeling is that, at close to the design pressure ratio, it always underpredicts OASPL's at lower angles θ (region of mixing noise dominance) and overpredicts at higher angles θ where the shock noise component is known to be dominant; however, the departures are reasonable, being within 5 dB. As compared to the ideal contoured plug-nozzle, the short conical PN computed levels are within 1 dB at ξ = 2.5 and 3 dB at ξ = 3.0. Thus, the short conical plug-nozzle of simple geometry and the longer ideal contoured plug-nozzle of complex geometry seem to be equivalent when operated at pressure ratios less than the design pressure ratio.

Now, the cases of operations of the short conical PN at pressure ratios greater than the design pressure ratio need to be examined. At close to the design pressure ratio of ξ = 4.0, the predictions are noted to be quite satisfactory at θ = 90°, except for a small range of frequencies in the middle of the spectrum where deviations of up to 10 dB are noted.

With increasing pressure ratio, the agreement is noted to improve and, at pressure ratio ξ = 4.5, the agreement between the predictions and measurements become quite satisfactory (see Fig. 17). It is important to note that the predicted noise levels of the short conical plug-nozzle jet and of the equivalent ideal contoured plug-nozzle jet approach one another as the pressure ratio increases from the design. At pressure ratio close to the design, ξ = 4.0, the predicted noise levels for the short conical PN are almost the same as those for the ideal contoured PN at frequencies f < 5 kHz, the levels being slightly higher for the higher frequencies. At higher pressure ratios, ξ = 4.5 and 5.0, there is little difference between the predicted noise levels of the short conical PN and the ideal PN for the entire range of frequencies at all angles to the jet axis. The predicted noise levels for the short conical plug-nozzle in general are quite comparable to those of the ideal contoured plug-nozzle as was the case in the reported experimental studies [14, 15]. It should be emphasized that the conical PN experimental noise data [14] as well as the predicted noise data indicate only a little sensitivity to changes in the pressure ratio above the design. This may be attributed to the basically different shock formation mechanism in the conical plug-nozzle jet flow which produces only weak shock structures, as explained in the earlier section.

Using the same codes as in this study, a computational noise prediction of a contoured CD nozzle (ξ_d = 3.12) in imperfectly expanded modes of operation has been recently reported [26]. This study reported the SPL's predictions to be fair except in the range of low one-third octave band center frequencies where the deviations were significant. According to this study, no noise suppression effectiveness of the CD nozzle, as compared to the equivalent underexpanded convergent nozzle, was observed at lower angles to the downstream jet axis at *any* frequency. However, significant noise suppressions of the CD nozzle were reported for high frequencies at higher angles θ where the shock associated noise is known to be a dominant component. Such is not the case for the short conical plug-nozzle of the present study, where one notices noise suppression effectiveness at all pressure ratios (even at low supercritical off-design pressure ratios) for all angles to the downstream jet axis - at lower angles where the

mixing noise is the dominant component as well as at higher angles where the shock-associated noise is the dominant component.

The predicted OASPL's vs θ variations for supercritical pressure ratios, $\xi > \xi_d$ (Fig. 18), exhibit a lack of any directivity pattern as was also reported to be the case with the measurements. The modeling is always noted to overpredict the OASPL's in the entire range of the angle θ, the deviations from the measurements not exceeding 4 dB. The predictions are, in general, quite satisfactory. As compared to the ideal contoured plug-nozzle predictions of the OASPL's, the short conical plug-nozzle values are up to 5 dB higher at close to the design pressure ratio. This difference in levels rapidly decreases with increasing pressure ratio above the design, there being little difference in levels between the short CPN and the ideal contoured PN at the highest pressure ratio, $\xi = 5.0$. Thus, the short conical plug-nozzle appears to be, in general, equivalent to the ideal contoured PN not only in the overexpanded modes of operations as noted before, but also in the underexpanded modes of operations.

It is of interest to compare the predicted mixing noise and shock-associated noise levels relative to the measurements. This is presented in Figure 19 for some typical pressure ratios at an angle $\theta = 90°$, where shock noise is known to be a dominant component in jets. It is observed that the mixing noise levels are only slightly less than the corresponding measurements even at very high frequencies where normally the shock-associated noise component is supposed to be dominant. If the gasdynamics data for the short conical PN were available to estimate a proper set of the empirical parameters, particularly for use in the shock-associated noise formulation, it may be possible to get a more satisfactory prediction of the total noise levels for frequencies of practical interest.

The sources of error in the present jet noise prediction for flows with significant shock structures may be primarily due to the shock-associated noise modeling and secondarily due to the mixing noise modeling problems discussed in the earlier section. As noted before, the mechanism of shock formation in a conical plug-nozzle jet flow is basically different from that in the convergent nozzle or in the convergent-divergent nozzle jet flows. The shock-associated noise formulation of Tam and his associates

incorporated in the code is based on the moderately imperfectly expanded jet flows from round convergent-divergent and convergent nozzles. Several empirical parameters such as Γ, L_w, n_1 and n_2 values for over- and underexpanded flows, etc. (see equations 12 and 15), need to be externally prescribed for implementation of this prediction scheme. These empirical constants have been assigned values so that a better match of the prediction with the measurements for the CD nozzle and convergent nozzle jets could be attained. The same set of values has also been used in the present plug-nozzle computations as no supporting experimental data are available for the short conical PN jet. It may be possible to change these values arbitrarily such that one obtains a better agreement between the short conical PN prediction and experiment at a particular pressure ratio. Efforts to get a set of values for the empirical parameters which would work reasonably for the whole realm of the short conical PN jet flows either above or below the design pressure ratios have been unsuccessful. In its present state of development, the modified GE/MGB code works well only for simple nozzle geometry. In addition, one should take into consideration the effect of possible coupling of the mixing noise and the shock noise radiation which is not incorporated in the code. In order to further modify the GE/MGB code, issues related to these need to be addressed.

7. CONCLUSIONS AND RECOMMENDATIONS

7.1 Conclusions

Some important conclusions of the computational noise study of the short conical plug-nozzle jet are follows.

1. The prediction of noise levels of the short conical plug-nozzle jet flow at design condition is noted to be good; the model often predicts noise levels within 4 dB. The trends as well as the magnitudes are well represented. The modeling, in general, predicts the noise levels at off-design supercritical pressure ratios within 5 dB except at very high 1/3-octave band center frequencies, when significant deviations are observed.

2. At the design condition, the short conical PN of simple geometry shows noise suppression comparable to the ideal contoured PN and the contoured CD nozzle jets which, being shockless, are slightly quieter. At off-design supercritical pressure ratios, the short conical plug-nozzle of simple geometry exhibits noise suppression better than the ideal nozzles.

3. The role of a short conical plug-nozzle as a jet noise suppressor for low to moderate supersonic pressure ratios is well supported by the computational study.

4. The computational noise prediction scheme consisting of a combination of the modified GE/MGB noise code and the NPARC CFD-code with k-ε turbulence modeling, is a useful engineering tool for *comparative* evaluations of jet noise suppression. The shock-associated noise formulation needs to be further improved.

7.2 Recommendations

The available experimental gasdynamics data for the plug-nozzle jet flows are very limited. This makes it difficult to assess the validity of the NPARC CFD-code with k-ε turbulence model in predicting the gasdynamics of such jet flows. A proper estimate of the empirical gasdynamic constants for use in the codes is rather difficult at this stage. The noise prediction code can at best be only as good as the CFD code that drives it. Therefore, there is a need for further experimental data for such jet flows.

The issues of possibly different mechanisms for both the mixing noise and the shock-associated noise radiation in plug-nozzle jet flows should to be examined in the future development of the noise code.

The performance of a short conical plug-nozzle of simple geometry as a supersonic jet noise suppressor could be further improved by providing suitable perforations on the plug surface. It is suggested that the possibility of use of a suitably optimized conical plug in jet noise suppression schemes be examined.

8. NOMENCLATURE

A	area of the jet
C, C_∞	local and ambient speed of sound
f	observer frequency
I_{ijkl}	source correlation tensor
J_1	Bessel function of order one
K	annulus radius ratio of the plug-nozzle (= R_P/R_N)
L_{max}	axial length of the plug from the sonic point to its tip
M	Mach number
p	absolute pressure
r	radial distance
R	radius (also source to observer distance)
R_P	radius of the plug at the sonic point
R_N	radius of the nozzle lip at the exit
U	mean velocity in the direction of the flow
V_i	local velocity component
v_i	fluctuating velocity component
W_t	annulus width of the throat from sonic point to the nozzle lip
y	source co-ordinate
α	inclination of the plug-nozzle lip to the jet axis
β	Harper-Bourne & Fisher parameter
γ	ratio of specific heats
ξ	ratio of reservoir absolute pressure to the ambient absolute pressure
ρ	density
ψ	wall slope of the plug at the sonic point
σ_m	m^{th} root of the zeroth order Bessel function
θ	polar angle with respect to the downstream jet axis

9. REFERENCES

1. L. E. Stitt 1990 *NASA RP*-1235. Exhaust nozzles for propulsion systems with emphasis on supersonic cruise aircraft.
2. J. M. Seiner and E. A., Krejsa 1989 *AIAA Paper* 89-2358. Supersonic jet noise and the high speed civil transport.
3. M. J. Lighthill, 1962 *Proceedings of the Royal Society London* **A267**, 147-182. The Bakerian lecture: sound generated aerodynamically.
4. A. Powell 1953 *Proceedings of the Physical Society* **66**(12B), 1039-1056. On the mechanism of choked jet noise.
5. J. C. Yu and D. S. Dosanjh 1972 *Journal of the Acoustical Society of America* **51**, 1400-1410. Noise field of a supersonic Mach 1.5 cold model jet.
6. M. Harper-Bourne and M. J. Fisher 1973 *AGARD CP*-131, 11-1 to 13. The noise from shock waves in supersonic jets, noise mechanisms, AGARD Conference on Propagation and Reduction of Jet Noise.
7. J. M. Seiner 1984 *AIAA Paper* 84-2275. Advances in high speed jet aeroacoustics.
8. H. S. Ribner 1985 *AIAA Journal* **43**, 1708-1715. Cylindrical sound waves generated by shock vortex interaction.
9. H. K. Tanna 1977 *Journal of Sound & Vibration* **50**, 429-444. An experimental study of jet noise, part II: shock associated noise.
10. C. K. W. Tam and H. K. Tanna 1982 *Journal of Sound and Vibration* **81**(3), 337-358. Shock-associated noise of supersonic jets from convergent-divergent nozzles.
11. L. Maestrello 1979 *AIAA Paper No.* 79-0673. An experimental study on porous plug jet noise suppressor.
12. V. Kibens and R.W. Wlezien 1985 *AIAA Journal* **23**(5), 678-684. Noise reduction mechanisms in supersonic jet with porous center-bodies.
13. K. Yamamoto, J. F. Brausch, T. F. Balsa, B. A. Janardan and P. R. Knott 1984 *NASA CR*-3845. Experimental investigation of shock-cell noise reduction for single stream nozzles in simulated flight.

14. I. S. Das and D. S. Dosanjh 1991 J. of Sound and Vibration, **146**(3), 391-406. Short conical solid/perforated plug-nozzle as supersonic jet noise suppressor.

15. D. S. Dosanjh and I. S. Das 1988 *AIAA Journal*, **6**(8), 924-931. Aeroacoustics of supersonic jet flows from a contoured plug-nozzle.

16. D. S. Dosanjh, P. K. Bhutiani and K. K. Ahuja 1978 *AIAA Journal* **16**(3), 268-270. Jet noise suppression by co-axial cold/heated jet flows.

17. H. K. Tanna, C. K. W. Tam and W. H. Brown 1981 *NASA CR*-3454. Shock-associated noise reduction from inverted-velocity profile coannular jets.

18. J. M. Seiner and M. K. Ponton 1986 *AIAA Paper No.* 86-1867. Acoustic properties associated with rectangular geometry supersonic nozzles.

19. P. J. Morris and T. R. S. Bhat 1993 *AIAA Paper No.* 93-4409. Supersonic elliptic jet noise.

20. A. Khavaran and N. J. Georgiadis 1996 *AIAA Paper No.* 96-0641. Aeroacoustics of supersonic elliptic jets.

21. E. A. Krejsa, B. A. Cooper, D. G. Hall and A. Khavaran 1990 *AIAA Paper No.* 99-3983, *NASA TM* 103628. Noise measurements from an ejector suppressor nozzle in the NASA Lewis 9- by 15-foot low speed wind tunnel.

22. I. S. Das, A. Khavaran and A. P. Das 1996 *NASA CR*- 198462. Computational study of a contoured plug-nozzle as a supersonic jet noise suppressor.

23. D. S. Dosanjh and I. S. Das 1987 *NASA CR*-178095. Aeroacoustics of contoured and solid/porous conical plug nozzle supersonic jet flows.

24. R. Mani, T. E. Balsa, P. R. Gliebe, R. A. Kantol, E. J. Stringas and J. F. C Wang 1977 *FAA-Rd*-76-79-2. High velocity jet noise source location and reduction, task 2: theoretical developments and basic experiments.

25. A. Khavaran, E. A. Krejsa and C. M. Kim 1994 *Journal of Aircraft*, **31**(3), 603-609. Computation of supersonic jet mixing noise for an axisymmetric convergent-divergent nozzle.

26. C. M. Kim, E. A. Krejsa and A. Khavaran 1993 *AIAA Paper No.* 93-0735. Computation of supersonic jet noise under imperfectly expanded conditions.

27. G. K. Cooper and J. R. Sirbaugh 1989 *Arnold Engineering Development Center Report No.* AEDC-TR-89-15. PARC code: theory and usage.

28. K. Y. Chien 1982 *AIAA Journal*, **20**(1), 33-38. Prediction of channel and boundary layer flows with a low Reynolds number turbulence.

29. R. Beam and R. F. Warming 1976 *Journal of Computational Physics*, **22**(1), 87-110. An implicit finite difference algorithm for hyperbolic systems in conservation form.

30. R. Mani 1976 *Journal of Fluid Mechanics* **76**, 753-778. The influence of jet flow on jet noise, part i the noise of unheated jets.

31. R. Mani 1972 *Journal of Sound and Vibration* **25**, 337-347. Moving source problem relevant to jet noise

32. M. E. Goldstein 1976 *Journal of Fluid Mechanics* **75**, 17-28. The low frequency sound from multipole sources in axisymmetric shear flows, part II.

33. T. F. Balsa 1977 *Journal of Fluid Mechanics* **79**, 33-47. The acoustic field of sources in shear flow with application to jet noise: convective amplification.

34. B. J. Tester and C. L. Morfey 1976 *Journal of Sound and Vibration*, **46**, 79-103. Developments in jet noise modeling - theoretical predictions and comparisons with measured data.

35. S. P. Pao. *Journal of Fluid Mechanics*, **59**, 451, 1973. Aerodynamic noise emission from turbulent shear layers.

36. M. E. Goldstein 1976 *Aeroacoustics*. McGraw-Hill Book Company, New York.

37. J. E. Ffowcs-Williams 1963 *Phil. Transactions of Roy. Soc. of London*, **A255**, 469-503. The noise from turbulence convected at high speed.

38. D. C. Pack 1950 *Quarterly J. of Mechanics and Applied Mathematics*, **3**, 173-181. A note on Prandtl's formula for the wavelength of a supersonic gas jet.

39. C. K.W. Tam, J. A. Jackson and J. M. Seiner 1987 *Journal of Fluid Mechanics*, **153**, 123-149. A multiple scales model of the shock cell structure of imperfectly expanded supersonic jets.

40. C. K.W. Tam 1987 *Journal of Fluid Mechanics*, **153**, 123-149. Stochastic model theory of broad band shock associated noise from supersonic jets.

41. C. K. W. Tam 1990 , *Journal of Sound and Vibration*, **140**, 55-71. Broadband shock associated noise of supersonic jets.

42. C. K. W. Tam 1989 *AIAA Paper No.* 89-1088. Forward flight effects on broadband shock associated noise of supersonic jets.

43. H. T. Nagamatsu, R. F. Sheer, Jr. and G. Horva 1969 *NASA SP*-207, 17-51. Basic Aerodynamic Research, Ed. I. R. Schwartz. Supersonic jet noise theory and experiments.

44. C.K.W. Tam, M. Golebioski and M.J. Seiner 1996 *AIAA Paper No.* 96-1716. On the two components of turbulence mixing noise from supersonic jets.

45. C.K.W. Tan. 1991 *NASA Reference Publication* 1258, Vol. 1, 311-390. Aerodynamics of flight vehicles: theory and practice.

46. C.K.W. Tam and P. Chen 1994 *AIAA Journal* , 32 (9), 1774-1780. Turbulence mixing noise from supersonic jets.

47. Ian S. F. Jones 1969 *J. of Fluid Mechanics. 36(3), 529-543.* Fluctuating turbulent stresses in the noise producing region of a jet.

48. M.E. Goldstein and B..M. Rosenbaum 1972 *NASA TN* D-6939. Emission of sound from axisymmetric turbulence convected by a mean flow with application to jet noise.

10. LIST OF FIGURES

Figure 1. Fully expanded jet flow from an ideal contoured plug-nozzle.

Figure 2. Computational grid for the plug-nozzle (aspect ratio = 3, axial length = 33D).

Figure 3. Contour plot of turbulence intensity (pressure ratio ξ = 3.62: design).

Figure 4. Contour plot of flow field Mach number (pressure ratio ξ = 3.62: design).

Figure 5. Radial distributions of the turbulence intensity and Mach number at some selected axial locations (pressure ratio ξ = 3.62: design).

Figure 6. Contour plot of turbulence intensity (pressure ratio ξ =2.50).

Figure 7. Contour plot of flow field Mach number (pressure ratio ξ =2.50).

Figure 8. Radial distributions of the turbulence intensity and Mach number at some selected axial locations (pressure ratio ξ =2.50).

Figure 9. Contour plot of turbulence intensity (pressure ratio ξ = 4.50).

Figure 10. Contour plot of flow field Mach number (pressure ratio ξ = 4.50).

Figure 11. Radial distributions of the turbulence intensity and Mach number at some selected axial locations (pressure ratio ξ = 4.50).

Figure 12. Some shadowgraphs of the short conical plug-nozzle jet flows.

Figure 13. Shock formations in conical plug-nozzle jet flows at off-design conditions.

Figure 14. Comparisons of the 1/3-octave SPL spectra for the jet flows at four typical angles θ (predictions vs measurements; pressure ratio ξ = 3.62).

Figure 15. Comparisons of the overall sound pressure level directivity for the conical PN (prediction vs measurements: design condition ξ = 3.62).

Figure 16. Comparisons of the 1/3-octave SPL spectra for the conical PN at four typical angles θ (predictions vs measurements : pressure ratio ξ = 3.0).

Figure 17. Comparisons of the 1/3-octave SPL spectra for the conical PN at four typical angles θ (predictions vs measurements : pressure ratio ξ = 4.5).

Figure 18. Comparisons of the overall sound pressure level directivity of the conical PN (predictions vs measurements : ξ = 3.0 and ξ = 4.5).

Figure 19. Comparisons of the predicted mixing and shock noise components

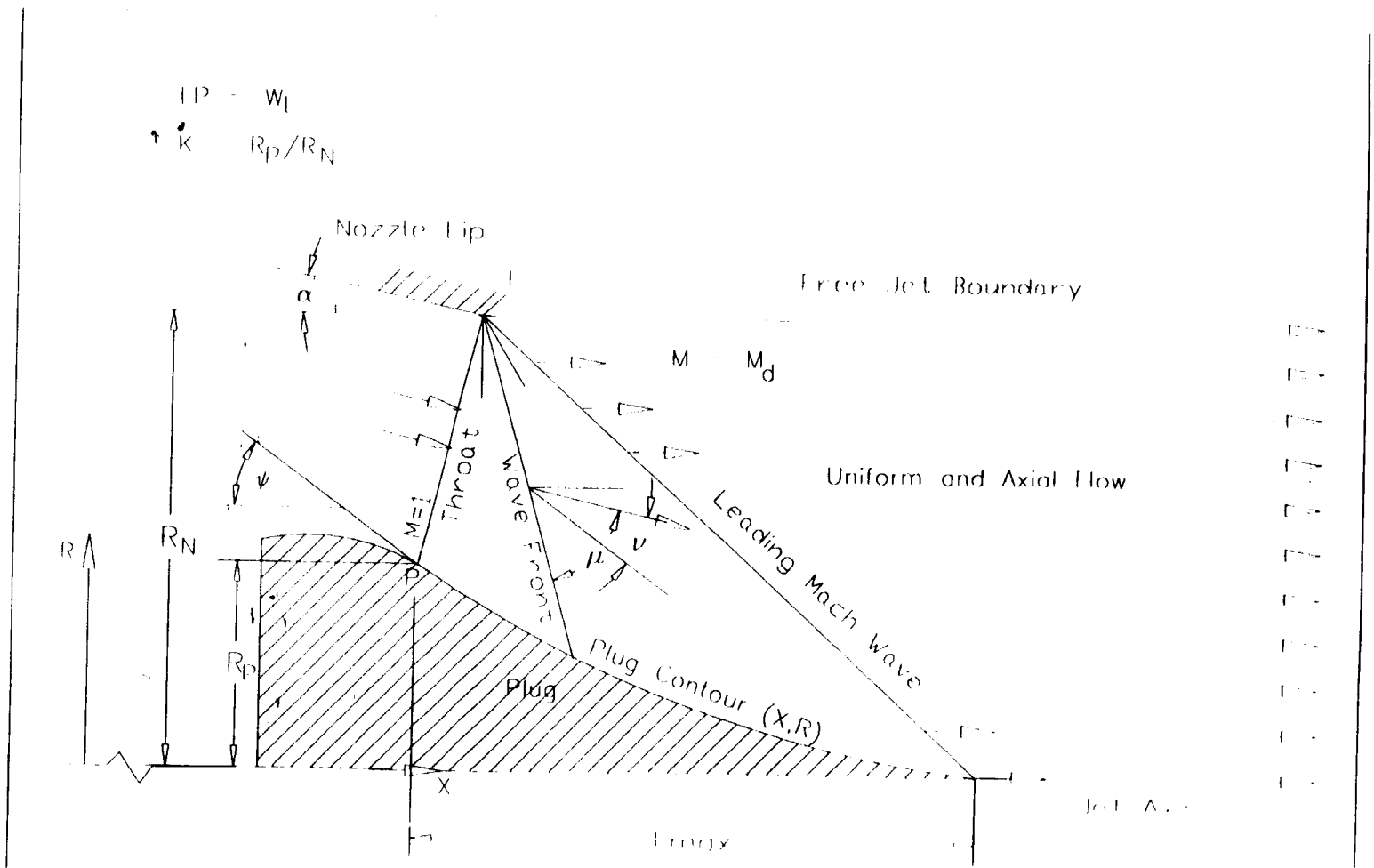

Fig 1 Fully expanded jet flow from an ideal contoured plug nozzle and

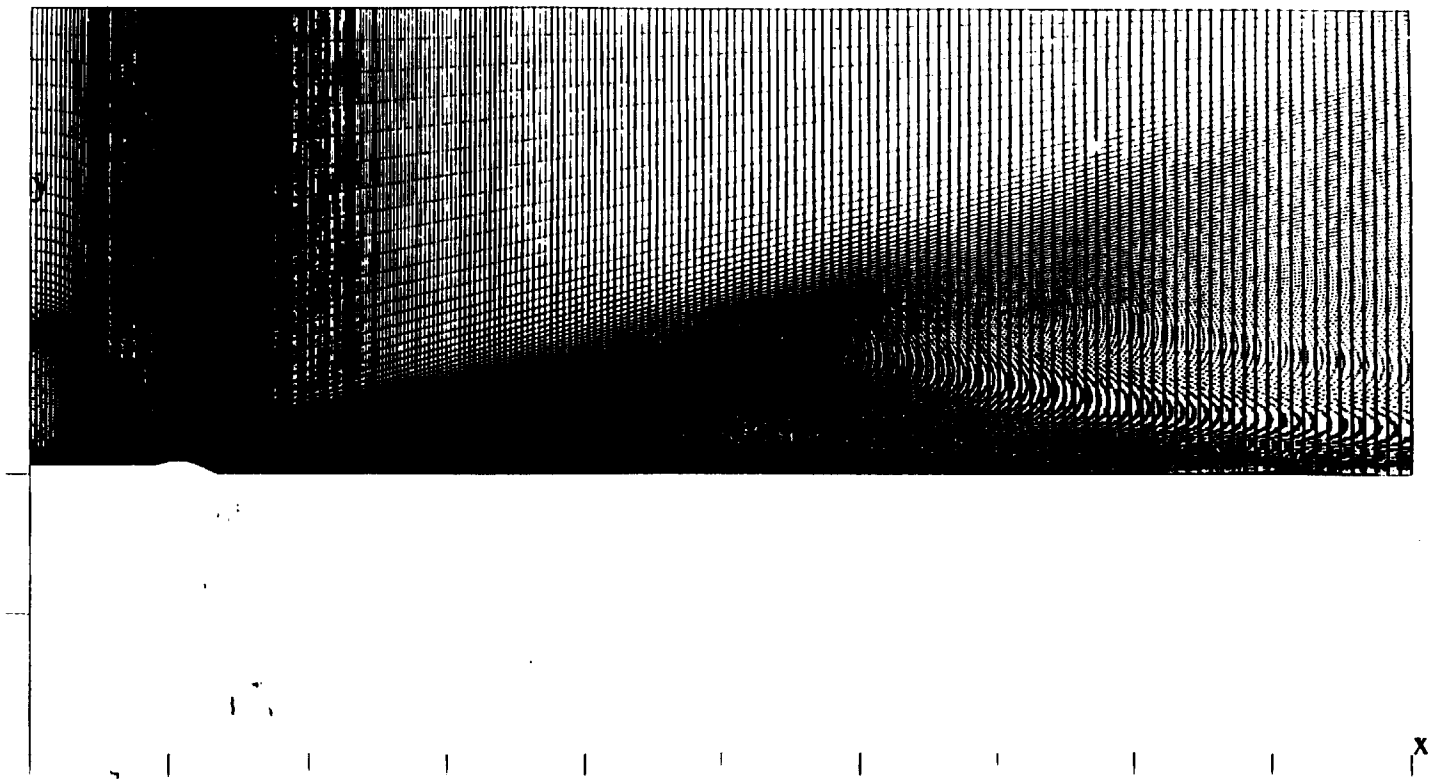

Fig. 2 Computational grid for the plug-nozzle (aspect ratio = 3, axial length = 33D).

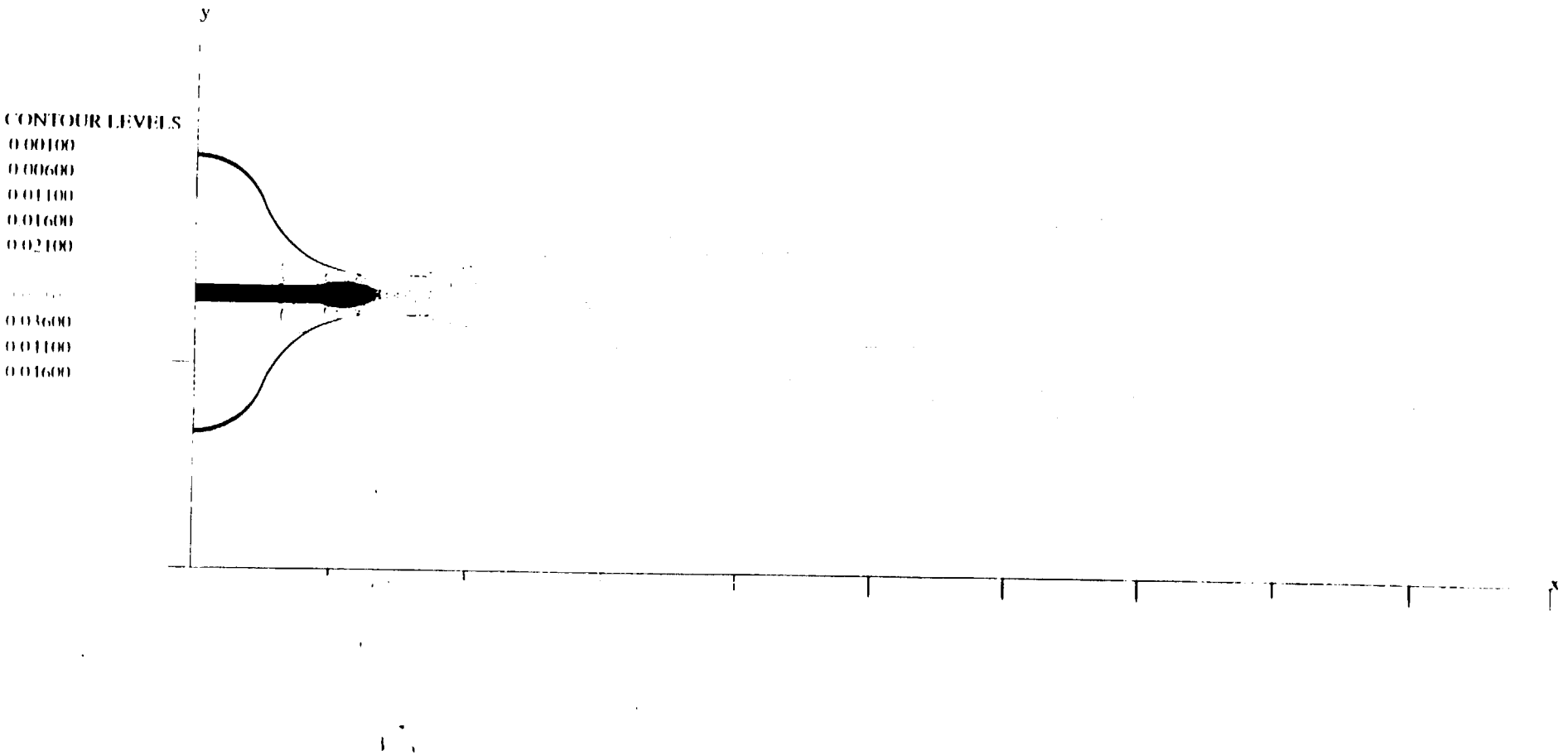

Fig. 3 Contour plot of the turbulence intensity for the plug-nozzle (ξ = 3.62 : design).

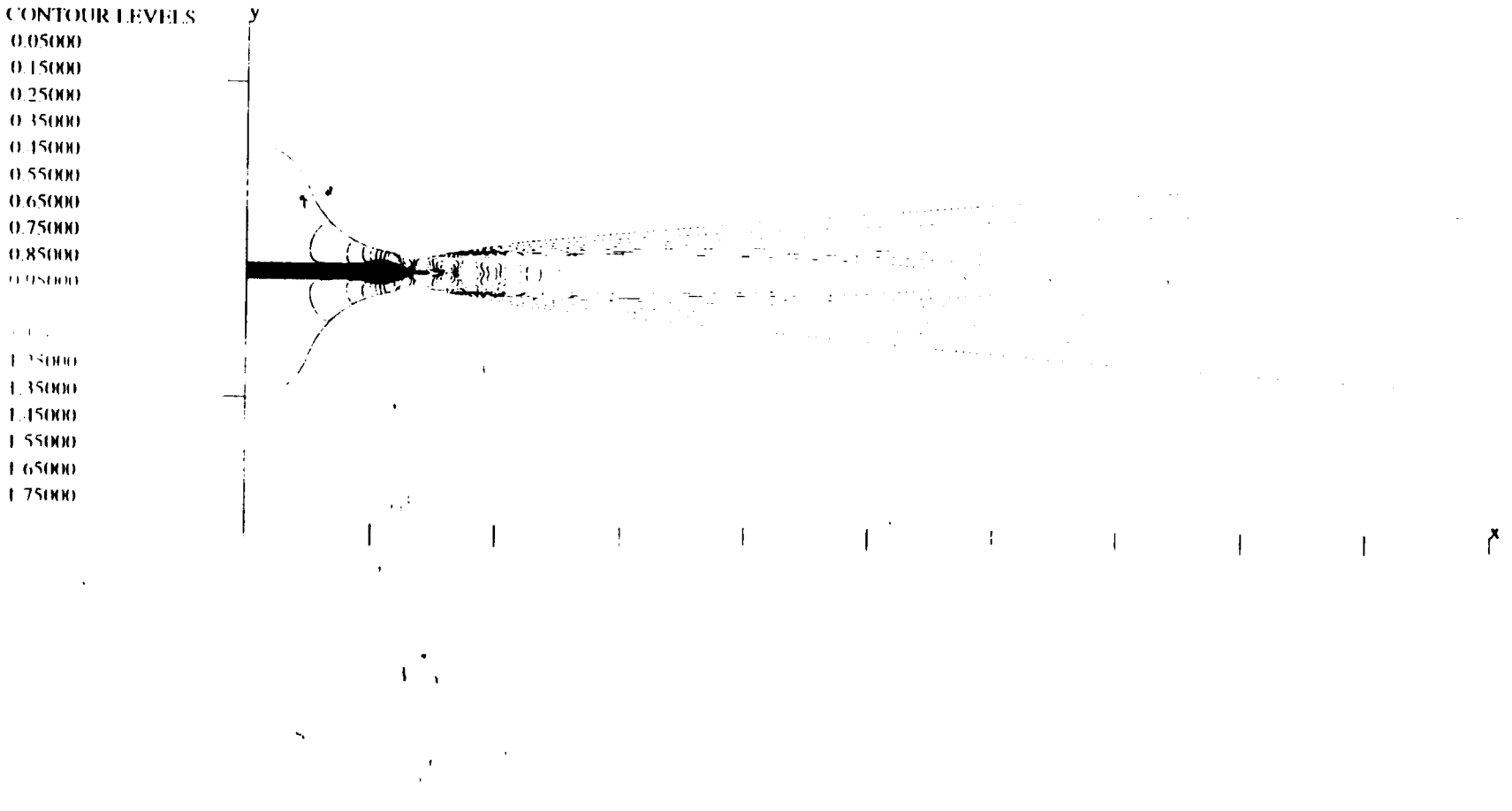

Fig. 4 Contour plot of the flow field Mach number for the plug-nozzle (ξ = 3.62).

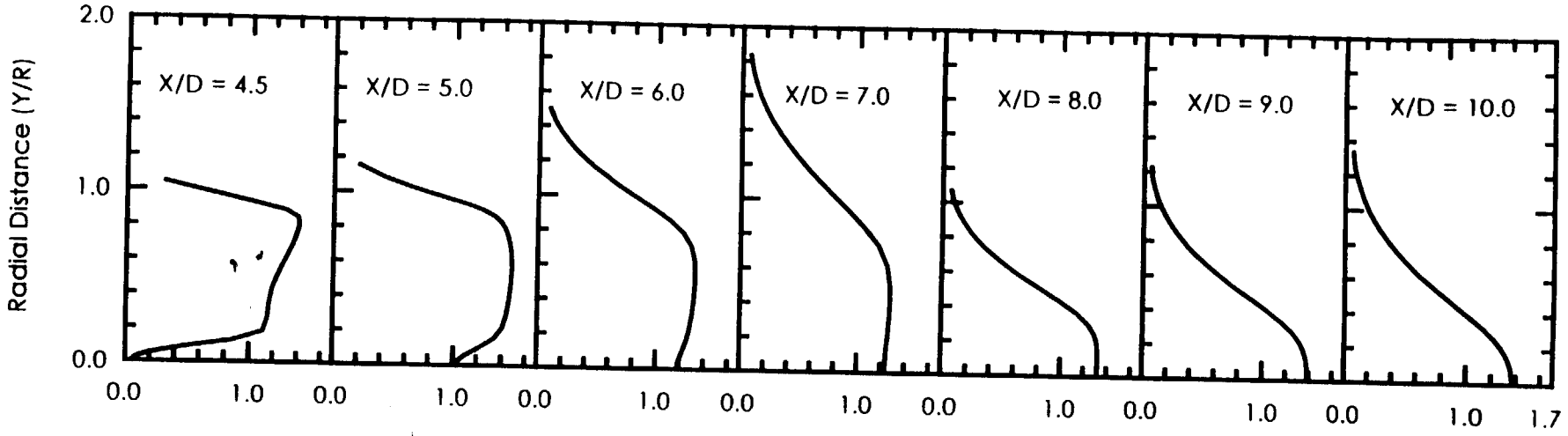

(a) Radial Mach number profiles at various axial locations.

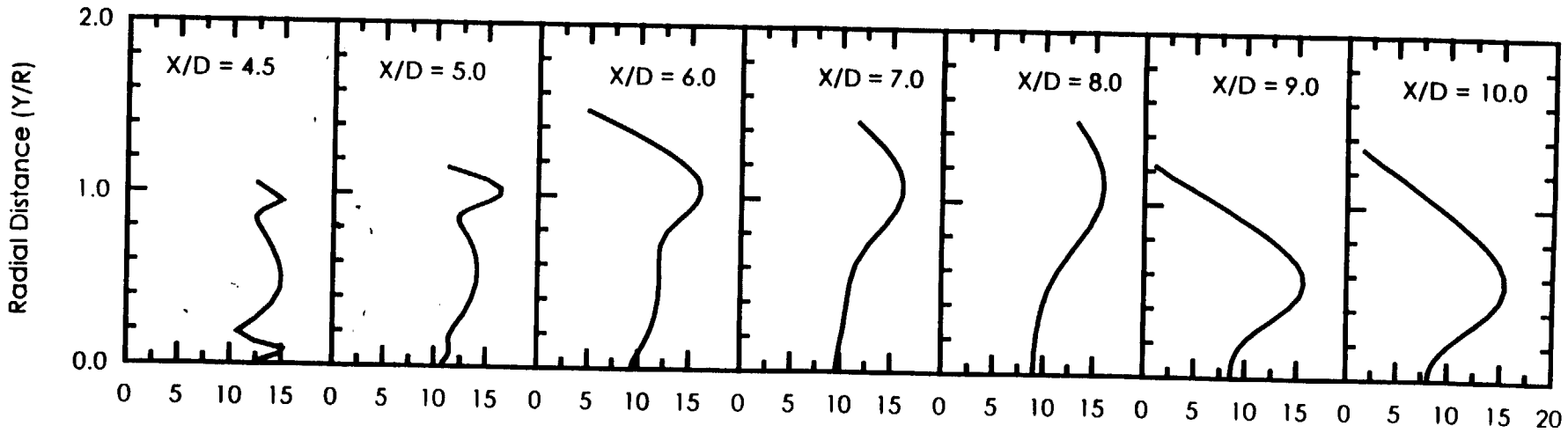

(b) Turbulence intensity profiles at various axial locations.

Fig. 5 Radial distribuutions of the turbulence intensity and Mach number at some selected axial locations (PR = 3.62).

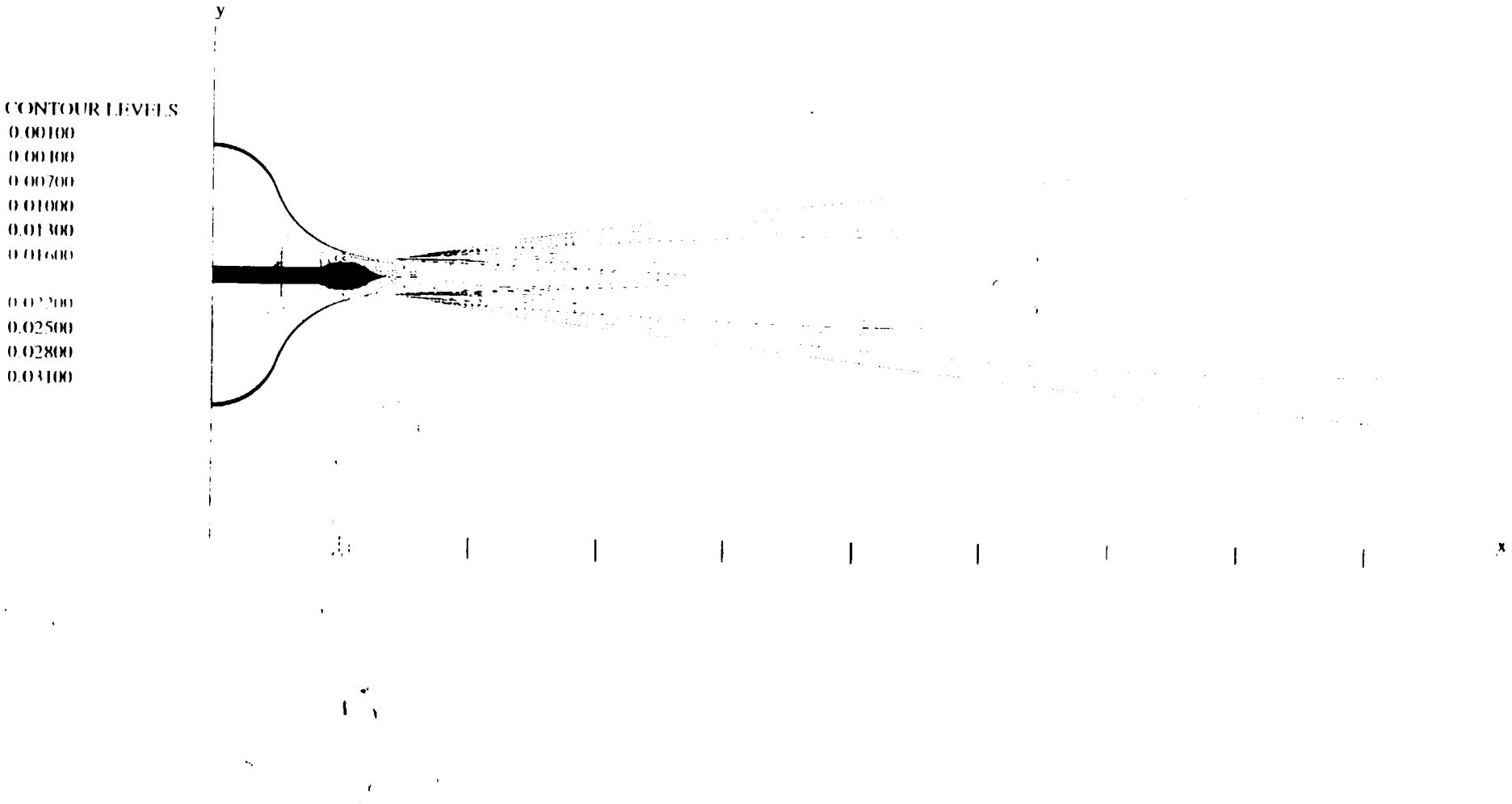

Fig. 6 Contour plot of the turbulence intensity for the plug-nozzle ($\xi = 2.5$).

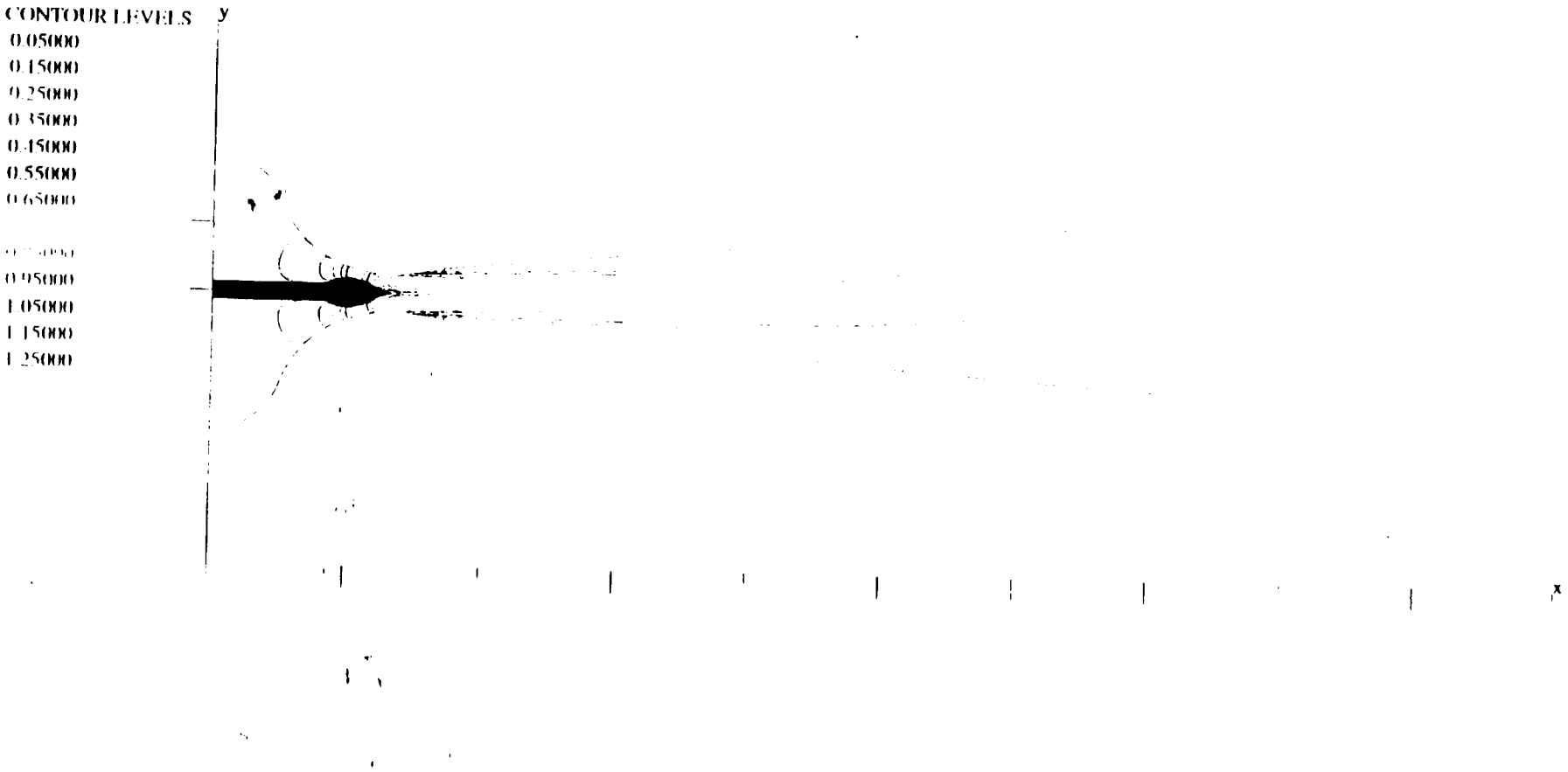

Fig. 7 Contour plot of the flow field Mach number for the plug-nozzle ($\xi = 2.5$).

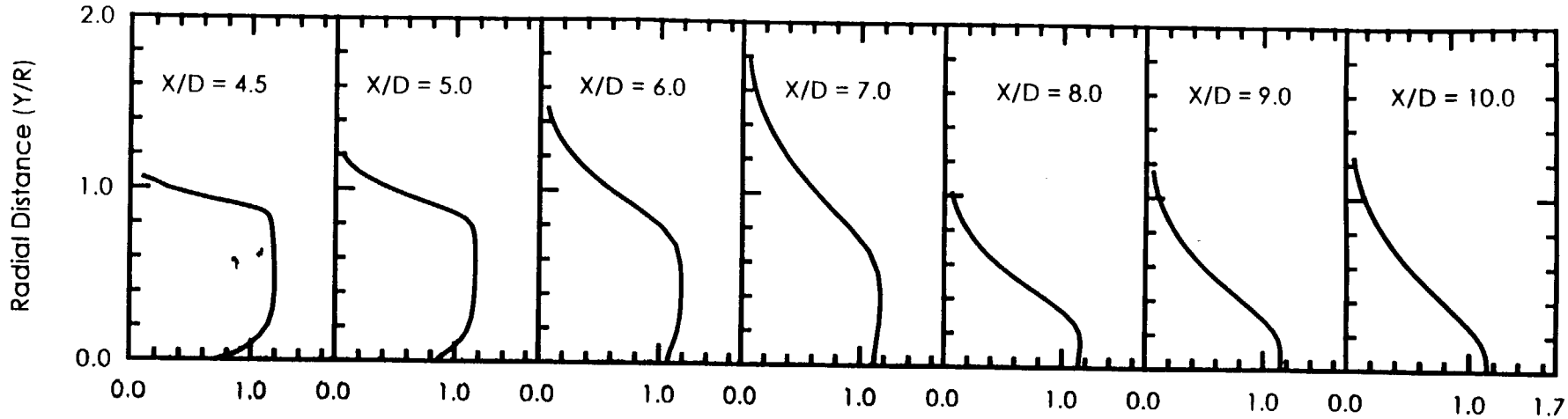

(a) Radial Mach number profiles at various axial locations.

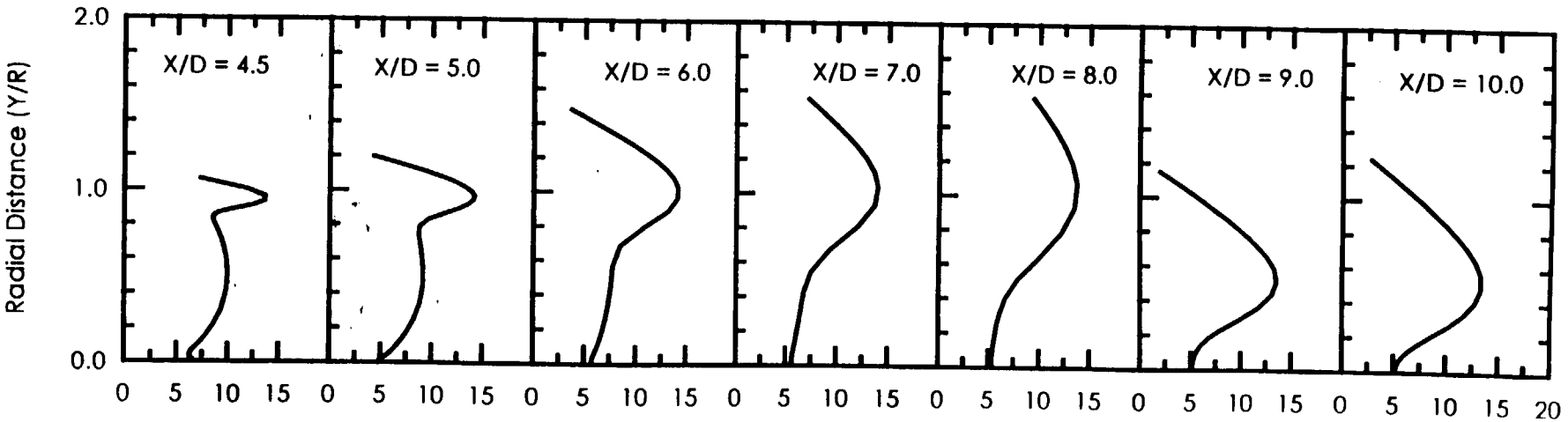

(b) Turbulence intensity profiles at various axial locations.

Fig. 8 Radial distribuutions of the turbulence intensity and Mach number at some selected axial locations (PR = 2.5).

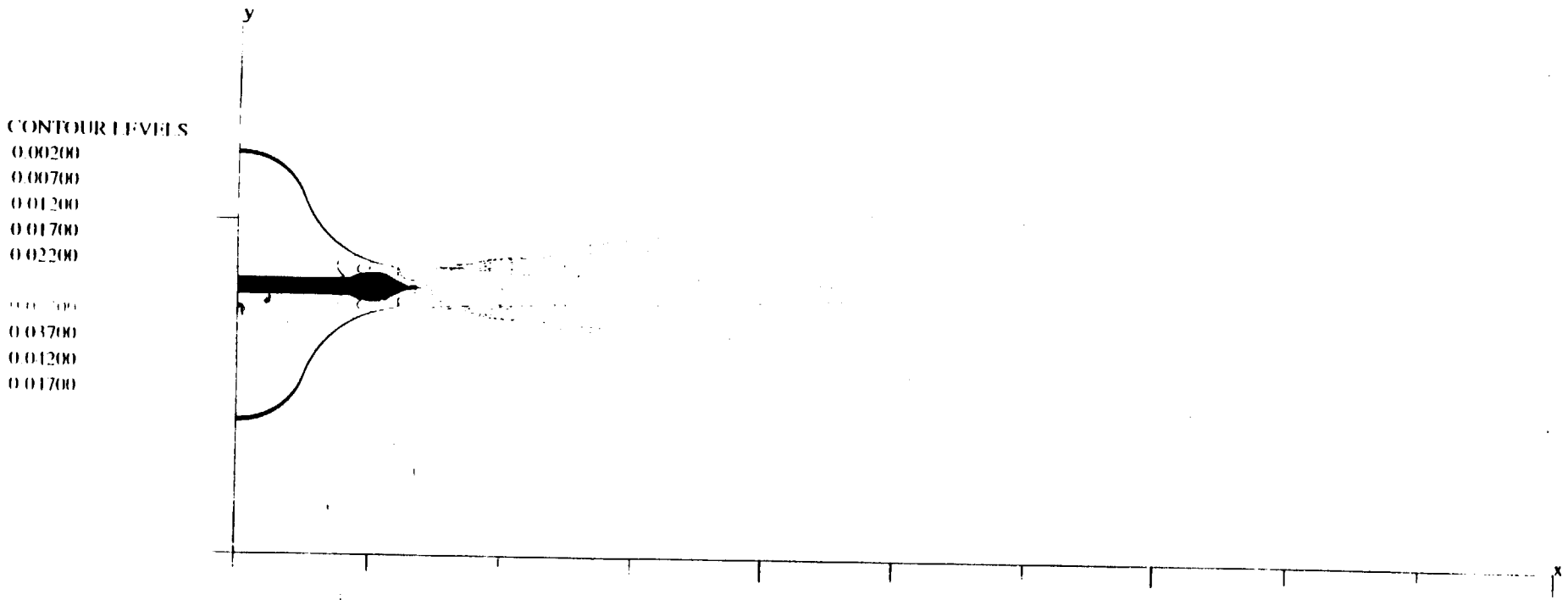

Fig. 9 Contour plot of the turbulence intensity for the plug-nozzle (ξ =4.5).

Fig. 10 Contour plot of the flow field Mach number for the plug-nozzle ($\xi = 4.5$).

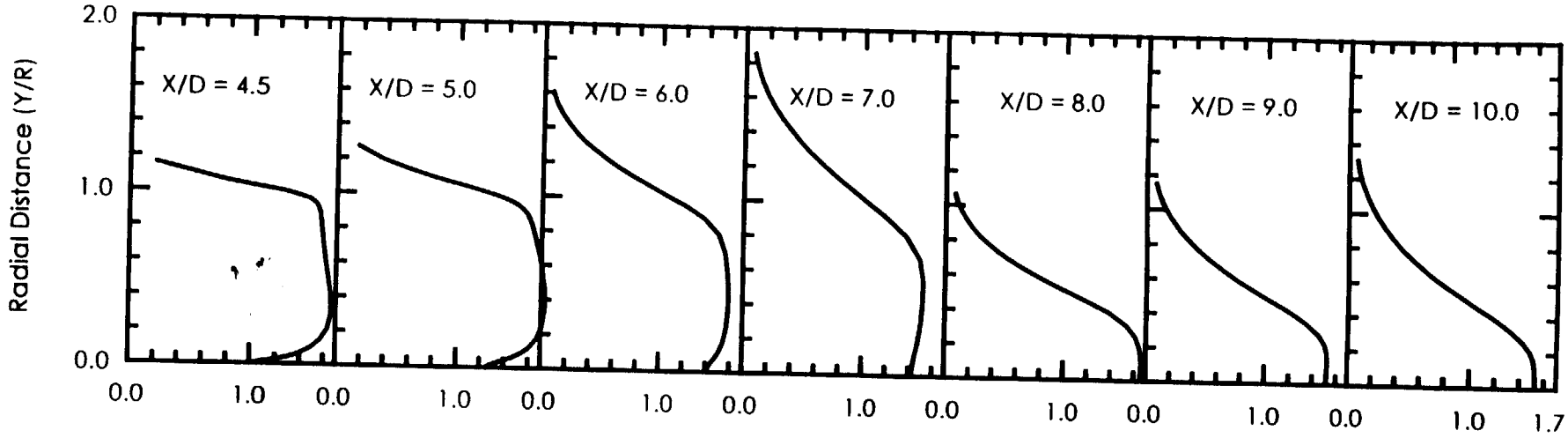

(a) Radial Mach number profiles at various axial locations.

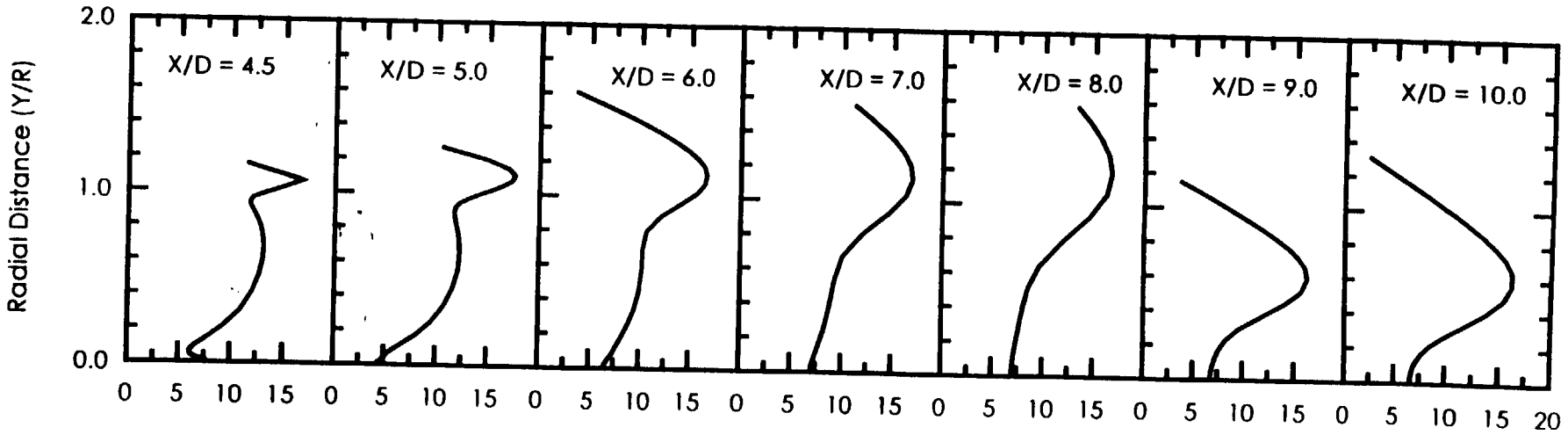

(b) Turbulence intensity profiles at various axial locations.

Fig. 11 Radial distribuutions of the turbulence intensity and Mach number at some selected axial locations (PR = 4.5).

$\xi = 4.5$

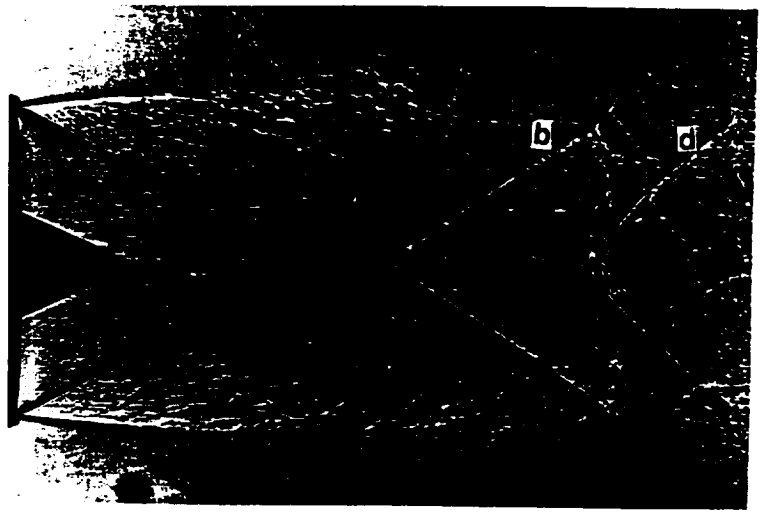

$\xi = 2.5$

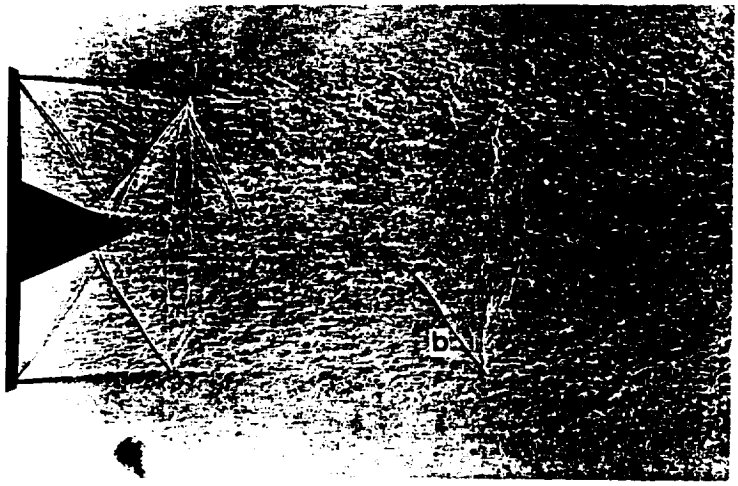

$\xi = 3.62$

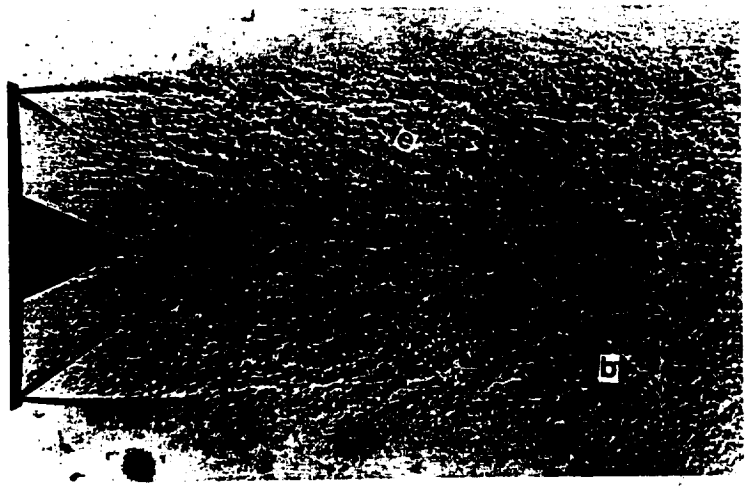

Fig. 12 Some shadowgraphs of the short conical plug-nozzle jet flows.

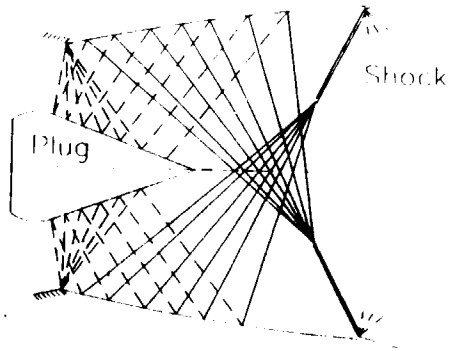

Jet Axis

One Family Of Repetitive Shocks

$M_j < M_d$

(a) Overexpanded conical plug nozzle jet

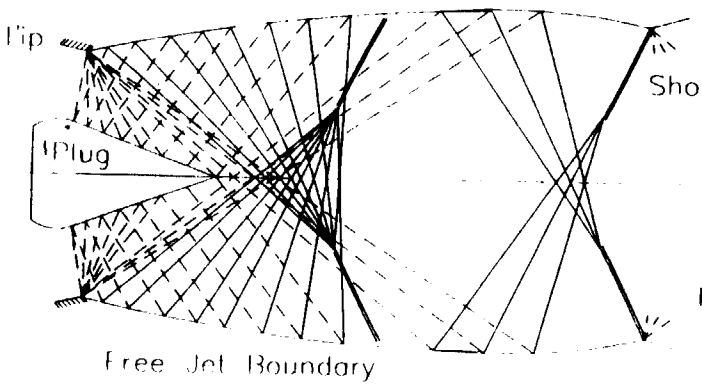

Jet Axis

Two Families Of Repetitive Shocks

$M_j > M_d$

(b) Underexpanded conical plug nozzle jet

Fig. 1.3 Shock formations in over- and underexpanded conical plug nozzle jets

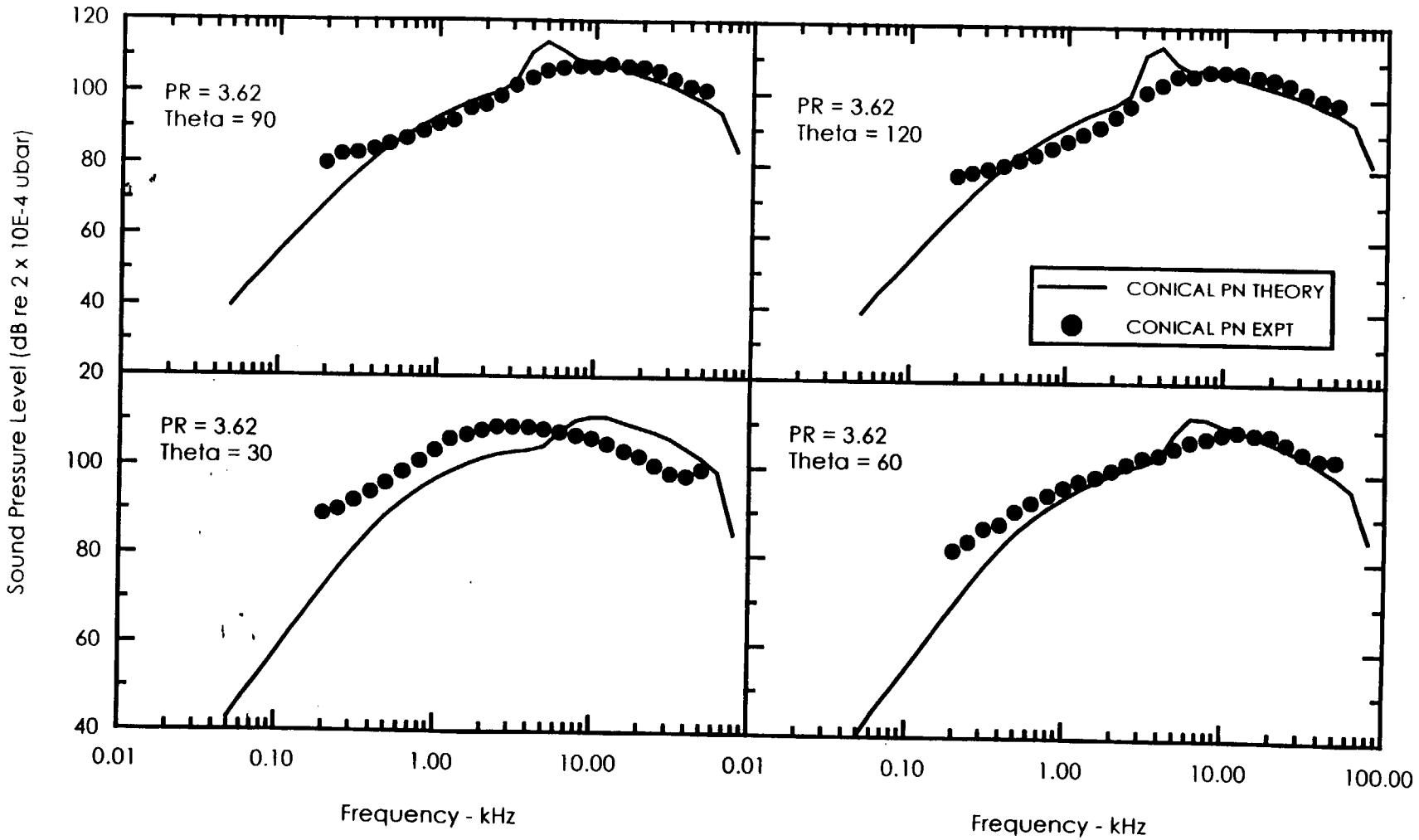

Fig. 14 Comparisons of the 1/3-octave SPL spectra for the conical PN jet flows at four typical angles theta (prediction vs measurements [14]; design pressure ratio = 3.62).

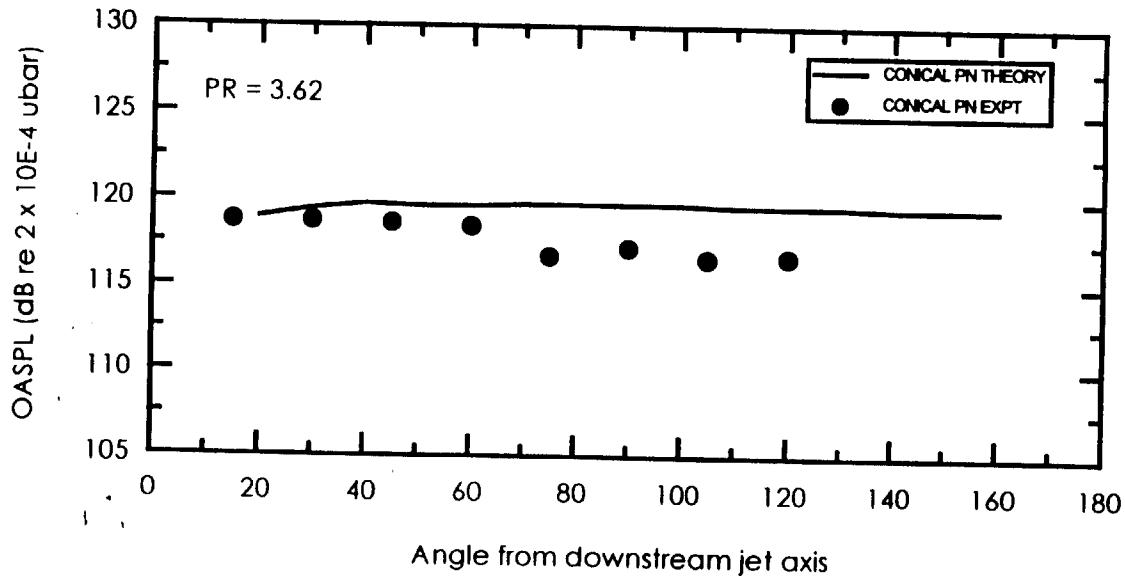

Fig. 15 Comparisons of the overall sound pressure level directivity for the conical PN theory and measurements [14] at design pressure ratio = 3.62.

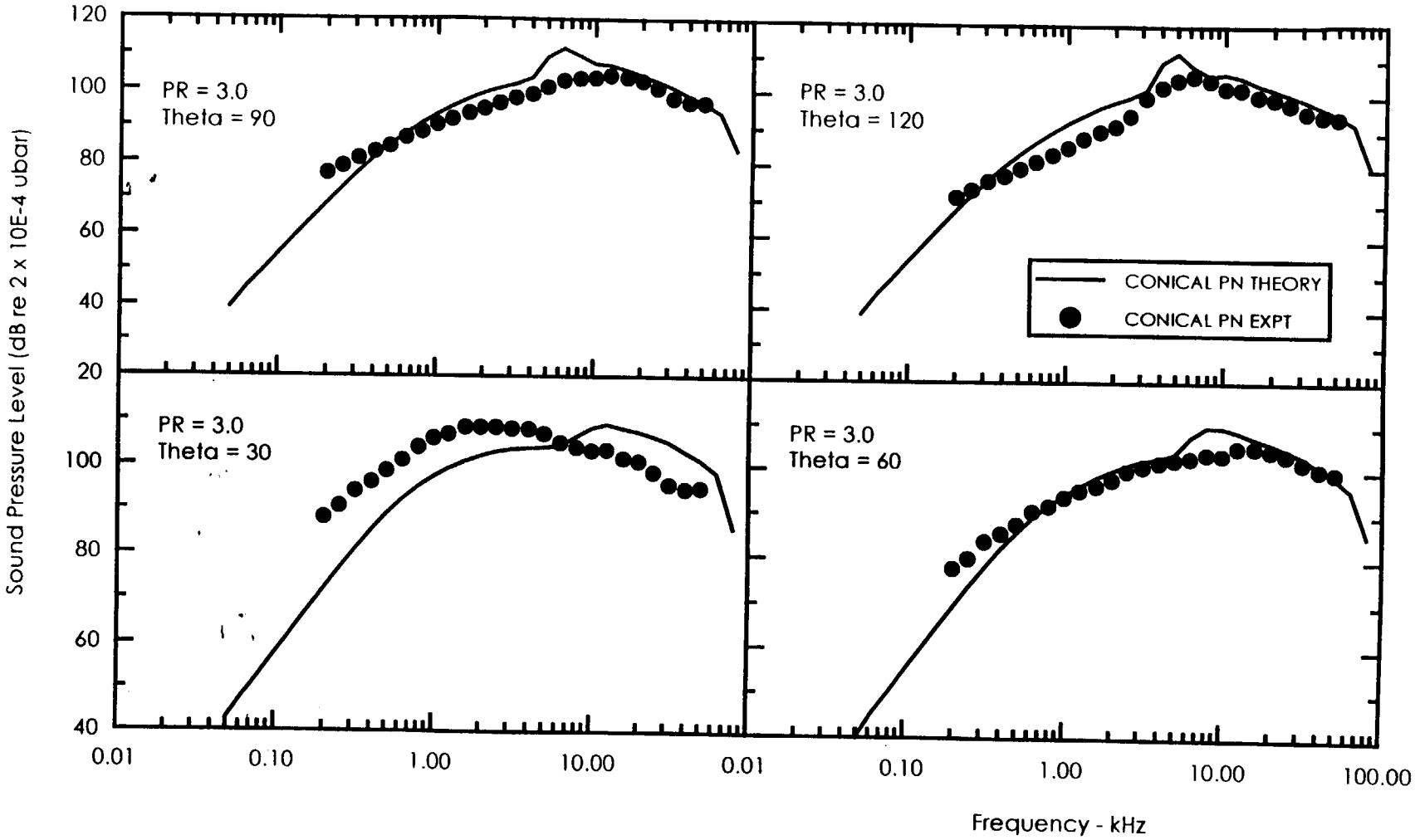

Fig. 16 Comparisons of the 1/3-octave SPL for the conical PN jet flows at four typical angles theta (prediction vs measurements [14]; pressure ratio = 3.0).

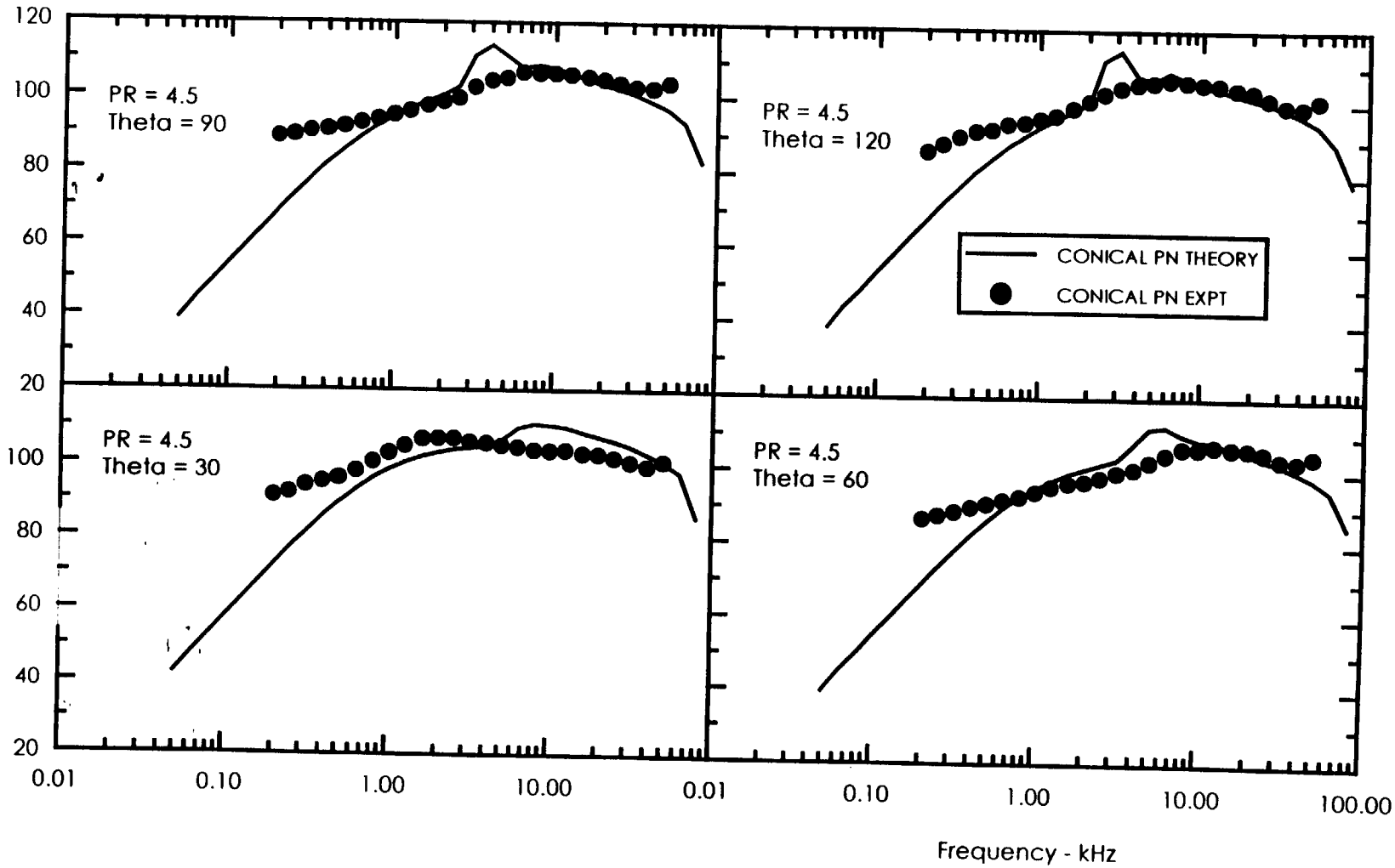

Fig. 17 Comparisons of the 1/3-octave SPL spectra for the conical PN jet flows at four typical angles theta (prediction vs measurements [14]; pressure ratio = 4.5).

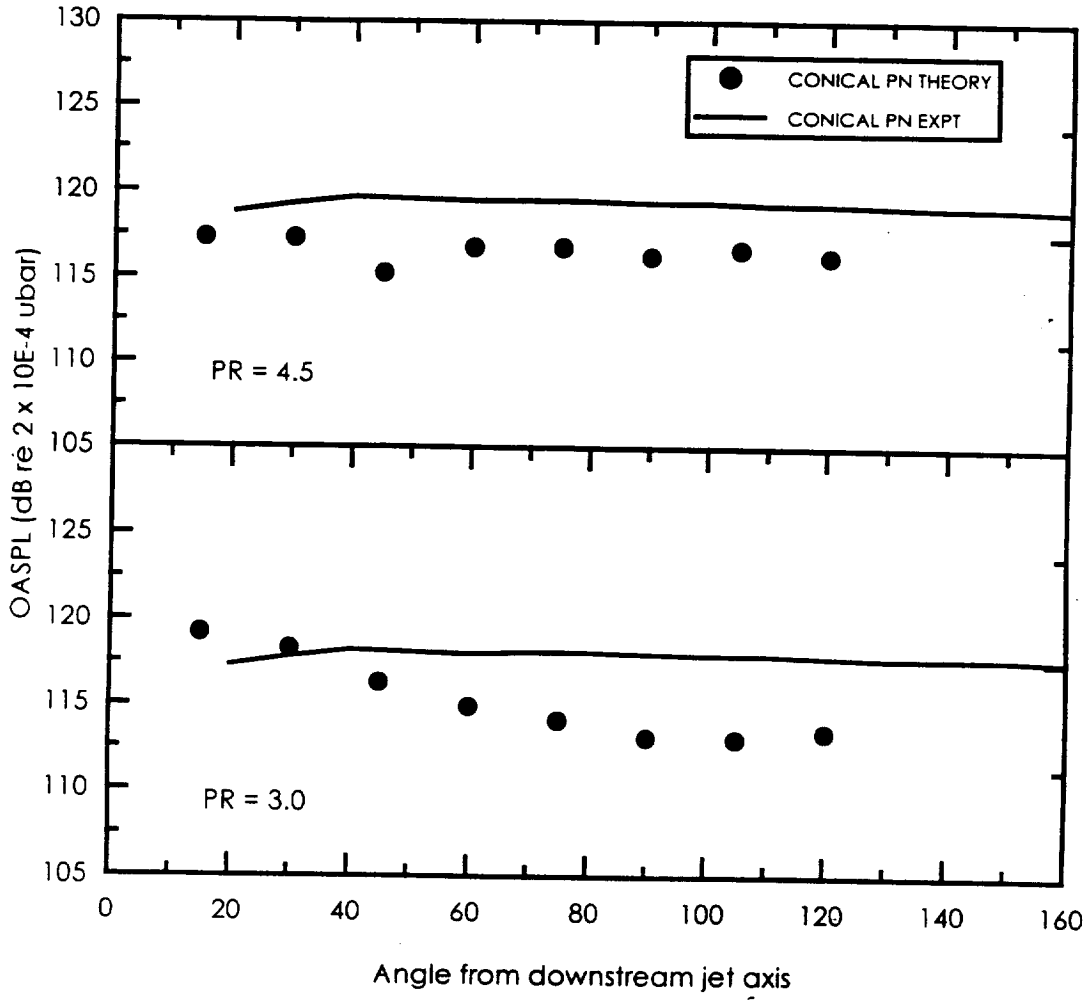

Figure 18 Comparisons of the overall sound pressure level directivity of the conical PN jet flows for off-design pressure ratios (prediction vs measurements [14]).

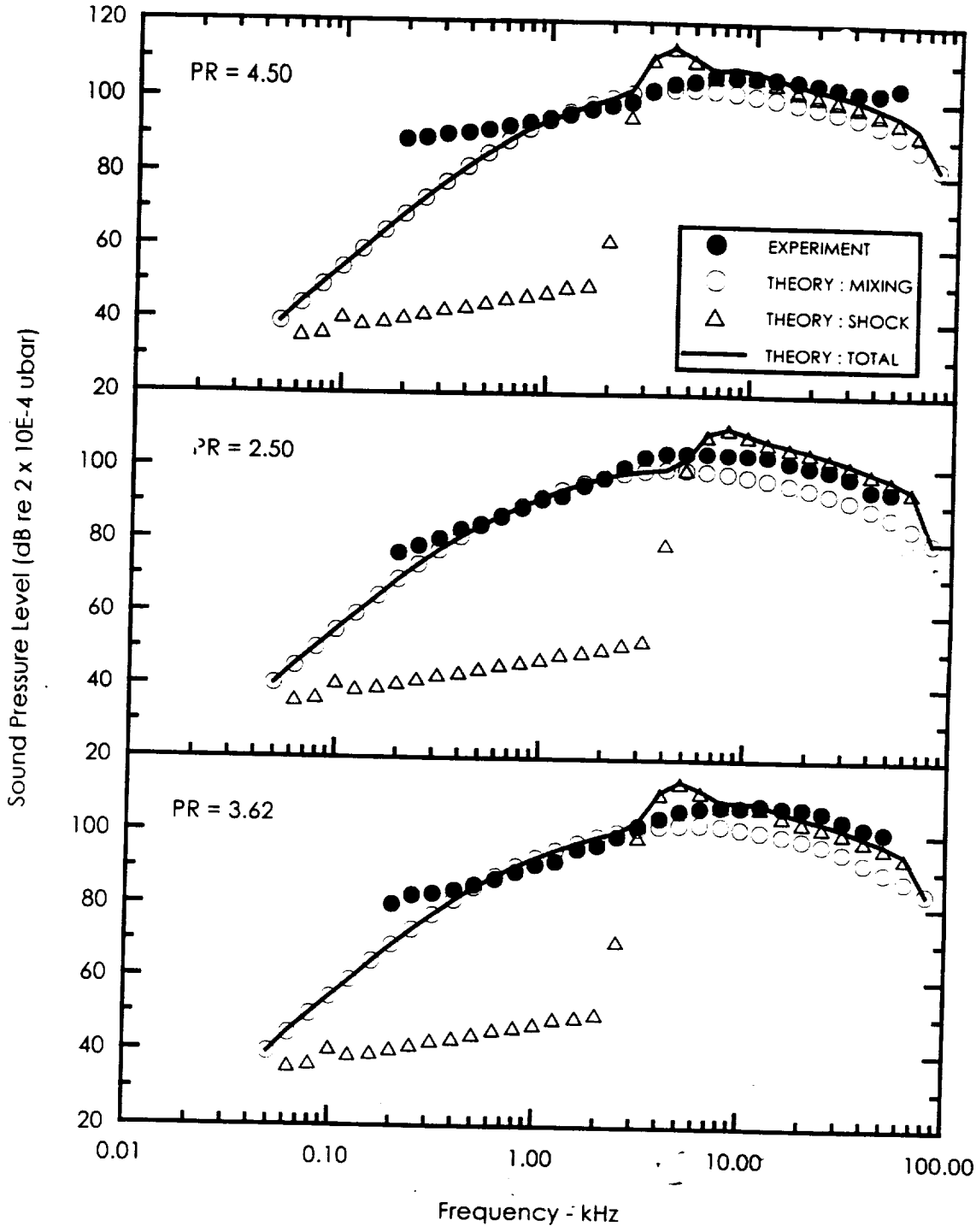

Figure 19 : Comparions of the predicted mixing and shock noise components with the measurements for conical PN at theta = 90 deg.

APPENDIX A

The profile of the short conical plug-nozzle, subject of the present computational study, is presented in Fig. A. The set of co-ordinates of the short conical plug-nozzle annulus is provided in Table A; the annulus is contained within the outer plug/stem surface and the inner converging nozzle surface. The X-axis is along the downstream jet axis and reference X = 0 is located at the start of the converging section on the jet axis; the radial R-axis is perpendicular to and measured from the jet axis.

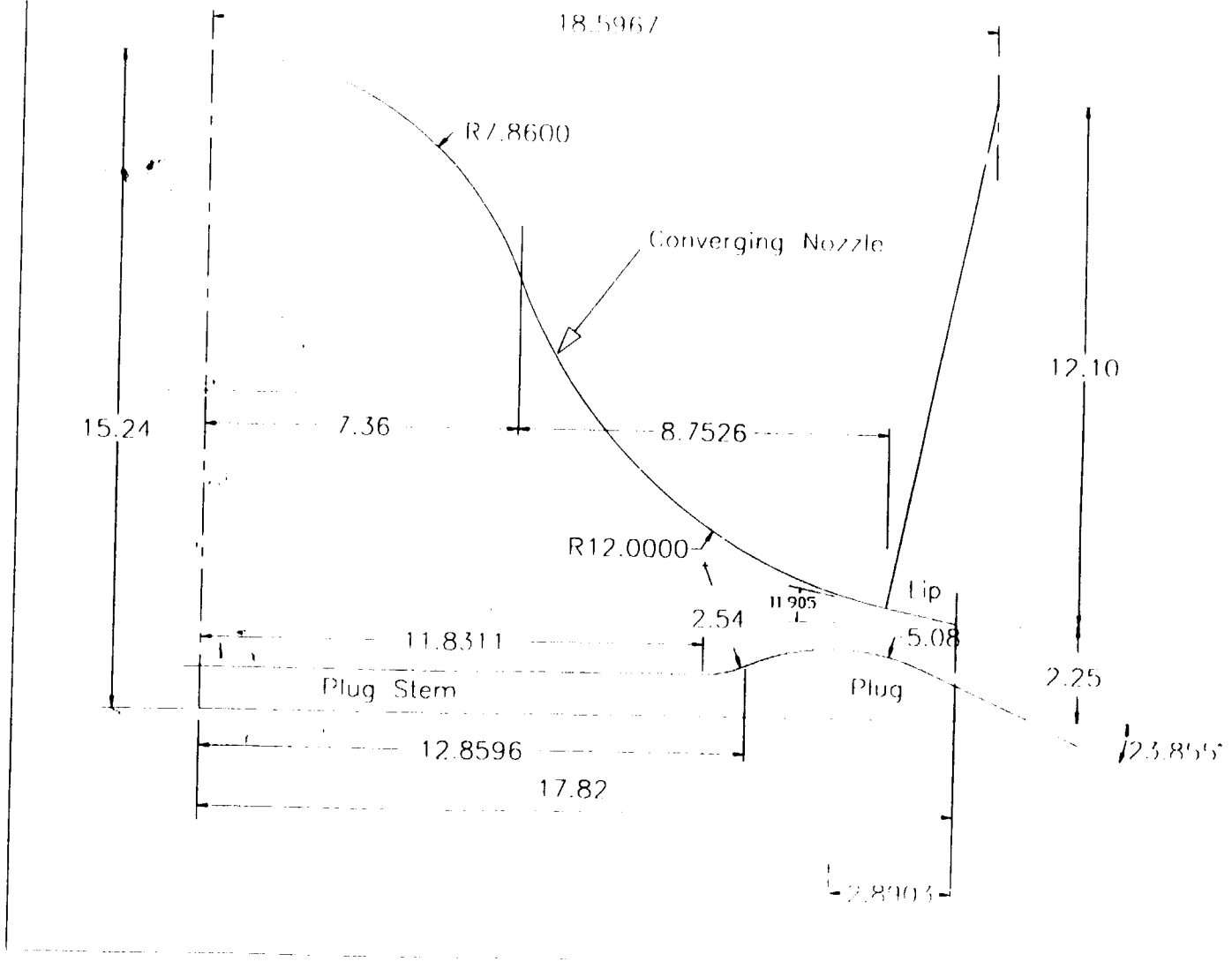

Fig. A Profile of the test conical plug nozzle

X- PLUG	R- PLUG	X - NOZ	R - NOZ	X- PLUG	R- PLUG	X - NOZ	R - NOZ
0.0000	0.9550	0.0000	15.2400	10.2618	0.9550	9.0882	7.0300
0.2012	0.9550	0.1782	15.2380	10.4630	0.9550	9.2664	6.8042
0.4024	0.9550	0.3564	15.2319	10.6642	0.9550	9.4446	6.5890
0.6036	0.9550	0.5346	15.2218	10.8654	0.9550	9.6228	6.3836
0.8048	0.9550	0.7128	15.2076	11.0667	0.9550	9.8010	6.1873
1.0061	0.9550	0.8910	15.1893	11.2679	0.9550	9.9792	5.9994
1.2073	0.9550	1.0692	15.1669	11.4691	0.9550	10.1574	5.8193
1.4085	0.9550	1.2474	15.1404	11.6703	0.9550	10.3356	5.6466
1.6097	0.9550	1.4256	15.1096	11.8715	0.9550	10.5138	5.4809
1.8109	0.9550	1.6038	15.0746	12.0727	0.9550	10.6920	5.3217
2.0121	0.9550	1.7820	15.0353	12.2739	0.9550	10.8702	5.1687
2.2133	0.9550	1.9602	14.9916	12.4751	0.9550	11.0484	5.0216
2.4145	0.9550	2.1384	14.9435	12.6764	0.9550	11.2266	4.8802
2.6158	0.9550	2.3166	14.8909	12.8776	0.9550	11.4048	4.7442
2.8170	0.9550	2.4948	14.8336	13.0788	0.9550	11.5830	4.6133
3.0182	0.9550	2.6730	14.7715	13.2800	0.9550	11.7612	4.4874
3.2194	0.9550	2.8512	14.7046	13.4812	0.9610	11.9394	4.3662
3.4206	0.9550	3.0294	14.6327	13.6824	0.9829	12.1176	4.2496
3.6218	0.9550	3.2076	14.5557	13.8836	1.0213	12.2958	4.1375
3.8230	0.9550	3.3858	14.4734	14.0848	1.0771	12.4740	4.0297
4.0242	0.9550	3.5640	14.3855	14.2861	1.1461	12.6522	3.9260
4.2255	0.9550	3.7422	14.2920	14.4873	1.2080	12.8304	3.8246
4.4267	0.9550	3.9204	14.1925	14.6885	1.2609	13.0086	3.7307
4.6279	0.9550	4.0986	14.0868	14.8897	1.3052	13.1868	3.6388
4.8291	0.9550	4.2768	13.9746	15.0909	1.3410	13.3650	3.5506
5.0303	0.9550	4.4550	13.8555	15.2921	1.3686	13.5432	3.4661
5.2315	0.9550	4.6332	13.7293	15.4933	1.3880	13.7214	3.3851
5.4327	0.9550	4.8114	13.5953	15.6945	1.3994	13.8996	3.3076
5.6339	0.9550	4.9896	13.4532	15.8957	1.4028	14.0778	3.2335
5.8351	0.9550	5.1678	13.3023	16.0970	1.3982	14.2560	3.1627
6.0364	0.9550	5.3460	13.1419	16.2982	1.3856	14.4342	3.0952
6.2376	0.9550	5.5242	12.9713	16.4994	1.3650	14.6124	3.0309
6.4388	0.9550	5.7024	12.7895	16.7006	1.3362	14.7906	2.9697
6.6400	0.9550	5.8806	12.5952	16.9018	1.2991	14.9688	2.9116
6.8412	0.9550	6.0588	12.3871	17.1030	1.2535	15.1470	2.8566
7.0424	0.9550	6.2370	12.1633	17.3042	1.1992	15.3252	2.8046
7.2436	0.9550	6.4152	11.9215	17.5054	1.1359	15.5034	2.7556
7.4448	0.9550	6.5934	11.6586	17.7067	1.0633	15.6816	2.7095
7.6461	0.9550	6.7716	11.3706	17.9079	0.9808	15.8598	2.6664
7.8473	0.9550	6.9498	11.0515	18.1091	0.8917	16.0380	2.6260
8.0485	0.9550	7.1280	10.6923	18.3103	0.8025	16.2162	2.5882
8.2497	0.9550	7.3062	10.2781	18.5115	0.7134	16.3944	2.5506
8.4509	0.9550	7.4844	9.8212	18.7127	0.6242	16.5726	2.5130
8.6521	0.9550	7.6626	9.4064	18.9139	0.5350	16.7507	2.4755
8.8533	0.9550	7.8408	9.0299	19.1151	0.4458	16.9289	2.4379
9.0545	0.9550	8.0190	8.6838	19.3164	0.3567	17.1071	2.4003
9.2558	0.9550	8.1972	8.3630	19.5176	0.2675	17.2853	2.3628
9.4570	0.9550	8.3754	8.0636	19.7188	0.1783	17.4635	2.3252
9.6582	0.9550	8.5536	7.7827	19.9200	0.0892	17.6417	2.2876
9.8594	0.9550	8.7318	7.5179	20.1212	0.0000		
10.0606	0.9550	8.9100	7.2675				

Table A. Coordinates of the Conical Plug and Converging Nozzle Surfaces

APPENDIX B

A complete set of the numerical noise data obtained as a result of the computational noise study of the short conical plug-nozzle of design Mach number 1.49 is presented in tabular forms in this Appendix. The tables consist of the mixing noise levels, the shock-associated noise levels, and the total noise levels at pressure ratios, ξ = 2.0, 2.5, 3.0, 3.62 (design), 4.0, 4.5, 5.0. The angles listed in the tables are referred to from the inlet, and not from the downstream jet axis. The numerical gasdynamics data for the contoured plug-nozzle jet flows obtained as outputs of the NPARC code are not included herein but these are also available.

ANGLE	20	30	40	50	60	70	80	90	100	110	120	130	140	150	160	PWL
FREQ																
50	38.7	38.8	38.9	39.0	39.1	39.3	39.5	39.8	40.1	40.6	41.0	41.5	42.1	42.9	44.3	68.3
63	43.7	43.7	43.8	43.9	44.0	44.2	44.4	44.7	45.1	45.5	46.0	46.5	47.0	47.8	49.2	73.3
80	48.7	48.7	48.8	48.9	49.1	49.2	49.5	49.8	50.1	50.5	51.0	51.5	52.1	52.9	54.3	78.3
100	53.3	53.3	53.4	53.5	53.7	53.9	54.1	54.4	54.8	55.2	55.7	56.2	56.8	57.6	58.9	83.0
125	57.8	57.8	57.9	58.0	58.2	58.4	58.7	59.0	59.3	59.8	60.3	60.8	61.4	62.2	63.5	87.5
160	62.5	62.6	62.7	62.8	63.0	63.2	63.5	63.8	64.2	64.7	65.2	65.7	66.3	67.1	68.4	92.4
200	66.6	66.6	66.8	66.9	67.1	67.3	67.6	68.0	68.4	68.9	69.4	69.9	70.5	71.4	72.7	96.6
250	70.3	70.4	70.5	70.7	70.9	71.2	71.5	71.9	72.3	72.8	73.3	73.9	74.5	75.4	76.6	100.5
315	73.9	74.0	74.1	74.3	74.5	74.8	75.1	75.5	76.0	76.5	77.1	77.7	78.3	79.2	80.4	104.2
400	77.3	77.4	77.5	77.7	77.9	78.2	78.5	78.9	79.4	79.9	80.5	81.1	81.7	82.7	83.8	107.6
500	80.2	80.3	80.4	80.6	80.8	81.1	81.4	81.8	82.2	82.7	83.3	83.9	84.5	85.6	86.6	110.4
630	83.1	83.2	83.3	83.4	83.6	83.9	84.2	84.5	84.9	85.4	85.9	86.4	87.1	88.1	89.1	113.1
800	85.8	85.9	86.0	86.2	86.3	86.6	86.8	87.1	87.5	87.9	88.4	88.9	89.5	90.6	91.3	115.7
1000	88.2	88.2	88.3	88.5	88.7	88.9	89.1	89.4	89.7	90.1	90.5	91.0	91.6	92.7	93.2	117.9
1250	90.2	90.2	90.4	90.5	90.7	90.9	91.2	91.5	91.8	92.1	92.5	92.9	93.5	94.6	94.9	119.8
1600	91.9	92.0	92.2	92.4	92.6	92.8	93.1	93.4	93.7	94.0	94.4	94.7	95.5	96.4	96.5	121.7
2000	93.1	93.2	93.4	93.6	93.9	94.2	94.5	94.8	95.1	95.5	95.8	96.2	97.0	97.8	97.6	123.1
2500	93.8	94.0	94.2	94.5	94.8	95.1	95.5	95.8	96.2	96.6	96.9	97.3	98.1	98.8	98.3	124.1
3150	94.1	94.3	94.6	94.9	95.2	95.6	96.1	96.5	96.9	97.3	97.7	98.1	99.0	99.4	98.7	124.8
4000	94.1	94.3	94.6	94.9	95.3	95.8	96.2	96.7	97.2	97.6	98.0	98.5	99.5	99.7	98.8	125.0
5000	93.7	94.0	94.3	94.6	95.1	95.6	96.1	96.6	97.1	97.6	98.1	98.5	99.6	99.6	98.6	125.0
6300	93.2	93.4	93.7	94.1	94.6	95.1	95.7	96.2	96.8	97.3	97.8	98.3	99.3	99.3	98.2	124.6
8000	92.4	92.7	93.0	93.4	93.9	94.4	95.0	95.6	96.2	96.7	97.3	97.8	98.8	98.7	97.7	124.1
10000	91.6	91.8	92.1	92.6	93.1	93.6	94.2	94.8	95.4	96.0	96.6	97.1	98.1	98.0	96.9	123.4
12500	90.5	90.8	91.1	91.6	92.1	92.7	93.3	93.9	94.6	95.2	95.7	96.3	97.3	97.1	96.0	122.7
16000	89.2	89.4	89.8	90.3	90.8	91.4	92.0	92.7	93.4	94.0	94.6	95.2	96.2	96.0	94.8	121.7
20000	87.7	88.0	88.4	88.8	89.4	90.0	90.7	91.4	92.1	92.7	93.3	94.0	95.0	94.8	93.6	120.7
25000	86.1	86.3	86.7	87.2	87.8	88.4	89.1	89.8	90.6	91.3	91.9	92.5	93.6	93.4	92.2	119.5
31500	84.2	84.5	84.8	85.3	85.9	86.5	87.2	88.0	88.7	89.4	90.1	90.8	91.8	91.6	90.5	118.3
40000	82.0	82.3	82.7	83.1	83.7	84.3	85.0	85.7	86.5	87.2	87.9	88.6	89.7	89.5	88.4	116.9
50000	79.8	80.0	80.4	80.8	81.4	82.0	82.7	83.4	84.1	84.8	85.5	86.1	87.3	87.1	86.0	115.6
63000	76.9	77.2	77.5	78.0	78.5	79.2	79.8	80.5	81.2	81.9	82.6	83.2	84.3	84.2	83.1	114.2
80000	73.1	73.4	73.8	74.3	74.8	75.5	76.2	76.9	77.6	78.3	78.9	79.5	80.7	80.5	79.3	112.9
OVERALL	103.9	104.1	104.4	104.7	105.1	105.6	106.0	106.5	107.0	107.5	108.0	108.5	109.4	109.6	108.9	135.2
PNL	116.2	116.3	116.6	116.9	117.3	117.7	118.1	118.6	119.0	119.5	119.9	120.3	121.3	121.6	121.0	
PNLT	116.2	116.3	116.6	116.9	117.3	117.7	118.1	118.6	119.0	119.5	119.9	120.3	121.3	121.6	121.0	

Table B-1. Computational Acoustic Data for Pressure Ratio 2.0 : Mixing Noise Component

ANGLE	20	30	40	50	60	70	80	90	100	110	120	130	140	150	160	PWL
FREQ																
50	0.0	0.0	0.0	0.0	0.0	0.0	0.0	0.0	0.0	0.0	0.0	0.0	0.0	0.0	0.0	27.9
63	35.8	35.8	35.8	35.8	35.8	35.8	35.8	35.8	35.8	35.8	35.8	35.8	35.8	35.8	35.8	63.7
80	36.5	36.5	36.5	36.5	36.5	36.5	36.5	36.5	36.5	36.5	36.5	36.5	36.5	36.5	36.5	64.4
100	40.6	40.6	40.6	40.6	40.6	40.6	40.6	40.6	40.6	40.6	40.6	40.6	40.6	40.6	40.6	68.4
125	38.9	38.9	38.9	38.9	38.9	38.9	38.9	38.9	38.9	38.9	38.9	38.9	38.9	38.9	38.9	66.8
160	39.5	39.5	39.5	39.5	39.5	39.5	39.5	39.5	39.5	39.5	39.5	39.5	39.5	39.5	39.5	67.4
200	40.5	40.5	40.5	40.5	40.5	40.5	40.5	40.5	40.5	40.5	40.5	40.5	40.5	40.5	40.5	68.4
250	41.6	41.6	41.6	41.6	41.6	41.6	41.6	41.6	41.6	41.6	41.6	41.6	41.6	41.6	41.6	69.5
315	42.8	42.8	42.8	42.8	42.8	42.8	42.8	42.8	42.8	42.8	42.8	42.8	42.8	42.8	42.8	70.7
400	43.5	43.5	43.5	43.5	43.5	43.5	43.5	43.5	43.5	43.5	43.5	43.5	43.5	43.5	43.5	71.4
500	44.6	44.6	44.6	44.6	44.6	44.6	44.6	44.6	44.6	44.6	44.6	44.6	44.6	44.6	44.6	72.5
630	45.8	45.8	45.8	45.8	45.8	45.8	45.8	45.8	45.8	45.8	45.8	45.8	45.8	45.8	45.8	73.7
800	46.5	46.5	46.5	46.5	46.5	46.5	46.5	46.5	46.5	46.5	46.5	46.5	46.5	46.5	46.5	74.4
1000	47.4	47.4	47.4	47.4	47.4	47.4	47.4	47.4	47.4	47.4	47.4	47.4	47.4	47.4	47.4	75.4
1250	48.9	48.9	48.9	48.9	48.9	48.9	48.9	48.9	48.9	48.9	48.9	48.9	48.9	48.9	48.9	76.8
1600	49.5	49.5	49.5	49.5	49.5	49.5	49.5	49.5	49.5	49.5	49.5	49.5	49.5	49.5	49.5	77.4
2000	50.4	50.4	50.4	50.4	50.4	50.4	50.4	50.4	50.4	50.4	50.4	50.4	50.4	50.4	50.4	78.4
2500	51.6	51.6	51.6	51.6	51.6	51.6	51.6	51.6	51.6	51.6	51.6	51.6	51.6	51.6	51.6	79.5
3150	52.7	52.7	52.7	52.7	52.7	52.7	52.7	52.7	52.7	52.7	52.7	52.7	52.7	52.7	52.7	80.7
4000	53.4	53.4	53.4	53.4	53.4	53.4	53.4	53.4	53.4	53.4	53.4	53.4	53.4	53.4	53.4	81.4
5000	54.5	54.5	54.5	54.5	54.5	54.5	54.5	54.5	54.5	54.5	54.5	54.5	54.5	54.5	54.5	82.5
6300	62.0	59.8	57.4	55.9	55.7	55.7	55.7	55.7	55.7	55.7	55.7	55.7	55.7	55.7	55.7	84.5
8000	85.3	83.8	81.5	78.5	74.6	69.9	64.5	59.3	56.5	56.3	56.3	56.3	56.3	56.3	56.3	103.9
10000	94.4	93.8	92.9	91.4	89.4	86.7	83.4	79.3	74.7	69.6	64.5	60.2	57.8	57.2	57.2	115.5
12500	95.0	95.3	95.4	95.4	95.0	94.1	92.6	90.5	87.9	84.8	81.4	77.9	74.6	71.7	69.4	120.1
16000	89.8	90.4	91.3	92.3	93.2	93.8	93.9	93.4	92.4	90.8	88.8	86.6	84.3	82.3	80.6	120.0
20000	89.3	89.2	89.2	89.4	90.0	90.9	91.9	92.6	92.8	92.4	91.6	90.4	89.0	87.7	86.6	119.7
25000	88.6	88.7	88.9	89.0	89.2	89.4	89.9	90.6	91.3	91.7	91.7	91.3	90.7	90.0	89.3	119.4
31500	86.4	86.6	87.0	87.4	87.8	88.2	88.6	89.1	89.6	90.2	90.5	90.6	90.5	90.2	89.9	118.8
40000	83.7	83.9	84.1	84.5	85.0	85.6	86.3	86.9	87.5	88.1	88.5	88.8	88.9	88.9	88.7	117.5
50000	81.7	81.8	82.0	82.3	82.7	83.2	83.9	84.6	85.3	86.1	86.7	87.0	87.3	87.4	87.2	116.6
63000	78.8	79.1	79.4	79.2	79.8	80.4	80.7	81.6	82.1	83.1	84.0	84.3	84.9	85.2	84.8	115.4
80000	0.0	0.0	0.0	0.0	0.0	0.0	0.0	0.0	0.0	0.0	0.0	0.0	0.0	0.0	0.0	27.9
OVERALL	99.9	99.8	99.8	99.7	99.6	99.5	99.3	99.1	98.8	98.5	98.1	97.5	97.0	96.5	96.0	128.0
PNL	100.2	99.6	98.6	97.2	95.4	93.0	90.2	87.1	83.9	80.9	78.3	76.9	76.8	76.7	76.7	
PNLT	100.9	100.7	99.7	98.0	95.4	93.0	91.9	89.8	86.8	83.0	79.5	76.9	76.8	76.7	76.7	

Table B-2. Computational Acoustic Data for Pressure Ratio 2.0 : Shock Noise Component

ANGLE	20	30	40	50	60	70	80	90	100	110	120	130	140	150	160	PWL
FREQ																
50	38.7	38.8	38.9	39.0	39.1	39.3	39.5	39.8	40.1	40.6	41.0	41.5	42.1	42.9	44.3	68.3
63	44.3	44.4	44.4	44.5	44.6	44.8	45.0	45.3	45.6	45.9	46.4	46.8	47.3	48.1	49.4	73.7
80	48.9	49.0	49.1	49.2	49.3	49.5	49.7	50.0	50.3	50.7	51.2	51.7	52.2	53.0	54.3	78.5
100	53.5	53.6	53.6	53.7	53.9	54.1	54.3	54.6	54.9	55.4	55.8	56.3	56.9	57.7	59.0	83.1
125	57.8	57.9	58.0	58.1	58.2	58.4	58.7	59.0	59.4	59.8	60.3	60.8	61.4	62.2	63.5	87.6
160	62.5	62.6	62.7	62.8	63.0	63.2	63.5	63.8	64.2	64.7	65.2	65.7	66.3	67.1	68.4	92.4
200	66.6	66.7	66.8	66.9	67.1	67.3	67.6	68.0	68.4	68.9	69.4	69.9	70.5	71.4	72.7	96.6
250	70.3	70.4	70.6	70.7	70.9	71.2	71.5	71.9	72.3	72.8	73.3	73.9	74.5	75.4	76.6	100.5
315	73.9	74.0	74.1	74.3	74.5	74.8	75.1	75.5	76.0	76.5	77.1	77.7	78.3	79.2	80.4	104.2
400	77.3	77.4	77.5	77.7	77.9	78.2	78.5	78.9	79.4	79.9	80.5	81.1	81.7	82.7	83.8	107.6
500	80.2	80.3	80.4	80.6	80.8	81.1	81.4	81.8	82.2	82.7	83.3	83.9	84.5	85.6	86.6	110.4
630	83.1	83.2	83.3	83.4	83.6	83.9	84.2	84.5	84.9	85.4	85.9	86.4	87.1	88.1	89.1	113.1
800	85.8	85.9	86.0	86.2	86.3	86.6	86.8	87.1	87.5	87.9	88.4	88.9	89.5	90.6	91.3	115.7
1000	88.2	88.2	88.3	88.5	88.7	88.9	89.1	89.4	89.7	90.1	90.5	91.0	91.6	92.7	93.2	117.9
1250	90.2	90.2	90.4	90.5	90.7	90.9	91.2	91.5	91.8	92.1	92.5	92.9	93.5	94.6	94.9	119.8
1600	91.9	92.0	92.2	92.4	92.6	92.8	93.1	93.4	93.7	94.0	94.4	94.7	95.5	96.4	96.5	121.7
2000	93.1	93.2	93.4	93.6	93.9	94.2	94.5	94.8	95.1	95.5	95.8	96.2	97.0	97.8	97.6	123.1
2500	93.8	94.0	94.2	94.5	94.8	95.1	95.5	95.8	96.2	96.6	96.9	97.3	98.1	98.8	98.3	124.1
3150	94.1	94.3	94.6	94.9	95.2	95.6	96.1	96.5	96.9	97.3	97.7	98.1	99.0	99.4	98.7	124.7
4000	94.1	94.3	94.6	94.9	95.3	95.8	96.2	96.7	97.2	97.6	98.1	98.5	99.5	99.7	98.8	124.9
5000	93.7	94.0	94.3	94.6	95.1	95.6	96.1	96.6	97.1	97.6	98.1	98.5	99.6	99.6	98.6	124.9
6300	93.2	93.4	93.7	94.1	94.6	95.1	95.7	96.2	96.8	97.3	97.8	98.3	99.3	99.3	98.2	124.5
8000	93.2	93.2	93.3	93.5	93.9	94.4	95.0	95.6	96.2	96.7	97.3	97.8	98.8	98.7	97.7	123.9
10000	96.2	96.0	95.5	95.0	94.6	94.4	94.6	95.0	95.5	96.0	96.6	97.1	98.1	98.0	96.9	123.8
12500	96.4	96.6	96.8	96.9	96.8	96.4	96.0	95.6	95.4	95.5	95.9	96.3	97.3	97.1	96.0	124.2
16000	92.5	93.0	93.6	94.4	95.2	95.8	96.1	96.1	95.9	95.7	95.6	95.7	96.5	96.1	95.0	123.4
20000	91.6	91.6	91.8	92.1	92.7	93.5	94.4	95.0	95.5	95.6	95.6	95.5	96.0	95.6	94.4	122.4
25000	90.5	90.7	90.9	91.2	91.5	92.0	92.5	93.2	93.9	94.5	94.8	95.0	95.4	95.0	94.0	121.3
31500	88.4	88.7	89.0	89.5	90.0	90.5	91.0	91.6	92.2	92.8	93.3	93.7	94.2	94.0	93.2	119.8
40000	85.9	86.2	86.5	86.9	87.4	88.0	88.7	89.4	90.0	90.7	91.2	91.7	92.3	92.2	91.5	117.6
50000	83.8	84.0	84.3	84.6	85.1	85.7	86.3	87.0	87.8	88.5	89.1	89.6	90.3	90.3	89.7	115.5
63000	81.0	81.2	81.5	81.7	82.2	82.8	83.3	84.1	84.7	85.6	86.4	86.8	87.6	87.7	87.0	112.7
80000	73.1	73.4	73.8	74.3	74.8	75.5	76.2	76.9	77.6	78.3	78.9	79.5	80.7	80.5	79.3	105.4
OVERALL	105.4	105.5	105.7	105.9	106.2	106.5	106.9	107.3	107.6	108.0	108.4	108.8	109.7	109.8	109.2	135.5
PNL	116.4	116.5	116.7	117.0	117.3	117.7	118.1	118.6	119.0	119.5	119.9	120.3	121.3	121.6	121.0	
PNLT	116.4	116.5	116.7	117.0	117.3	117.7	118.1	118.6	119.0	119.5	119.9	120.3	121.3	121.6	121.0	

Table B-3. Computational Acoustic Data for Pressure Ratio 2.0 : Total Noise Levels

ANGLE	20	30	40	50	60	70	80	90	100	110	120	130	140	150	160	PWL
FREQ																
50	39.3	39.3	39.3	39.4	39.5	39.6	39.8	40.1	40.4	40.7	41.2	41.7	42.2	43.2	44.8	69.6
63	44.2	44.2	44.3	44.4	44.5	44.6	44.8	45.0	45.3	45.7	46.1	46.6	47.2	48.2	49.8	74.6
80	49.3	49.3	49.4	49.4	49.5	49.7	49.9	50.1	50.4	50.8	51.2	51.7	52.3	53.3	54.8	79.6
100	53.9	54.0	54.0	54.1	54.2	54.4	54.6	54.8	55.1	55.5	56.0	56.5	57.0	58.0	59.5	84.4
125	58.5	58.6	58.6	58.7	58.8	59.0	59.2	59.4	59.8	60.2	60.6	61.1	61.7	62.7	64.2	89.0
160	63.4	63.5	63.5	63.6	63.8	63.9	64.2	64.4	64.8	65.2	65.6	66.2	66.7	67.8	69.2	94.0
200	67.7	67.7	67.8	67.9	68.1	68.2	68.5	68.8	69.1	69.5	70.0	70.6	71.1	72.2	73.6	98.3
250	71.6	71.7	71.8	71.9	72.1	72.3	72.6	72.9	73.3	73.7	74.2	74.8	75.4	76.4	77.8	102.5
315	75.5	75.5	75.6	75.8	76.0	76.2	76.5	76.8	77.2	77.7	78.2	78.8	79.5	80.6	81.8	106.5
400	79.0	79.1	79.2	79.4	79.6	79.8	80.2	80.5	81.0	81.5	82.0	82.6	83.3	84.4	85.6	110.2
500	82.1	82.2	82.3	82.4	82.6	82.9	83.2	83.6	84.0	84.6	85.1	85.7	86.4	87.7	88.7	113.3
630	85.0	85.1	85.2	85.3	85.5	85.8	86.1	86.4	86.9	87.4	87.9	88.5	89.3	90.5	91.4	116.1
800	87.8	87.9	88.0	88.1	88.3	88.5	88.8	89.1	89.5	90.0	90.5	91.1	91.8	93.1	93.8	118.8
1000	90.2	90.3	90.4	90.5	90.7	90.9	91.1	91.4	91.8	92.2	92.7	93.2	94.0	95.2	95.6	121.0
1250	92.3	92.4	92.5	92.6	92.8	93.0	93.3	93.6	93.9	94.3	94.7	95.1	95.9	97.1	97.3	123.0
1600	94.2	94.3	94.5	94.6	94.8	95.1	95.3	95.6	95.9	96.3	96.6	97.0	97.9	98.9	98.8	125.0
2000	95.5	95.6	95.8	96.0	96.3	96.5	96.8	97.2	97.5	97.8	98.2	98.5	99.5	100.3	99.9	126.4
2500	96.3	96.5	96.7	97.0	97.3	97.6	98.0	98.3	98.7	99.0	99.4	99.8	100.8	101.3	100.6	127.6
3150	96.7	96.9	97.2	97.5	97.9	98.3	98.7	99.1	99.5	99.9	100.3	100.7	101.8	102.0	101.0	128.3
4000	96.6	96.9	97.2	97.6	98.0	98.5	99.0	99.5	99.9	100.4	100.8	101.3	102.3	102.2	101.0	128.7
5000	96.3	96.6	96.9	97.3	97.8	98.3	98.9	99.4	100.0	100.5	100.9	101.5	102.5	102.1	100.8	128.7
6300	95.8	96.0	96.4	96.8	97.3	97.9	98.5	99.1	99.7	100.2	100.7	101.3	102.3	101.8	100.4	128.4
8000	95.0	95.3	95.7	96.1	96.6	97.2	97.8	98.5	99.1	99.7	100.2	100.9	101.8	101.2	99.9	127.9
10000	94.2	94.5	94.8	95.3	95.8	96.4	97.1	97.7	98.4	99.0	99.5	100.2	101.1	100.5	99.2	127.3
12500	93.2	93.5	93.9	94.4	94.9	95.5	96.2	96.9	97.5	98.1	98.7	99.4	100.3	99.6	98.3	126.5
16000	92.0	92.3	92.6	93.1	93.7	94.3	95.0	95.7	96.4	97.0	97.6	98.3	99.2	98.5	97.1	125.6
20000	90.6	90.9	91.3	91.8	92.4	93.0	93.7	94.5	95.2	95.9	96.5	97.2	98.0	97.3	95.9	124.6
25000	89.1	89.4	89.8	90.3	90.9	91.6	92.3	93.0	93.8	94.5	95.1	95.9	96.7	96.0	94.6	123.6
31500	87.2	87.5	88.0	88.5	89.1	89.8	90.5	91.3	92.1	92.8	93.4	94.2	95.1	94.4	93.0	122.4
40000	85.0	85.3	85.7	86.2	86.9	87.6	88.3	89.1	89.9	90.7	91.4	92.2	93.0	92.4	91.0	121.1
50000	82.6	82.9	83.3	83.8	84.4	85.1	85.9	86.7	87.5	88.3	89.0	89.9	90.7	90.1	88.7	119.9
63000	79.6	79.9	80.3	80.8	81.5	82.2	82.9	83.7	84.5	85.3	86.0	86.9	87.8	87.1	85.7	118.4
80000	75.7	76.0	76.5	77.0	77.7	78.4	79.1	79.9	80.7	81.5	82.2	83.0	84.0	83.3	81.9	117.0
OVERALL	106.5	106.7	107.0	107.3	107.7	108.2	108.7	109.2	109.8	110.3	110.7	111.3	112.3	112.2	111.2	138.8
PNL	118.6	118.8	119.1	119.4	119.8	120.2	120.7	121.1	121.6	122.1	122.5	123.0	124.0	124.1	123.2	
PNLT	118.6	118.8	119.1	119.4	119.8	120.2	120.7	121.1	121.6	122.1	122.5	123.0	124.0	124.1	123.2	

Table B-4. Computational Acoustic Data for Pressure Ratio 2.5 : Mixing Noise Component

ANGLE	20	30	40	50	60	70	80	90	100	110	120	130	140	150	160	PWL
FREQ																
50	0.0	0.0	0.0	0.0	0.0	0.0	0.0	0.0	0.0	0.0	0.0	0.0	0.0	0.0	0.0	28.9
63	35.8	35.8	35.8	35.8	35.8	35.8	35.8	35.8	35.8	35.8	35.8	35.8	35.8	35.8	35.8	64.6
80	36.5	36.5	36.5	36.5	36.5	36.5	36.5	36.5	36.5	36.5	36.5	36.5	36.5	36.5	36.5	65.4
100	40.6	40.6	40.6	40.6	40.6	40.6	40.6	40.6	40.6	40.6	40.6	40.6	40.6	40.6	40.6	69.4
125	38.9	38.9	38.9	38.9	38.9	38.9	38.9	38.9	38.9	38.9	38.9	38.9	38.9	38.9	38.9	67.8
160	39.5	39.5	39.5	39.5	39.5	39.5	39.5	39.5	39.5	39.5	39.5	39.5	39.5	39.5	39.5	68.4
200	40.5	40.5	40.5	40.5	40.5	40.5	40.5	40.5	40.5	40.5	40.5	40.5	40.5	40.5	40.5	69.3
250	41.6	41.6	41.6	41.6	41.6	41.6	41.6	41.6	41.6	41.6	41.6	41.6	41.6	41.6	41.6	70.5
315	42.8	42.8	42.8	42.8	42.8	42.8	42.8	42.8	42.8	42.8	42.8	42.8	42.8	42.8	42.8	71.6
400	43.5	43.5	43.5	43.5	43.5	43.5	43.5	43.5	43.5	43.5	43.5	43.5	43.5	43.5	43.5	72.3
500	44.6	44.6	44.6	44.6	44.6	44.6	44.6	44.6	44.6	44.6	44.6	44.6	44.6	44.6	44.6	73.5
630	45.8	45.8	45.8	45.8	45.8	45.8	45.8	45.8	45.8	45.8	45.8	45.8	45.8	45.8	45.8	74.6
800	46.5	46.5	46.5	46.5	46.5	46.5	46.5	46.5	46.5	46.5	46.5	46.5	46.5	46.5	46.5	75.4
1000	47.4	47.4	47.4	47.4	47.4	47.4	47.4	47.4	47.4	47.4	47.4	47.4	47.4	47.4	47.4	76.3
1250	48.9	48.9	48.9	48.9	48.9	48.9	48.9	48.9	48.9	48.9	48.9	48.9	48.9	48.9	48.9	77.8
1600	49.5	49.5	49.5	49.5	49.5	49.5	49.5	49.5	49.5	49.5	49.5	49.5	49.5	49.5	49.5	78.4
2000	50.4	50.4	50.4	50.4	50.4	50.4	50.4	50.4	50.4	50.4	50.4	50.4	50.4	50.4	50.4	79.3
2500	51.6	51.6	51.6	51.6	51.6	51.6	51.6	51.6	51.6	51.6	51.6	51.6	51.6	51.6	51.6	80.5
3150	88.3	85.5	81.5	76.1	69.4	61.4	54.4	52.7	52.7	52.7	52.7	52.7	52.7	52.7	52.7	105.8
4000	107.5	106.1	104.1	101.2	97.3	92.3	86.3	79.1	71.1	62.7	55.7	53.4	53.4	53.4	53.4	127.1
5000	112.9	112.7	112.2	111.2	109.6	107.2	103.9	99.7	94.7	89.0	82.9	76.7	70.9	66.0	62.3	135.8
6300	109.2	110.1	111.0	111.8	112.1	111.9	110.9	109.1	106.4	103.0	99.1	95.0	90.9	87.3	84.5	137.8
8000	104.6	104.6	105.2	106.5	108.2	109.8	110.7	110.9	110.2	108.6	106.4	103.8	101.1	98.6	96.6	137.1
10000	106.5	106.4	106.3	106.0	105.8	106.4	107.7	109.1	109.9	109.9	109.1	107.8	106.2	104.6	103.2	136.9
12500	105.4	105.6	105.9	106.2	106.4	106.6	106.7	107.3	108.3	109.1	109.4	109.1	108.5	107.6	106.8	136.9
16000	102.7	102.9	103.3	103.8	104.4	105.0	105.5	105.9	106.5	107.1	107.7	108.0	107.9	107.6	107.2	135.6
20000	101.2	101.4	101.6	102.0	102.4	103.1	103.8	104.6	105.3	105.9	106.5	106.9	107.1	107.1	106.9	134.6
25000	100.0	100.2	100.4	100.6	101.0	101.4	102.1	102.9	103.8	104.6	105.3	105.9	106.2	106.3	106.3	133.7
31500	98.6	98.7	98.9	99.2	99.5	99.9	100.4	101.1	101.9	102.9	103.8	104.5	105.0	105.2	105.3	132.8
40000	96.5	96.6	96.8	97.1	97.4	97.8	98.2	98.8	99.6	100.5	101.4	102.3	102.9	103.3	103.5	131.4
50000	94.6	94.7	94.9	95.2	95.5	95.9	96.3	96.9	97.5	98.4	99.3	100.1	100.9	101.4	101.7	130.5
63000	91.9	92.1	92.2	92.4	92.6	93.0	93.4	94.0	94.6	95.4	96.3	97.2	98.2	98.7	99.2	129.3
80000	0.0	0.0	0.0	0.0	0.0	0.0	0.0	0.0	0.0	0.0	0.0	0.0	0.0	0.0	0.0	28.9
OVERALL	117.0	117.0	116.9	116.9	116.9	116.8	116.7	116.7	116.5	116.3	116.1	115.8	115.4	115.1	114.7	145.9
PNL	127.2	126.9	126.5	125.7	125.4	124.9	123.9	122.2	120.3	118.5	116.2	114.3	112.4	110.5	109.0	
PNLT	130.2	129.7	129.0	127.3	128.7	127.8	126.2	123.8	122.4	119.6	118.1	114.9	112.4	111.5	109.9	

Table B-5. *Computational Acoustic Data for Pressure Ratio 2.5 : Shock Noise Component*

ANGLE	20	30	40	50	60	70	80	90	100	110	120	130	140	150	160	PWL
FREQ																
50	39.3	39.3	39.3	39.4	39.5	39.6	39.8	40.1	40.4	40.7	41.2	41.7	42.2	43.2	44.8	69.6
63	44.8	44.8	44.9	44.9	45.0	45.1	45.3	45.5	45.8	46.1	46.5	47.0	47.5	48.4	49.9	75.0
80	49.5	49.5	49.6	49.6	49.7	49.9	50.1	50.3	50.6	51.0	51.4	51.9	52.4	53.4	54.9	79.8
100	54.1	54.2	54.2	54.3	54.4	54.5	54.7	55.0	55.3	55.6	56.1	56.6	57.1	58.1	59.6	84.5
125	58.6	58.6	58.7	58.7	58.9	59.0	59.2	59.5	59.8	60.2	60.6	61.1	61.7	62.7	64.2	89.0
160	63.4	63.5	63.6	63.7	63.8	64.0	64.2	64.4	64.8	65.2	65.6	66.2	66.7	67.8	69.2	94.0
200	67.7	67.7	67.8	67.9	68.1	68.2	68.5	68.8	69.1	69.6	70.0	70.6	71.2	72.2	73.6	98.3
250	71.7	71.7	71.8	71.9	72.1	72.3	72.6	72.9	73.3	73.7	74.2	74.8	75.4	76.4	77.8	102.5
315	75.5	75.5	75.6	75.8	76.0	76.2	76.5	76.8	77.3	77.7	78.2	78.8	79.5	80.6	81.8	106.5
400	79.0	79.1	79.2	79.4	79.6	79.8	80.2	80.5	81.0	81.5	82.0	82.6	83.3	84.4	85.6	110.2
500	82.1	82.2	82.3	82.4	82.6	82.9	83.2	83.6	84.0	84.6	85.1	85.7	86.4	87.7	88.7	113.3
630	85.0	85.1	85.2	85.3	85.5	85.8	86.1	86.4	86.9	87.4	87.9	88.5	89.3	90.5	91.4	116.1
800	87.8	87.9	88.0	88.1	88.3	88.5	88.8	89.1	89.5	90.0	90.5	91.1	91.8	93.1	93.8	118.8
1000	90.2	90.3	90.4	90.5	90.7	90.9	91.1	91.4	91.8	92.2	92.7	93.2	94.0	95.2	95.6	121.0
1250	92.3	92.4	92.5	92.6	92.8	93.0	93.3	93.6	93.9	94.3	94.7	95.1	95.9	97.1	97.3	123.0
1600	94.2	94.3	94.5	94.6	94.8	95.1	95.3	95.6	95.9	96.3	96.6	97.0	97.9	98.9	98.8	125.0
2000	95.5	95.6	95.8	96.0	96.3	96.5	96.8	97.2	97.5	97.8	98.2	98.5	99.5	100.3	99.9	126.4
2500	96.3	96.5	96.7	97.0	97.3	97.6	98.0	98.3	98.7	99.0	99.4	99.8	100.8	101.3	100.6	127.5
3150	97.3	97.2	97.3	97.5	97.9	98.3	98.7	99.1	99.5	99.9	100.3	100.7	101.8	102.0	101.0	128.3
4000	107.8	106.6	104.9	102.7	100.7	99.4	99.2	99.5	99.9	100.4	100.8	101.3	102.4	102.2	101.0	130.9
5000	113.0	112.8	112.3	111.4	109.9	107.8	105.1	102.6	101.1	100.8	101.0	101.5	102.5	102.1	100.8	136.5
6300	109.4	110.3	111.2	111.9	112.3	112.1	111.2	109.5	107.2	104.9	103.0	102.2	102.6	101.9	100.5	138.1
8000	105.0	105.1	105.7	106.9	108.5	110.0	110.9	111.1	110.5	109.1	107.4	105.6	104.5	103.1	101.5	137.4
10000	106.8	106.7	106.6	106.3	106.2	106.8	108.1	109.4	110.2	110.2	109.6	108.5	107.4	106.0	104.6	137.1
12500	105.7	105.9	106.2	106.5	106.7	106.9	107.1	107.7	108.6	109.4	109.7	109.6	109.1	108.2	107.3	136.8
16000	103.0	103.3	103.7	104.2	104.8	105.4	105.9	106.3	106.9	107.5	108.1	108.4	108.4	108.1	107.6	135.4
20000	101.6	101.8	102.0	102.4	102.8	103.5	104.2	105.0	105.7	106.3	106.9	107.4	107.6	107.5	107.2	134.2
25000	100.4	100.5	100.7	101.0	101.4	101.9	102.5	103.3	104.2	105.0	105.7	106.3	106.7	106.7	106.6	132.9
31500	98.9	99.0	99.3	99.5	99.9	100.3	100.9	101.5	102.4	103.3	104.1	104.9	105.4	105.6	105.6	131.4
40000	96.8	96.9	97.1	97.4	97.8	98.2	98.7	99.3	100.0	100.9	101.8	102.7	103.3	103.6	103.7	129.2
50000	94.8	95.0	95.2	95.5	95.8	96.2	96.7	97.3	98.0	98.8	99.7	100.5	101.3	101.7	101.9	127.2
63000	92.1	92.4	92.5	92.7	93.0	93.3	93.8	94.4	95.0	95.8	96.7	97.6	98.6	99.0	99.4	124.4
80000	75.7	76.0	76.5	77.0	77.7	78.4	79.1	79.9	80.7	81.5	82.2	83.0	84.0	83.3	81.9	109.4
OVERALL	117.4	117.4	117.4	117.4	117.4	117.4	117.4	117.4	117.4	117.3	117.2	117.1	117.2	116.9	116.3	146.1
PNL	129.5	129.3	129.1	128.5	128.4	128.3	127.7	126.8	125.7	125.0	124.2	123.7	124.4	124.4	123.5	
PNLT	132.0	131.6	131.0	129.8	130.6	129.9	128.4	126.8	125.7	125.0	124.2	123.7	124.4	124.4	123.5	

Table B-6. Computational Acoustic Data for Pressure Ratio 2.5 : Total Noise Levels

ANGLE	20	30	40	50	60	70	80	90	100	110	120	130	140	150	160	PWL
FREQ																
50	39.2	39.2	39.1	39.1	39.1	39.1	39.2	39.3	39.5	39.7	40.0	40.4	41.0	42.5	44.3	70.9
63	44.1	44.1	44.1	44.1	44.1	44.1	44.2	44.3	44.5	44.7	45.0	45.4	46.0	47.5	49.3	75.9
80	49.3	49.2	49.2	49.2	49.2	49.2	49.3	49.4	49.6	49.8	50.2	50.5	51.2	52.6	54.3	81.0
100	54.0	54.0	54.0	54.0	54.0	54.0	54.1	54.2	54.4	54.6	54.9	55.3	55.9	57.4	59.1	85.8
125	58.7	58.7	58.7	58.7	58.7	58.7	58.8	58.9	59.1	59.3	59.7	60.1	60.7	62.1	63.8	90.5
160	63.8	63.8	63.8	63.8	63.8	63.8	63.9	64.0	64.2	64.5	64.8	65.2	65.8	67.3	68.9	95.6
200	68.2	68.2	68.2	68.2	68.3	68.3	68.4	68.6	68.8	69.0	69.4	69.8	70.4	71.8	73.4	100.2
250	72.5	72.5	72.5	72.6	72.6	72.7	72.8	72.9	73.2	73.4	73.8	74.2	74.9	76.3	77.8	104.5
315	76.7	76.7	76.7	76.8	76.8	76.9	77.1	77.3	77.5	77.8	78.2	78.6	79.3	80.7	82.1	108.9
400	80.6	80.7	80.7	80.8	80.9	81.0	81.2	81.4	81.7	82.0	82.4	82.9	83.6	85.0	86.2	113.0
500	84.0	84.0	84.1	84.2	84.3	84.5	84.7	84.9	85.2	85.6	86.0	86.5	87.3	88.7	89.8	116.6
630	87.1	87.1	87.2	87.3	87.4	87.6	87.8	88.1	88.4	88.8	89.3	89.8	90.7	92.1	92.9	119.8
800	90.0	90.0	90.1	90.2	90.3	90.5	90.7	91.0	91.3	91.7	92.2	92.7	93.7	95.0	95.6	122.7
1000	92.5	92.5	92.6	92.7	92.8	92.9	93.1	93.4	93.7	94.1	94.5	95.0	96.0	97.3	97.6	125.0
1250	94.7	94.7	94.8	94.9	95.0	95.2	95.3	95.5	95.8	96.1	96.5	97.0	98.1	99.1	99.1	127.1
1600	96.8	96.8	96.9	97.1	97.2	97.3	97.5	97.7	97.9	98.2	98.5	98.9	100.0	100.8	100.5	129.1
2000	98.3	98.4	98.5	98.7	98.8	99.0	99.2	99.4	99.6	99.8	100.0	100.4	101.6	102.0	101.4	130.7
2500	99.4	99.6	99.7	99.9	100.1	100.3	100.5	100.7	100.9	101.1	101.3	101.7	102.9	103.0	102.0	131.9
3150	100.2	100.4	100.6	100.8	101.0	101.3	101.5	101.8	102.0	102.2	102.4	102.8	103.9	103.6	102.4	132.9
4000	100.5	100.7	101.0	101.3	101.6	101.9	102.2	102.5	102.7	102.9	103.1	103.6	104.5	103.9	102.5	133.5
5000	100.4	100.6	101.0	101.3	101.7	102.2	102.5	102.9	103.1	103.3	103.4	104.0	104.7	104.0	102.5	133.8
6300	99.9	100.2	100.5	101.0	101.5	102.0	102.5	102.9	103.2	103.4	103.5	104.1	104.7	103.9	102.6	133.7
8000	99.3	99.6	99.9	100.4	100.9	101.4	102.0	102.5	103.0	103.2	103.3	104.0	104.5	103.7	102.8	133.5
10000	98.7	98.9	99.3	99.7	100.2	100.8	101.3	101.9	102.4	102.8	102.9	103.6	104.1	103.4	102.7	133.1
12500	98.0	98.2	98.6	99.0	99.5	100.0	100.6	101.2	101.7	102.1	102.3	103.0	103.4	102.8	102.4	132.5
16000	96.8	97.1	97.5	98.0	98.5	99.1	99.7	100.3	100.8	101.2	101.4	102.2	102.5	101.9	101.4	131.8
20000	95.2	95.5	96.0	96.6	97.2	97.9	98.6	99.3	99.8	100.3	100.5	101.3	101.5	100.8	100.1	131.0
25000	93.0	93.4	93.9	94.5	95.3	96.1	97.0	97.8	98.5	99.1	99.4	100.2	100.4	99.5	98.5	129.9
31500	91.0	91.3	91.7	92.3	92.9	93.7	94.6	95.5	96.4	97.2	97.7	98.6	98.8	97.7	96.5	128.5
40000	89.0	89.3	89.7	90.2	90.8	91.4	92.1	92.8	93.6	94.4	95.0	96.2	96.4	95.3	93.9	126.8
50000	86.6	86.9	87.4	87.9	88.6	89.3	89.9	90.6	91.2	91.7	92.1	93.2	93.6	92.5	91.1	125.3
63000	83.0	83.4	83.9	84.6	85.4	86.2	87.1	87.9	88.5	88.9	89.2	90.1	90.6	89.5	87.9	123.9
80000	77.9	78.4	79.1	79.9	80.8	81.8	82.8	83.8	84.7	85.4	85.7	86.7	87.0	85.8	84.1	122.4
OVERALL	110.2	110.4	110.7	111.0	111.4	111.8	112.3	112.7	113.0	113.3	113.5	114.2	114.8	114.4	113.6	144.0
PNL	122.1	122.3	122.5	122.8	123.1	123.4	123.7	124.0	124.3	124.5	124.7	125.2	126.1	125.8	124.9	
PNLT	122.1	122.3	122.5	122.8	123.1	123.4	123.7	124.0	124.3	124.5	124.7	125.2	126.1	125.8	124.9	

Table B-7. Computational Acoustic Data for Pressure Ratio 3.0 : Mixing Noise Component

ANGLE	20	30	40	50	60	70	80	90	100	110	120	130	140	150	160	PWL
FREQ																
50	0.0	0.0	0.0	0.0	0.0	0.0	0.0	0.0	0.0	0.0	0.0	0.0	0.0	0.0	0.0	30.9
63	35.8	35.8	35.8	35.8	35.8	35.8	35.8	35.8	35.8	35.8	35.8	35.8	35.8	35.8	35.8	66.7
80	36.5	36.5	36.5	36.5	36.5	36.5	36.5	36.5	36.5	36.5	36.5	36.5	36.5	36.5	36.5	67.4
100	40.6	40.6	40.6	40.6	40.6	40.6	40.6	40.6	40.6	40.6	40.6	40.6	40.6	40.6	40.6	71.5
125	38.9	38.9	38.9	38.9	38.9	38.9	38.9	38.9	38.9	38.9	38.9	38.9	38.9	38.9	38.9	69.8
160	39.5	39.5	39.5	39.5	39.5	39.5	39.5	39.5	39.5	39.5	39.5	39.5	39.5	39.5	39.5	70.4
200	40.5	40.5	40.5	40.5	40.5	40.5	40.5	40.5	40.5	40.5	40.5	40.5	40.5	40.5	40.5	71.4
250	41.6	41.6	41.6	41.6	41.6	41.6	41.6	41.6	41.6	41.6	41.6	41.6	41.6	41.6	41.6	72.5
315	42.8	42.8	42.8	42.8	42.8	42.8	42.8	42.8	42.8	42.8	42.8	42.8	42.8	42.8	42.8	73.7
400	43.5	43.5	43.5	43.5	43.5	43.5	43.5	43.5	43.5	43.5	43.5	43.5	43.5	43.5	43.5	74.4
500	44.6	44.6	44.6	44.6	44.6	44.6	44.6	44.6	44.6	44.6	44.6	44.6	44.6	44.6	44.6	75.5
630	45.8	45.8	45.8	45.8	45.8	45.8	45.8	45.8	45.8	45.8	45.8	45.8	45.8	45.8	45.8	76.7
800	46.5	46.5	46.5	46.5	46.5	46.5	46.5	46.5	46.5	46.5	46.5	46.5	46.5	46.5	46.5	77.4
1000	47.4	47.4	47.4	47.4	47.4	47.4	47.4	47.4	47.4	47.4	47.4	47.4	47.4	47.4	47.4	78.4
1250	48.9	48.9	48.9	48.9	48.9	48.9	48.9	48.9	48.9	48.9	48.9	48.9	48.9	48.9	48.9	79.8
1600	49.5	49.5	49.5	49.5	49.5	49.5	49.5	49.5	49.5	49.5	49.5	49.5	49.5	49.5	49.5	80.4
2000	50.4	50.4	50.4	50.4	50.4	50.4	50.4	50.4	50.4	50.4	50.4	50.4	50.4	50.4	50.4	81.4
2500	83.7	80.3	75.3	68.7	60.6	53.2	51.6	51.6	51.6	51.6	51.6	51.6	51.6	51.6	51.6	102.7
3150	107.5	106.0	103.6	100.3	95.8	89.9	82.6	74.1	64.4	55.6	52.7	52.7	52.7	52.7	52.7	128.7
4000	112.8	112.6	112.1	111.1	109.3	106.4	102.5	97.4	91.2	84.2	76.6	69.0	61.9	56.7	54.2	137.5
5000	108.4	109.5	110.7	111.6	112.1	111.9	110.6	108.3	105.0	100.8	95.9	90.6	85.5	81.0	77.4	139.4
6300	103.5	103.3	103.9	105.7	107.9	109.9	111.1	111.3	110.4	108.5	105.7	102.5	99.1	95.9	93.4	139.0
8000	106.4	106.4	106.1	105.5	104.8	105.2	107.0	108.9	109.9	110.0	109.0	107.4	105.4	103.3	101.5	138.5
10000	104.8	105.0	105.4	105.7	105.9	105.8	105.7	106.2	107.5	108.7	109.1	108.8	107.9	106.7	105.6	138.2
12500	102.9	103.2	103.6	104.2	104.8	105.4	105.8	106.1	106.6	107.3	108.1	108.6	108.5	108.1	107.5	137.8
16000	101.1	101.2	101.5	101.8	102.2	102.9	103.7	104.5	105.2	105.8	106.4	107.0	107.2	107.2	107.0	136.3
20000	99.9	100.0	100.2	100.5	100.8	101.3	101.9	102.7	103.6	104.5	105.3	105.9	106.3	106.4	106.4	135.3
25000	98.7	98.8	99.0	99.2	99.6	100.0	100.5	101.1	102.0	103.0	103.9	104.7	105.2	105.5	105.6	134.4
31500	97.2	97.4	97.6	97.8	98.1	98.5	99.0	99.6	100.3	101.2	102.2	103.1	103.9	104.3	104.5	133.5
40000	95.1	95.3	95.5	95.7	96.0	96.4	96.9	97.4	98.1	98.9	99.9	100.9	101.7	102.3	102.6	132.1
50000	93.2	93.4	93.6	93.8	94.1	94.5	95.0	95.5	96.1	96.9	97.8	98.8	99.7	100.3	100.6	131.2
63000	90.6	90.8	91.0	91.3	91.5	91.9	92.4	92.8	93.5	94.1	95.0	96.1	97.0	97.6	97.9	130.1
80000	0.0	0.0	0.0	0.0	0.0	0.0	0.0	0.0	0.0	0.0	0.0	0.0	0.0	0.0	0.0	30.9
OVERALL	116.8	116.8	116.7	116.7	116.7	116.6	116.6	116.5	116.4	116.3	116.1	115.8	115.5	115.2	114.8	147.7
PNL	128.5	128.3	127.9	127.1	126.9	126.5	125.4	124.7	123.6	121.8	119.5	117.6	115.4	113.6	112.2	
PNLT	131.6	131.2	130.5	130.8	130.3	129.8	127.3	126.1	126.3	123.8	120.8	119.2	116.4	115.1	113.4	

Table B-8. Computational Acoustic Data for Pressure Ratio 3.0 : Shock Noise Component

ANGLE	20	30	40	50	60	70	80	90	100	110	120	130	140	150	160	PWL
FREQ																
50	39.2	39.2	39.1	39.1	39.1	39.1	39.2	39.3	39.5	39.7	40.0	40.4	41.0	42.5	44.3	70.9
63	44.7	44.7	44.7	44.7	44.7	44.7	44.8	44.9	45.0	45.2	45.5	45.9	46.4	47.8	49.4	76.4
80	49.5	49.5	49.5	49.4	49.4	49.5	49.5	49.6	49.8	50.0	50.3	50.7	51.3	52.7	54.4	81.2
100	54.2	54.2	54.2	54.2	54.2	54.2	54.3	54.4	54.5	54.8	55.1	55.5	56.1	57.5	59.1	85.9
125	58.7	58.7	58.7	58.7	58.7	58.7	58.8	58.9	59.1	59.4	59.7	60.1	60.7	62.1	63.8	90.5
160	63.8	63.8	63.8	63.8	63.8	63.8	63.9	64.0	64.2	64.5	64.8	65.2	65.8	67.3	68.9	95.6
200	68.2	68.2	68.2	68.2	68.3	68.3	68.4	68.6	68.8	69.0	69.4	69.8	70.4	71.9	73.4	100.2
250	72.5	72.5	72.5	72.6	72.6	72.7	72.8	72.9	73.2	73.5	73.8	74.2	74.9	76.3	77.8	104.5
315	76.7	76.7	76.7	76.8	76.8	76.9	77.1	77.3	77.5	77.8	78.2	78.6	79.3	80.7	82.1	108.9
400	80.6	80.7	80.7	80.8	80.9	81.0	81.2	81.4	81.7	82.0	82.4	82.9	83.6	85.0	86.2	113.0
500	84.0	84.0	84.1	84.2	84.3	84.5	84.7	84.9	85.2	85.6	86.0	86.5	87.3	88.7	89.8	116.5
630	87.1	87.1	87.2	87.3	87.4	87.6	87.8	88.1	88.4	88.8	89.3	89.8	90.7	92.1	92.9	119.8
800	90.0	90.0	90.1	90.2	90.3	90.5	90.7	91.0	91.3	91.7	92.2	92.8	93.7	95.0	95.6	122.7
1000	92.5	92.5	92.6	92.7	92.8	92.9	93.1	93.4	93.7	94.1	94.5	95.0	96.0	97.3	97.6	125.0
1250	94.7	94.7	94.8	94.9	95.0	95.2	95.3	95.5	95.8	96.1	96.5	97.0	98.1	99.1	99.1	127.1
1600	96.8	96.8	96.9	97.1	97.2	97.3	97.5	97.7	97.9	98.2	98.5	98.9	100.0	100.8	100.5	129.1
2000	98.3	98.4	98.5	98.7	98.8	99.0	99.2	99.4	99.6	99.8	100.0	100.4	101.6	102.0	101.4	130.6
2500	99.6	99.6	99.7	99.9	100.1	100.3	100.5	100.7	100.9	101.1	101.3	101.7	102.9	103.0	102.0	131.9
3150	108.2	107.0	105.4	103.6	102.2	101.6	101.6	101.8	102.0	102.2	102.4	102.8	103.9	103.6	102.4	134.2
4000	113.1	112.9	112.5	111.5	109.9	107.8	105.4	103.7	103.0	103.0	103.1	103.6	104.5	103.9	102.5	138.9
5000	109.1	110.0	111.1	112.0	112.5	112.3	111.3	109.4	107.2	105.2	104.1	104.2	104.8	104.0	102.6	140.4
6300	105.1	105.0	105.6	106.9	108.8	110.6	111.7	111.9	111.1	109.6	107.8	106.4	105.8	104.5	103.1	140.0
8000	107.2	107.2	107.0	106.6	106.3	106.7	108.2	109.8	110.7	110.8	110.1	109.0	108.0	106.5	105.2	139.5
10000	105.8	106.0	106.3	106.7	106.9	107.0	107.0	107.6	108.7	109.7	110.0	109.9	109.4	108.4	107.4	139.1
12500	104.1	104.4	104.8	105.3	105.9	106.5	107.0	107.3	107.8	108.5	109.1	109.6	109.7	109.2	108.7	138.5
16000	102.5	102.7	102.9	103.3	103.8	104.4	105.2	105.9	106.5	107.1	107.6	108.2	108.5	108.3	108.1	137.1
20000	101.1	101.3	101.6	101.9	102.4	102.9	103.6	104.3	105.2	105.9	106.5	107.2	107.5	107.5	107.3	135.8
25000	99.7	99.9	100.2	100.5	100.9	101.5	102.1	102.8	103.6	104.4	105.2	106.0	106.5	106.5	106.4	134.5
31500	98.2	98.3	98.6	98.9	99.3	99.8	100.3	101.0	101.8	102.7	103.5	104.5	105.0	105.2	105.2	132.9
40000	96.1	96.3	96.5	96.8	97.2	97.6	98.1	98.7	99.4	100.2	101.1	102.1	102.8	103.0	103.1	130.7
50000	94.1	94.3	94.5	94.8	95.2	95.6	96.2	96.7	97.3	98.0	98.9	99.9	100.6	101.0	101.1	128.6
63000	91.3	91.5	91.8	92.1	92.5	92.9	93.5	94.0	94.7	95.2	96.0	97.0	97.9	98.2	98.3	125.8
80000	77.9	78.4	79.1	79.9	80.8	81.8	82.8	83.8	84.7	85.4	85.7	86.7	87.0	85.8	84.1	114.9
OVERALL	117.6	117.7	117.7	117.7	117.8	117.9	117.9	118.0	118.1	118.1	118.0	118.1	118.2	117.8	117.3	148.8
PNL	130.8	130.8	130.5	130.0	130.0	129.8	129.3	129.0	128.6	127.8	126.8	126.3	126.6	126.3	125.2	
PNLT	133.2	132.9	131.9	131.2	132.0	130.9	129.3	129.0	128.6	127.8	126.8	126.3	126.6	126.3	125.2	

Table B-9. Computational Acoustic Data for Pressure Ratio 3.0 : Total Noise Levels

ANGLE	20	30	40	50	60	70	80	90	100	110	120	130	140	150	160	PWL
FREQ																
50	39.2	39.2	39.2	39.2	39.2	39.3	39.4	39.5	39.7	40.0	40.3	40.7	41.3	42.7	44.4	70.7
63	44.2	44.2	44.2	44.2	44.2	44.3	44.3	44.5	44.7	45.0	45.3	45.7	46.3	47.7	49.4	75.6
80	49.3	49.3	49.3	49.3	49.3	49.4	49.5	49.6	49.8	50.1	50.4	50.9	51.4	52.8	54.5	80.8
100	54.0	54.0	54.0	54.0	54.1	54.1	54.2	54.4	54.6	54.8	55.2	55.6	56.2	57.6	59.2	85.5
125	58.7	58.7	58.7	58.7	58.7	58.8	58.9	59.1	59.3	59.6	59.9	60.3	60.9	62.3	63.9	90.2
160	63.7	63.7	63.7	63.8	63.8	63.9	64.0	64.2	64.4	64.7	65.0	65.5	66.1	67.4	69.0	95.3
200	68.1	68.2	68.2	68.2	68.3	68.4	68.5	68.7	68.9	69.2	69.6	70.0	70.6	72.0	73.5	99.8
250	72.4	72.4	72.4	72.5	72.5	72.6	72.8	73.0	73.2	73.6	74.0	74.4	75.0	76.4	77.8	104.1
315	76.5	76.5	76.5	76.6	76.7	76.8	77.0	77.2	77.5	77.9	78.3	78.7	79.4	80.7	82.1	108.4
400	80.3	80.4	80.4	80.5	80.6	80.8	81.0	81.3	81.6	82.0	82.4	82.9	83.6	85.0	86.2	112.5
500	83.6	83.6	83.7	83.8	84.0	84.1	84.4	84.7	85.0	85.4	85.9	86.4	87.1	88.5	89.6	115.9
630	86.6	86.7	86.8	86.9	87.0	87.2	87.4	87.8	88.1	88.5	89.0	89.6	90.4	91.8	92.6	119.0
800	89.5	89.5	89.6	89.7	89.9	90.0	90.3	90.6	90.9	91.3	91.8	92.4	93.3	94.6	95.2	121.8
1000	92.0	92.0	92.1	92.2	92.3	92.5	92.7	92.9	93.2	93.6	94.1	94.6	95.5	96.8	97.1	124.1
1250	94.2	94.2	94.3	94.4	94.5	94.7	94.9	95.1	95.3	95.7	96.1	96.5	97.5	98.6	98.6	126.2
1600	96.3	96.3	96.4	96.5	96.7	96.8	97.0	97.2	97.4	97.7	98.0	98.4	99.5	100.3	100.0	128.2
2000	97.8	97.9	98.0	98.1	98.3	98.5	98.7	98.9	99.1	99.3	99.6	100.0	101.1	101.6	101.0	129.7
2500	98.9	99.1	99.2	99.4	99.6	99.8	100.0	100.2	100.4	100.6	100.9	101.3	102.4	102.6	101.7	131.0
3150	99.8	99.9	100.1	100.3	100.5	100.8	101.0	101.3	101.5	101.7	101.9	102.3	103.4	103.2	102.1	132.0
4000	100.2	100.4	100.6	100.9	101.2	101.4	101.7	102.0	102.2	102.4	102.6	103.1	104.0	103.6	102.2	132.6
5000	100.1	100.3	100.6	101.0	101.4	101.7	102.1	102.4	102.6	102.8	102.9	103.5	104.3	103.7	102.3	132.9
6300	99.5	99.8	100.2	100.6	101.1	101.6	102.1	102.5	102.8	102.9	103.0	103.6	104.3	103.6	102.4	132.9
8000	98.8	99.1	99.5	99.9	100.4	101.0	101.6	102.2	102.6	102.8	102.8	103.5	104.1	103.5	102.6	132.7
10000	98.1	98.4	98.7	99.2	99.7	100.3	100.9	101.5	102.0	102.4	102.5	103.1	103.7	103.2	102.6	132.2
12500	97.3	97.6	97.9	98.4	98.9	99.5	100.1	100.7	101.2	101.6	101.9	102.6	103.1	102.6	102.2	131.6
16000	96.2	96.5	96.8	97.3	97.8	98.4	99.1	99.7	100.2	100.7	100.9	101.7	102.2	101.6	101.1	130.8
20000	94.7	95.0	95.5	96.0	96.6	97.3	98.0	98.6	99.2	99.6	99.9	100.7	101.1	100.4	99.7	130.0
25000	92.6	92.9	93.5	94.1	94.8	95.6	96.4	97.2	97.9	98.4	98.8	99.6	99.9	99.0	98.1	129.0
31500	90.2	90.5	91.0	91.6	92.3	93.2	94.1	95.1	96.0	96.7	97.2	98.0	98.4	97.4	96.2	127.6
40000	88.3	88.5	88.9	89.3	89.9	90.5	91.3	92.2	93.1	94.0	94.7	95.7	96.1	94.9	93.5	125.9
50000	86.4	86.7	87.0	87.5	88.0	88.5	89.1	89.7	90.3	91.0	91.6	92.7	93.1	92.0	90.4	124.2
63000	83.8	84.1	84.5	85.0	85.5	86.1	86.7	87.3	87.8	88.1	88.4	89.1	89.6	88.5	87.0	122.9
80000	80.1	80.4	80.8	81.4	82.0	82.7	83.4	84.1	84.6	85.0	85.2	85.6	86.0	84.9	83.3	121.8
OVERALL	109.7	109.9	110.2	110.5	110.9	111.3	111.8	112.2	112.6	112.9	113.1	113.7	114.4	114.1	113.3	143.2
PNL	121.7	121.9	122.1	122.4	122.7	123.0	123.3	123.6	123.8	124.0	124.2	124.8	125.7	125.5	124.6	
PNLT	121.7	121.9	122.1	122.4	122.7	123.0	123.3	123.6	123.8	124.0	124.2	124.8	125.7	125.5	124.6	

Table B-10. Computational Acoustic Data for Pressure Ratio 3.62 : Mixing Noise Component

ANGLE	20	30	40	50	60	70	80	90	100	110	120	130	140	150	160	PWL
FREQ																
50	0.0	0.0	0.0	0.0	0.0	0.0	0.0	0.0	0.0	0.0	0.0	0.0	0.0	0.0	0.0	30.5
63	35.8	35.8	35.8	35.8	35.8	35.8	35.8	35.8	35.8	35.8	35.8	35.8	35.8	35.8	35.8	66.3
80	36.5	36.5	36.5	36.5	36.5	36.5	36.5	36.5	36.5	36.5	36.5	36.5	36.5	36.5	36.5	67.0
100	40.6	40.6	40.6	40.6	40.6	40.6	40.6	40.6	40.6	40.6	40.6	40.6	40.6	40.6	40.6	71.0
125	38.9	38.9	38.9	38.9	38.9	38.9	38.9	38.9	38.9	38.9	38.9	38.9	38.9	38.9	38.9	69.4
160	39.5	39.5	39.5	39.5	39.5	39.5	39.5	39.5	39.5	39.5	39.5	39.5	39.5	39.5	39.5	70.0
200	40.5	40.5	40.5	40.5	40.5	40.5	40.5	40.5	40.5	40.5	40.5	40.5	40.5	40.5	40.5	70.9
250	41.6	41.6	41.6	41.6	41.6	41.6	41.6	41.6	41.6	41.6	41.6	41.6	41.6	41.6	41.6	72.1
315	42.8	42.8	42.8	42.8	42.8	42.8	42.8	42.8	42.8	42.8	42.8	42.8	42.8	42.8	42.8	73.2
400	43.5	43.5	43.5	43.5	43.5	43.5	43.5	43.5	43.5	43.5	43.5	43.5	43.5	43.5	43.5	73.9
500	44.6	44.6	44.6	44.6	44.6	44.6	44.6	44.6	44.6	44.6	44.6	44.6	44.6	44.6	44.6	75.1
630	45.8	45.8	45.8	45.8	45.8	45.8	45.8	45.8	45.8	45.8	45.8	45.8	45.8	45.8	45.8	76.3
800	46.5	46.5	46.5	46.5	46.5	46.5	46.5	46.5	46.5	46.5	46.5	46.5	46.5	46.5	46.5	77.0
1000	47.4	47.4	47.4	47.4	47.4	47.4	47.4	47.4	47.4	47.4	47.4	47.4	47.4	47.4	47.4	77.9
1250	48.9	48.9	48.9	48.9	48.9	48.9	48.9	48.9	48.9	48.9	48.9	48.9	48.9	48.9	48.9	79.4
1600	49.5	49.5	49.5	49.5	49.5	49.5	49.5	49.5	49.5	49.5	49.5	49.5	49.5	49.5	49.5	80.0
2000	82.4	78.4	72.8	65.2	56.2	50.8	50.4	50.4	50.4	50.4	50.4	50.4	50.4	50.4	50.4	100.5
2500	109.2	107.5	104.9	101.0	95.8	88.9	80.4	70.3	59.3	52.0	51.6	51.6	51.6	51.6	51.6	129.6
3150	115.6	115.5	115.0	113.9	112.0	109.0	104.7	99.0	92.1	84.1	75.4	66.7	58.9	54.1	52.8	139.8
4000	109.5	110.9	112.4	113.7	114.5	114.3	113.1	110.7	106.9	102.1	96.5	90.5	84.6	79.3	75.1	141.1
5000	104.1	103.6	104.2	106.5	109.4	111.9	113.4	113.8	112.8	110.7	107.6	103.8	99.9	96.2	93.2	140.6
6300	109.1	109.0	108.6	107.7	106.6	106.7	108.8	111.3	112.7	112.9	111.9	110.1	107.8	105.5	103.5	140.6
8000	107.0	107.2	107.6	108.0	108.3	108.1	107.6	107.7	109.3	110.9	111.7	111.5	110.5	109.3	108.0	139.9
10000	104.7	105.0	105.5	106.1	106.7	107.3	107.8	107.9	108.0	108.8	110.0	110.7	110.7	110.3	109.7	139.1
12500	103.9	104.1	104.2	104.5	105.0	105.7	106.6	107.4	107.9	108.4	109.0	109.7	110.2	110.3	110.2	138.5
16000	102.2	102.4	102.6	102.8	103.2	103.6	104.2	105.0	105.9	106.8	107.5	108.2	108.7	109.0	109.0	137.0
20000	101.0	101.2	101.3	101.6	101.9	102.3	102.8	103.4	104.2	105.2	106.2	107.0	107.6	108.0	108.2	136.0
25000	99.8	99.9	100.1	100.4	100.7	101.1	101.5	102.1	102.8	103.6	104.6	105.6	106.4	106.9	107.2	135.0
31500	98.4	98.5	98.7	99.0	99.3	99.7	100.1	100.6	101.2	102.0	103.0	104.0	104.9	105.5	105.9	134.1
40000	96.3	96.4	96.6	96.9	97.2	97.6	98.0	98.5	99.1	99.8	100.7	101.7	102.7	103.4	103.8	132.7
50000	94.3	94.4	94.7	95.0	95.3	95.6	96.1	96.6	97.2	97.9	98.7	99.6	100.6	101.3	101.8	131.8
63000	89.3	90.0	90.9	91.7	92.5	92.9	93.2	93.9	94.4	94.9	95.9	96.7	97.7	98.5	99.0	130.4
80000	0.0	0.0	0.0	0.0	0.0	0.0	0.0	0.0	0.0	0.0	0.0	0.0	0.0	0.0	0.0	30.5
OVERALL	119.0	119.0	119.0	119.0	119.0	118.9	118.9	118.8	118.8	118.7	118.5	118.4	118.1	117.8	117.6	149.6
PNL	131.6	131.4	131.1	130.4	130.6	130.3	129.4	128.8	127.8	126.7	125.5	123.7	121.5	119.8	118.5	
PNLT	134.9	134.5	137.8	137.1	134.2	133.4	131.5	132.1	130.6	129.1	126.8	125.9	123.3	121.2	119.6	

Table B-11 Computational Acoustic Data for Pressure Ratio 3.62 : Shock Noise Component

ANGLE	20	30	40	50	60	70	80	90	100	110	120	130	140	150	160	PWL
FREQ																
50	39.2	39.2	39.2	39.2	39.2	39.3	39.4	39.5	39.7	40.0	40.3	40.7	41.3	42.7	44.4	70.7
63	44.8	44.8	44.8	44.8	44.8	44.8	44.9	45.0	45.2	45.5	45.8	46.1	46.7	47.9	49.6	76.1
80	49.5	49.5	49.5	49.5	49.5	49.6	49.7	49.8	50.0	50.3	50.6	51.0	51.6	52.9	54.6	80.9
100	54.2	54.2	54.2	54.2	54.2	54.3	54.4	54.5	54.7	55.0	55.3	55.8	56.3	57.6	59.3	85.7
125	58.7	58.7	58.7	58.7	58.8	58.8	58.9	59.1	59.3	59.6	59.9	60.4	60.9	62.3	63.9	90.2
160	63.7	63.7	63.8	63.8	63.8	63.9	64.0	64.2	64.4	64.7	65.1	65.5	66.1	67.4	69.0	95.3
200	68.1	68.2	68.2	68.2	68.3	68.4	68.5	68.7	68.9	69.2	69.6	70.0	70.6	72.0	73.5	99.8
250	72.4	72.4	72.4	72.5	72.5	72.6	72.8	73.0	73.2	73.6	74.0	74.4	75.0	76.4	77.8	104.1
315	76.5	76.5	76.5	76.6	76.7	76.8	77.0	77.2	77.5	77.9	78.3	78.7	79.4	80.7	82.1	108.4
400	80.3	80.4	80.4	80.5	80.6	80.8	81.0	81.3	81.6	82.0	82.4	82.9	83.6	85.0	86.2	112.5
500	83.6	83.6	83.7	83.8	84.0	84.1	84.4	84.7	85.0	85.4	85.9	86.4	87.1	88.5	89.6	115.9
630	86.6	86.7	86.8	86.9	87.0	87.2	87.5	87.8	88.1	88.5	89.0	89.6	90.4	91.8	92.6	119.0
800	89.5	89.5	89.6	89.7	89.9	90.0	90.3	90.6	90.9	91.3	91.8	92.4	93.3	94.6	95.2	121.8
1000	92.0	92.0	92.1	92.2	92.3	92.5	92.7	92.9	93.2	93.6	94.1	94.6	95.5	96.8	97.1	124.1
1250	94.2	94.2	94.3	94.4	94.5	94.7	94.9	95.1	95.3	95.7	96.1	96.5	97.5	98.6	98.6	126.2
1600	96.3	96.3	96.4	96.5	96.7	96.8	97.0	97.2	97.4	97.7	98.0	98.4	99.5	100.3	100.0	128.2
2000	97.9	97.9	98.0	98.1	98.3	98.5	98.7	98.9	99.1	99.3	99.6	100.0	101.1	101.6	101.0	129.7
2500	109.6	108.1	105.9	103.3	101.1	100.1	100.0	100.2	100.4	100.6	100.9	101.3	102.4	102.6	101.7	133.3
3150	115.7	115.6	115.1	114.1	112.3	109.6	106.2	103.3	101.9	101.8	101.9	102.3	103.4	103.2	102.1	140.4
4000	110.0	111.3	112.7	113.9	114.7	114.6	113.4	111.2	108.2	105.3	103.5	103.3	104.1	103.6	102.3	141.6
5000	105.5	105.3	105.8	107.6	110.1	112.3	113.8	114.1	113.2	111.3	108.8	106.7	105.7	104.4	102.8	141.2
6300	109.6	109.5	109.2	108.5	107.7	107.8	109.6	111.8	113.1	113.3	112.5	111.0	109.4	107.7	106.0	141.1
8000	107.6	107.8	108.2	108.6	108.9	108.9	108.5	108.8	110.1	111.6	112.2	112.1	111.4	110.3	109.1	140.5
10000	105.5	105.9	106.3	106.9	107.5	108.1	108.6	108.8	109.0	109.7	110.7	111.4	111.5	111.1	110.5	139.7
12500	104.8	104.9	105.2	105.5	105.9	106.6	107.4	108.2	108.8	109.2	109.8	110.5	111.0	111.0	110.8	138.9
16000	103.2	103.4	103.6	103.9	104.3	104.7	105.3	106.1	107.0	107.7	108.4	109.1	109.6	109.7	109.7	137.3
20000	101.9	102.1	102.3	102.7	103.0	103.5	104.0	104.6	105.4	106.3	107.1	107.9	108.5	108.7	108.7	136.1
25000	100.6	100.7	101.0	101.3	101.7	102.2	102.7	103.3	104.0	104.8	105.6	106.6	107.3	107.6	107.7	134.8
31500	99.0	99.2	99.4	99.7	100.1	100.5	101.1	101.7	102.4	103.1	104.0	105.0	105.8	106.2	106.4	133.2
40000	96.9	97.1	97.3	97.6	97.9	98.3	98.8	99.4	100.1	100.8	101.7	102.7	103.5	104.0	104.2	131.0
50000	94.9	95.1	95.4	95.7	96.0	96.4	96.9	97.4	98.0	98.7	99.5	100.4	101.3	101.8	102.1	128.9
63000	90.3	91.0	91.8	92.6	93.3	93.7	94.1	94.7	95.2	95.8	96.6	97.4	98.3	98.9	99.3	125.9
80000	80.1	80.4	80.8	81.4	82.0	82.7	83.4	84.1	84.6	85.0	85.2	85.6	86.0	84.9	83.3	114.3
OVERALL	119.5	119.5	119.5	119.6	119.6	119.6	119.7	119.7	119.7	119.7	119.6	119.6	119.7	119.4	118.9	150.1
PNL	133.0	133.0	132.7	132.2	132.5	132.4	131.7	131.4	130.9	130.3	129.7	128.9	128.3	127.4	126.3	
PNLT	136.3	135.9	135.2	134.0	135.2	134.5	131.7	131.4	130.9	130.3	129.7	128.9	128.3	127.4	126.3	

Table B-12. Computational Acoustic Data for Pressure Ratio 3.62 : Total Noise Levels

ANGLE	20	30	40	50	60	70	80	90	100	110	120	130	140	150	160	PWL
FREQ																
50	39.2	39.2	39.1	39.1	39.1	39.1	39.2	39.3	39.5	39.7	40.0	40.4	41.0	42.5	44.3	70.9
63	44.1	44.1	44.1	44.1	44.1	44.1	44.2	44.3	44.5	44.7	45.0	45.4	46.0	47.5	49.3	75.9
80	49.3	49.2	49.2	49.2	49.2	49.2	49.3	49.4	49.6	49.8	50.2	50.5	51.2	52.6	54.3	81.0
100	54.0	54.0	54.0	54.0	54.0	54.0	54.1	54.2	54.4	54.6	54.9	55.3	55.9	57.4	59.1	85.8
125	58.7	58.7	58.7	58.7	58.7	58.7	58.8	58.9	59.1	59.3	59.7	60.1	60.7	62.1	63.8	90.5
160	63.8	63.8	63.8	63.8	63.8	63.8	63.9	64.0	64.2	64.5	64.8	65.2	65.8	67.3	68.9	95.6
200	68.2	68.2	68.2	68.2	68.3	68.3	68.4	68.6	68.8	69.0	69.4	69.8	70.4	71.8	73.4	100.2
250	72.5	72.5	72.5	72.6	72.6	72.7	72.8	72.9	73.2	73.4	73.8	74.2	74.9	76.3	77.8	104.5
315	76.7	76.7	76.7	76.8	76.8	76.9	77.1	77.3	77.5	77.8	78.2	78.6	79.3	80.7	82.1	108.9
400	80.6	80.7	80.7	80.8	80.9	81.0	81.2	81.4	81.7	82.0	82.4	82.9	83.6	85.0	86.2	113.0
500	84.0	84.0	84.1	84.2	84.3	84.5	84.7	84.9	85.2	85.6	86.0	86.5	87.3	88.7	89.8	116.6
630	87.1	87.1	87.2	87.3	87.4	87.6	87.8	88.1	88.4	88.8	89.3	89.8	90.7	92.1	92.9	119.8
800	90.0	90.0	90.1	90.2	90.3	90.5	90.7	91.0	91.3	91.7	92.2	92.7	93.7	95.0	95.6	122.7
1000	92.5	92.5	92.6	92.7	92.8	92.9	93.1	93.4	93.7	94.1	94.5	95.0	96.0	97.3	97.6	125.0
1250	94.7	94.7	94.8	94.9	95.0	95.2	95.3	95.5	95.8	96.1	96.5	97.0	98.1	99.1	99.1	127.1
1600	96.8	96.8	96.9	97.1	97.2	97.3	97.5	97.7	97.9	98.2	98.5	98.9	100.0	100.8	100.5	129.1
2000	98.3	98.4	98.5	98.7	98.8	99.0	99.2	99.4	99.6	99.8	100.0	100.4	101.6	102.0	101.4	130.7
2500	99.4	99.6	99.7	99.9	100.1	100.3	100.5	100.7	100.9	101.1	101.3	101.7	102.9	103.0	102.0	131.9
3150	100.2	100.4	100.6	100.8	101.0	101.3	101.5	101.8	102.0	102.2	102.4	102.8	103.9	103.6	102.4	132.9
4000	100.5	100.7	101.0	101.3	101.6	101.9	102.2	102.5	102.7	102.9	103.1	103.6	104.5	103.9	102.5	133.5
5000	100.4	100.6	101.0	101.3	101.7	102.2	102.5	102.9	103.1	103.3	103.4	104.0	104.7	104.0	102.5	133.8
6300	99.9	100.2	100.5	101.0	101.5	102.0	102.5	102.9	103.2	103.4	103.5	104.1	104.7	103.9	102.6	133.7
8000	99.3	99.6	99.9	100.4	100.9	101.4	102.0	102.5	103.0	103.2	103.3	104.0	104.5	103.7	102.8	133.5
10000	98.7	98.9	99.3	99.7	100.2	100.8	101.3	101.9	102.4	102.8	102.9	103.6	104.1	103.4	102.7	133.1
12500	98.0	98.2	98.6	99.0	99.5	100.0	100.6	101.2	101.7	102.1	102.3	103.0	103.4	102.8	102.4	132.5
16000	96.8	97.1	97.5	98.0	98.5	99.1	99.7	100.3	100.8	101.2	101.4	102.2	102.5	101.9	101.4	131.8
20000	95.2	95.5	96.0	96.6	97.2	97.9	98.6	99.3	99.8	100.3	100.5	101.3	101.5	100.8	100.1	131.0
25000	93.0	93.4	93.9	94.5	95.3	96.1	97.0	97.8	98.5	99.1	99.4	100.2	100.4	99.5	98.5	129.9
31500	91.0	91.3	91.7	92.3	92.9	93.7	94.6	95.5	96.4	97.2	97.7	98.6	98.8	97.7	96.5	128.5
40000	89.0	89.3	89.7	90.2	90.8	91.4	92.1	92.8	93.6	94.4	95.0	96.2	96.4	95.3	93.9	126.8
50000	86.6	86.9	87.4	87.9	88.6	89.3	89.9	90.6	91.2	91.7	92.1	93.2	93.6	92.5	91.1	125.3
63000	83.0	83.4	83.9	84.6	85.4	86.2	87.1	87.9	88.5	88.9	89.2	90.1	90.6	89.5	87.9	123.9
80000	77.9	78.4	79.1	79.9	80.8	81.8	82.8	83.8	84.7	85.4	85.7	86.7	87.0	85.8	84.1	122.4
OVERALL	110.2	110.4	110.7	111.0	111.4	111.8	112.3	112.7	113.0	113.3	113.5	114.2	114.8	114.4	113.6	144.0
PNL	122.1	122.3	122.5	122.8	123.1	123.4	123.7	124.0	124.3	124.5	124.7	125.2	126.1	125.8	124.9	
PNLT	122.1	122.3	122.5	122.8	123.1	123.4	123.7	124.0	124.3	124.5	124.7	125.2	126.1	125.8	124.9	

Table B-13. Computational Acoustic Data for Pressure Ratio 4.0 : Mixing Noise Component

ANGLE	20	30	40	50	60	70	80	90	100	110	120	130	140	150	160	PWL
FREQ																
50	0.0	0.0	0.0	0.0	0.0	0.0	0.0	0.0	0.0	0.0	0.0	0.0	0.0	0.0	0.0	30.9
63	35.8	35.8	35.8	35.8	35.8	35.8	35.8	35.8	35.8	35.8	35.8	35.8	35.8	35.8	35.8	66.7
80	36.5	36.5	36.5	36.5	36.5	36.5	36.5	36.5	36.5	36.5	36.5	36.5	36.5	36.5	36.5	67.4
100	40.6	40.6	40.6	40.6	40.6	40.6	40.6	40.6	40.6	40.6	40.6	40.6	40.6	40.6	40.6	71.5
125	38.9	38.9	38.9	38.9	38.9	38.9	38.9	38.9	38.9	38.9	38.9	38.9	38.9	38.9	38.9	69.8
160	39.5	39.5	39.5	39.5	39.5	39.5	39.5	39.5	39.5	39.5	39.5	39.5	39.5	39.5	39.5	70.4
200	40.5	40.5	40.5	40.5	40.5	40.5	40.5	40.5	40.5	40.5	40.5	40.5	40.5	40.5	40.5	71.4
250	41.6	41.6	41.6	41.6	41.6	41.6	41.6	41.6	41.6	41.6	41.6	41.6	41.6	41.6	41.6	72.5
315	42.8	42.8	42.8	42.8	42.8	42.8	42.8	42.8	42.8	42.8	42.8	42.8	42.8	42.8	42.8	73.7
400	43.5	43.5	43.5	43.5	43.5	43.5	43.5	43.5	43.5	43.5	43.5	43.5	43.5	43.5	43.5	74.4
500	44.6	44.6	44.6	44.6	44.6	44.6	44.6	44.6	44.6	44.6	44.6	44.6	44.6	44.6	44.6	75.5
630	45.8	45.8	45.8	45.8	45.8	45.8	45.8	45.8	45.8	45.8	45.8	45.8	45.8	45.8	45.8	76.7
800	46.5	46.5	46.5	46.5	46.5	46.5	46.5	46.5	46.5	46.5	46.5	46.5	46.5	46.5	46.5	77.4
1000	47.4	47.4	47.4	47.4	47.4	47.4	47.4	47.4	47.4	47.4	47.4	47.4	47.4	47.4	47.4	78.4
1250	48.9	48.9	48.9	48.9	48.9	48.9	48.9	48.9	48.9	48.9	48.9	48.9	48.9	48.9	48.9	79.8
1600	51.1	49.8	49.5	49.5	49.5	49.5	49.5	49.5	49.5	49.5	49.5	49.5	49.5	49.5	49.5	80.5
2000	95.5	92.3	87.6	81.1	72.6	62.2	52.3	50.4	50.4	50.4	50.4	50.4	50.4	50.4	50.4	114.5
2500	113.3	112.2	110.5	107.7	103.7	98.0	90.7	81.7	71.2	59.8	52.1	51.6	51.6	51.6	51.6	135.3
3150	113.9	114.5	114.9	114.9	114.1	112.2	109.1	104.5	98.4	91.2	83.1	74.7	66.7	59.9	55.6	141.2
4000	103.1	105.2	107.8	110.4	112.5	113.7	113.8	112.5	109.7	105.7	100.7	95.1	89.5	84.4	80.3	140.9
5000	106.8	105.8	104.4	103.4	105.0	108.4	111.3	112.9	113.1	111.8	109.4	106.1	102.5	99.0	96.2	140.4
6300	108.1	108.4	108.6	108.4	107.6	106.4	106.4	108.7	111.1	112.3	112.1	110.8	108.9	106.8	105.0	140.5
8000	105.7	106.0	106.3	106.8	107.3	107.7	107.6	107.1	107.6	109.4	110.7	111.1	110.6	109.6	108.5	139.6
10000	103.6	103.7	104.0	104.6	105.4	106.2	106.9	107.3	107.4	107.8	108.8	109.8	110.2	110.0	109.6	138.7
12500	103.0	103.1	103.4	103.6	103.9	104.4	105.3	106.2	107.0	107.6	108.1	108.8	109.4	109.7	109.7	138.0
16000	101.3	101.5	101.7	101.9	102.2	102.6	103.1	103.8	104.8	105.8	106.6	107.3	107.9	108.3	108.4	136.5
20000	100.1	100.3	100.4	100.7	101.0	101.4	101.8	102.4	103.1	104.1	105.1	106.1	106.8	107.3	107.5	135.5
25000	98.9	99.0	99.2	99.5	99.8	100.2	100.6	101.1	101.8	102.6	103.6	104.6	105.5	106.1	106.5	134.6
31500	97.5	97.6	97.8	98.1	98.4	98.8	99.2	99.7	100.3	101.1	102.0	103.0	104.0	104.7	105.2	133.6
40000	95.4	95.5	95.7	96.0	96.3	96.7	97.1	97.6	98.2	98.9	99.7	100.7	101.7	102.5	103.1	132.2
50000	92.9	93.2	93.6	94.0	94.4	94.7	95.2	95.7	96.3	96.9	97.8	98.7	99.7	100.5	101.1	131.3
63000	85.5	86.8	88.2	89.6	90.9	91.9	92.4	92.9	93.4	94.0	95.0	95.8	96.9	97.8	98.3	129.8
80000	0.0	0.0	0.0	0.0	0.0	0.0	0.0	0.0	0.0	0.0	0.0	0.0	0.0	0.0	0.0	30.9
OVERALL	118.6	118.6	118.6	118.6	118.5	118.5	118.5	118.4	118.4	118.3	118.2	118.0	117.8	117.5	117.3	149.6
PNL	130.6	130.9	131.1	131.0	130.4	130.1	129.9	128.8	128.2	127.0	126.0	124.5	122.6	120.6	119.2	
PNLT	135.0	134.8	134.6	134.1	137.1	133.8	133.2	131.0	131.4	129.4	128.2	125.7	124.7	122.4	120.7	

Table B-14. Computational Acoustic Data for Pressure Ratio 4.0 : Shock Noise Component

ANGLE	20	30	40	50	60	70	80	90	100	110	120	130	140	150	160	PWL
FREQ																
50	39.2	39.2	39.1	39.1	39.1	39.1	39.2	39.3	39.5	39.7	40.0	40.4	41.0	42.5	44.3	70.9
63	44.7	44.7	44.7	44.7	44.7	44.7	44.8	44.9	45.0	45.2	45.5	45.9	46.4	47.8	49.4	76.4
80	49.5	49.5	49.5	49.4	49.4	49.5	49.5	49.6	49.8	50.0	50.3	50.7	51.3	52.7	54.4	81.2
100	54.2	54.2	54.2	54.2	54.2	54.2	54.3	54.4	54.5	54.8	55.1	55.5	56.1	57.5	59.1	85.9
125	58.7	58.7	58.7	58.7	58.7	58.7	58.8	58.9	59.1	59.4	59.7	60.1	60.7	62.1	63.8	90.5
160	63.8	63.8	63.8	63.8	63.8	63.8	63.9	64.0	64.2	64.5	64.8	65.2	65.8	67.3	68.9	95.6
200	68.2	68.2	68.2	68.2	68.3	68.3	68.4	68.6	68.8	69.0	69.4	69.8	70.4	71.9	73.4	100.2
250	72.5	72.5	72.5	72.6	72.6	72.7	72.8	72.9	73.2	73.5	73.8	74.2	74.9	76.3	77.8	104.5
315	76.7	76.7	76.7	76.8	76.8	76.9	77.1	77.3	77.5	77.8	78.2	78.6	79.3	80.7	82.1	108.9
400	80.6	80.7	80.7	80.8	80.9	81.0	81.2	81.4	81.7	82.0	82.4	82.9	83.6	85.0	86.2	113.0
500	84.0	84.0	84.1	84.2	84.3	84.5	84.7	84.9	85.2	85.6	86.0	86.5	87.3	88.7	89.8	116.5
630	87.1	87.1	87.2	87.3	87.4	87.6	87.8	88.1	88.4	88.8	89.3	89.8	90.7	92.1	92.9	119.8
800	90.0	90.0	90.1	90.2	90.3	90.5	90.7	91.0	91.3	91.7	92.2	92.8	93.7	95.0	95.6	122.7
1000	92.5	92.5	92.6	92.7	92.8	92.9	93.1	93.4	93.7	94.1	94.5	95.0	96.0	97.3	97.6	125.0
1250	94.7	94.7	94.8	94.9	95.0	95.2	95.3	95.5	95.8	96.1	96.5	97.0	98.1	99.1	99.1	127.1
1600	96.8	96.8	96.9	97.1	97.2	97.3	97.5	97.7	97.9	98.2	98.5	98.9	100.0	100.8	100.5	129.1
2000	100.1	99.4	98.9	98.7	98.8	99.0	99.2	99.4	99.6	99.8	100.0	100.4	101.6	102.0	101.4	130.7
2500	113.4	112.5	110.8	108.4	105.2	102.3	101.0	100.8	100.9	101.1	101.3	101.7	102.9	103.0	102.0	136.9
3150	114.1	114.7	115.1	115.1	114.3	112.6	109.8	106.3	103.6	102.5	102.4	102.8	103.9	103.6	102.4	141.7
4000	105.0	106.5	108.6	110.9	112.8	114.0	114.1	112.9	110.5	107.6	105.1	104.2	104.6	104.0	102.5	141.5
5000	107.7	107.0	106.0	105.5	106.7	109.3	111.9	113.3	113.5	112.4	110.4	108.2	106.8	105.2	103.4	141.1
6300	108.7	109.0	109.2	109.1	108.6	107.7	107.8	109.7	111.8	112.8	112.6	111.7	110.3	108.6	107.0	141.2
8000	106.6	106.9	107.2	107.7	108.2	108.6	108.6	108.4	108.9	110.3	111.4	111.8	111.5	110.6	109.5	140.4
10000	104.8	105.0	105.3	105.8	106.5	107.3	107.9	108.4	108.6	109.0	109.8	110.7	111.1	110.9	110.4	139.5
12500	104.2	104.4	104.6	104.9	105.3	105.8	106.6	107.4	108.1	108.7	109.1	109.8	110.4	110.5	110.4	138.7
16000	102.7	102.8	103.1	103.4	103.8	104.2	104.8	105.4	106.2	107.1	107.8	108.5	109.0	109.2	109.2	137.2
20000	101.3	101.5	101.8	102.1	102.5	103.0	103.5	104.1	104.8	105.6	106.4	107.3	107.9	108.1	108.2	136.0
25000	99.9	100.1	100.4	100.7	101.1	101.6	102.2	102.8	103.5	104.2	105.0	106.0	106.7	107.0	107.1	134.6
31500	98.4	98.5	98.8	99.1	99.5	99.9	100.5	101.1	101.8	102.5	103.3	104.3	105.1	105.5	105.7	133.0
40000	96.3	96.5	96.7	97.0	97.4	97.8	98.3	98.9	99.5	100.2	101.0	102.0	102.8	103.3	103.6	130.8
50000	93.8	94.2	94.5	94.9	95.4	95.8	96.3	96.9	97.4	98.1	98.8	99.8	100.6	101.2	101.5	128.7
63000	87.4	88.4	89.6	90.8	92.0	92.9	93.6	94.1	94.6	95.2	96.0	96.8	97.8	98.4	98.7	125.6
80000	77.9	78.4	79.1	79.9	80.8	81.8	82.8	83.8	84.7	85.4	85.7	86.7	87.0	85.8	84.1	114.9
OVERALL	119.2	119.2	119.2	119.3	119.3	119.4	119.4	119.5	119.5	119.5	119.4	119.5	119.6	119.3	118.8	150.3
PNL	132.1	132.4	132.7	132.7	132.3	132.1	132.1	131.5	131.2	130.5	130.0	129.4	128.9	128.0	126.9	
PNLT	136.0	136.0	135.9	135.4	134.0	134.8	134.1	131.5	131.2	130.5	130.0	129.4	128.9	128.0	126.9	

Table B-15. Computational Acoustic Data for Pressure Ratio 4.0 : Total Noise Levels

ANGLE	20	30	40	50	60	70	80	90	100	110	120	130	140	150	160	PWL
FREQ																
50	39.1	39.1	39.1	39.0	39.0	39.0	39.0	39.0	39.1	39.3	39.6	39.9	40.6	42.3	44.2	71.2
63	44.1	44.1	44.0	44.0	44.0	43.9	44.0	44.0	44.1	44.3	44.6	44.9	45.6	47.3	49.1	76.2
80	49.3	49.2	49.2	49.1	49.1	49.1	49.1	49.1	49.3	49.5	49.7	50.1	50.8	52.4	54.2	81.3
100	54.0	54.0	53.9	53.9	53.9	53.9	53.9	53.9	54.0	54.2	54.5	54.9	55.6	57.2	59.0	86.1
125	58.7	58.7	58.7	58.6	58.6	58.6	58.6	58.7	58.8	59.0	59.3	59.6	60.3	61.9	63.7	90.8
160	63.9	63.9	63.8	63.8	63.8	63.8	63.8	63.9	64.0	64.2	64.5	64.8	65.5	67.1	68.8	96.0
200	68.4	68.4	68.4	68.3	68.3	68.3	68.4	68.4	68.6	68.8	69.1	69.5	70.2	71.8	73.3	100.6
250	72.8	72.8	72.8	72.8	72.8	72.8	72.8	72.9	73.1	73.3	73.6	74.0	74.7	76.3	77.8	105.0
315	77.1	77.1	77.1	77.1	77.1	77.2	77.3	77.4	77.5	77.8	78.1	78.5	79.2	80.8	82.2	109.5
400	81.3	81.3	81.3	81.3	81.4	81.5	81.6	81.7	81.9	82.2	82.5	82.9	83.7	85.2	86.5	113.8
500	84.8	84.8	84.9	84.9	85.0	85.1	85.2	85.4	85.7	86.0	86.3	86.8	87.6	89.1	90.2	117.6
630	88.0	88.1	88.1	88.2	88.3	88.5	88.6	88.9	89.1	89.5	89.9	90.3	91.2	92.7	93.6	121.0
800	91.0	91.0	91.1	91.2	91.3	91.5	91.7	92.0	92.3	92.6	93.1	93.6	94.6	95.9	96.5	124.1
1000	93.4	93.5	93.6	93.7	93.8	94.0	94.2	94.4	94.7	95.1	95.5	96.1	97.2	98.4	98.7	126.6
1250	95.6	95.6	95.7	95.8	96.0	96.2	96.4	96.6	96.9	97.2	97.6	98.1	99.3	100.3	100.3	128.7
1600	97.5	97.6	97.8	97.9	98.1	98.3	98.5	98.7	98.9	99.2	99.6	100.1	101.3	102.0	101.5	130.6
2000	98.9	99.0	99.2	99.4	99.6	99.8	100.1	100.3	100.5	100.8	101.1	101.6	102.8	103.1	102.3	132.1
2500	99.8	99.9	100.1	100.4	100.7	101.0	101.3	101.6	101.8	102.1	102.3	102.8	103.9	103.9	102.7	133.2
3150	100.2	100.4	100.7	101.0	101.4	101.7	102.1	102.4	102.8	103.0	103.3	103.8	104.8	104.3	102.9	134.0
4000	100.3	100.5	100.8	101.2	101.6	102.1	102.5	102.9	103.3	103.6	103.8	104.5	105.2	104.4	102.7	134.4
5000	100.0	100.2	100.6	101.0	101.5	102.0	102.5	103.0	103.4	103.8	104.0	104.7	105.3	104.2	102.3	134.5
6300	99.4	99.7	100.0	100.5	101.0	101.6	102.2	102.7	103.2	103.6	103.8	104.6	105.0	103.7	102.0	134.2
8000	98.7	99.0	99.4	99.8	100.4	101.0	101.6	102.2	102.7	103.1	103.4	104.2	104.4	103.2	101.6	133.7
10000	98.0	98.3	98.6	99.1	99.6	100.2	100.9	101.5	102.0	102.5	102.7	103.6	103.8	102.6	101.3	133.2
12500	97.1	97.4	97.7	98.2	98.8	99.4	100.0	100.7	101.2	101.7	102.0	102.8	103.0	101.9	100.9	132.5
16000	96.0	96.3	96.6	97.1	97.7	98.3	98.9	99.6	100.2	100.7	100.9	101.8	101.9	100.9	99.9	131.6
20000	95.0	95.3	95.6	96.1	96.6	97.2	97.8	98.5	99.1	99.6	99.9	100.7	100.8	99.7	98.7	130.8
25000	93.7	94.0	94.4	94.9	95.5	96.1	96.7	97.3	97.8	98.3	98.6	99.5	99.6	98.4	97.3	129.9
31500	91.7	92.1	92.6	93.1	93.8	94.5	95.3	95.9	96.5	96.9	97.2	98.0	98.1	97.0	95.8	129.0
40000	88.9	89.3	89.8	90.5	91.3	92.2	93.0	93.9	94.7	95.2	95.5	96.4	96.5	95.3	93.8	127.9
50000	85.6	86.0	86.6	87.4	88.2	89.2	90.2	91.2	92.1	92.9	93.4	94.3	94.5	93.2	91.4	126.5
63000	81.2	81.7	82.4	83.2	84.2	85.2	86.3	87.5	88.5	89.4	90.1	91.3	91.5	90.0	88.0	124.6
80000	74.9	75.6	76.4	77.4	78.6	79.9	81.2	82.5	83.7	84.8	85.6	86.9	87.2	85.6	83.3	122.2
OVERALL	110.1	110.3	110.6	111.0	111.4	111.8	112.3	112.8	113.2	113.6	113.9	114.6	115.2	114.5	113.4	144.7
PNL	122.1	122.3	122.5	122.9	123.2	123.6	124.0	124.4	124.8	125.1	125.4	126.0	126.8	126.3	125.1	
PNLT	122.1	122.3	122.5	122.9	123.2	123.6	124.0	124.4	124.8	125.1	125.4	126.0	126.8	126.3	125.1	

Table B-16. Computational Acoustic Data for Pressure Ratio 4.5 : Mixing Noise Component

ANGLE	20	30	40	50	60	70	80	90	100	110	120	130	140	150	160	PWL
FREQ																
50	0.0	0.0	0.0	0.0	0.0	0.0	0.0	0.0	0.0	0.0	0.0	0.0	0.0	0.0	0.0	31.4
63	35.8	35.8	35.8	35.8	35.8	35.8	35.8	35.8	35.8	35.8	35.8	35.8	35.8	35.8	35.8	67.2
80	36.5	36.5	36.5	36.5	36.5	36.5	36.5	36.5	36.5	36.5	36.5	36.5	36.5	36.5	36.5	67.9
100	40.6	40.6	40.6	40.6	40.6	40.6	40.6	40.6	40.6	40.6	40.6	40.6	40.6	40.6	40.6	72.0
125	38.9	38.9	38.9	38.9	38.9	38.9	38.9	38.9	38.9	38.9	38.9	38.9	38.9	38.9	38.9	70.3
160	39.5	39.5	39.5	39.5	39.5	39.5	39.5	39.5	39.5	39.5	39.5	39.5	39.5	39.5	39.5	70.9
200	40.5	40.5	40.5	40.5	40.5	40.5	40.5	40.5	40.5	40.5	40.5	40.5	40.5	40.5	40.5	71.9
250	41.6	41.6	41.6	41.6	41.6	41.6	41.6	41.6	41.6	41.6	41.6	41.6	41.6	41.6	41.6	73.0
315	42.8	42.8	42.8	42.8	42.8	42.8	42.8	42.8	42.8	42.8	42.8	42.8	42.8	42.8	42.8	74.2
400	43.5	43.5	43.5	43.5	43.5	43.5	43.5	43.5	43.5	43.5	43.5	43.5	43.5	43.5	43.5	74.9
500	44.6	44.6	44.6	44.6	44.6	44.6	44.6	44.6	44.6	44.6	44.6	44.6	44.6	44.6	44.6	76.0
630	45.8	45.8	45.8	45.8	45.8	45.8	45.8	45.8	45.8	45.8	45.8	45.8	45.8	45.8	45.8	77.2
800	46.5	46.5	46.5	46.5	46.5	46.5	46.5	46.5	46.5	46.5	46.5	46.5	46.5	46.5	46.5	77.9
1000	47.4	47.4	47.4	47.4	47.4	47.4	47.4	47.4	47.4	47.4	47.4	47.4	47.4	47.4	47.4	78.9
1250	48.9	48.9	48.9	48.9	48.9	48.9	48.9	48.9	48.9	48.9	48.9	48.9	48.9	48.9	48.9	80.3
1600	80.3	75.7	68.9	59.8	51.1	49.5	49.5	49.5	49.5	49.5	49.5	49.5	49.5	49.5	49.5	98.9
2000	108.8	107.0	103.9	99.4	93.1	84.8	74.2	61.6	51.3	50.4	50.4	50.4	50.4	50.4	50.4	129.8
2500	115.2	115.2	114.8	113.8	111.7	108.1	102.8	95.7	86.8	76.4	65.1	54.9	51.6	51.6	51.6	140.4
3150	107.3	109.2	111.3	113.2	114.4	114.6	113.3	110.5	106.0	100.1	93.0	85.3	77.7	70.8	65.4	141.8
4000	102.3	100.8	100.2	102.7	106.9	110.5	112.9	113.6	112.5	109.9	105.9	101.1	96.0	91.1	87.2	140.7
5000	108.8	108.7	108.2	107.0	105.0	104.0	106.9	110.4	112.4	112.7	111.4	109.0	105.9	102.8	100.0	140.7
6300	106.6	106.8	107.2	107.8	108.3	108.0	106.9	106.4	108.5	110.9	111.9	111.6	110.3	108.6	106.9	140.6
8000	103.8	104.2	104.8	105.4	106.1	106.8	107.4	107.4	107.1	107.8	109.4	110.5	110.6	110.1	109.2	139.5
10000	103.0	103.2	103.3	103.5	103.9	104.7	105.7	106.5	107.1	107.3	107.9	108.9	109.6	109.8	109.6	138.5
12500	102.3	102.4	102.6	102.8	103.2	103.6	104.1	105.0	106.0	106.9	107.5	108.2	108.8	109.3	109.4	137.8
16000	100.6	100.7	100.9	101.2	101.5	101.9	102.3	102.9	103.7	104.8	105.8	106.7	107.4	107.8	108.0	136.3
20000	99.4	99.5	99.7	99.9	100.3	100.6	101.1	101.6	102.3	103.2	104.2	105.3	106.2	106.8	107.1	135.3
25000	98.2	98.3	98.5	98.7	99.1	99.4	99.9	100.4	101.0	101.8	102.7	103.8	104.8	105.6	106.0	134.3
31500	96.7	96.9	97.1	97.3	97.6	98.0	98.5	99.0	99.6	100.3	101.2	102.2	103.2	104.1	104.7	133.4
40000	94.5	94.7	94.9	95.2	95.5	95.9	96.4	96.9	97.5	98.2	99.0	100.0	101.0	101.9	102.5	132.0
50000	89.9	90.8	91.7	92.6	93.3	93.9	94.4	94.9	95.5	96.2	97.0	97.9	98.9	99.8	100.5	131.0
63000	77.1	79.4	82.2	85.1	87.7	89.8	91.3	91.8	92.4	93.0	93.8	95.0	95.9	96.9	97.6	129.1
80000	0.0	0.0	0.0	0.0	0.0	0.0	0.0	0.0	0.0	0.0	0.0	0.0	0.0	0.0	0.0	31.4
OVERALL	118.4	118.4	118.5	118.5	118.5	118.5	118.4	118.4	118.3	118.3	118.2	118.0	117.8	117.6	117.3	150.0
PNL	130.9	130.8	130.6	130.2	130.9	130.8	130.0	129.9	129.0	128.1	126.8	125.6	124.1	122.4	120.7	
PNLT	134.3	133.9	137.3	136.9	134.8	134.0	132.4	133.3	131.7	129.7	129.3	128.1	125.5	122.4	122.7	

Table B-17. Computational Acoustic Data for Pressure Ratio 4.5 : Shock Noise Component

ANGLE	20	30	40	50	60	70	80	90	100	110	120	130	140	150	160	PWL
FREQ																
50	39.1	39.1	39.1	39.0	39.0	39.0	39.0	39.0	39.1	39.3	39.6	39.9	40.6	42.3	44.2	71.2
63	44.7	44.7	44.7	44.6	44.6	44.6	44.6	44.6	44.7	44.9	45.1	45.4	46.1	47.6	49.3	76.7
80	49.5	49.5	49.4	49.4	49.3	49.3	49.3	49.4	49.5	49.7	49.9	50.3	50.9	52.5	54.3	81.5
100	54.2	54.2	54.1	54.1	54.1	54.1	54.1	54.1	54.2	54.4	54.7	55.0	55.7	57.3	59.0	86.2
125	58.8	58.8	58.7	58.7	58.6	58.6	58.7	58.7	58.8	59.0	59.3	59.7	60.4	62.0	63.7	90.8
160	63.9	63.9	63.8	63.8	63.8	63.8	63.8	63.9	64.0	64.2	64.5	64.8	65.5	67.1	68.8	96.0
200	68.4	68.4	68.4	68.4	68.3	68.3	68.4	68.5	68.6	68.8	69.1	69.5	70.2	71.8	73.3	100.6
250	72.8	72.8	72.8	72.8	72.8	72.8	72.8	72.9	73.1	73.3	73.6	74.0	74.7	76.3	77.8	105.0
315	77.1	77.1	77.1	77.1	77.1	77.2	77.3	77.4	77.5	77.8	78.1	78.5	79.2	80.8	82.2	109.5
400	81.3	81.3	81.3	81.3	81.4	81.5	81.6	81.7	81.9	82.2	82.5	82.9	83.7	85.2	86.5	113.8
500	84.8	84.8	84.9	84.9	85.0	85.1	85.2	85.4	85.7	86.0	86.3	86.8	87.6	89.1	90.2	117.5
630	88.0	88.1	88.1	88.2	88.3	88.5	88.6	88.9	89.1	89.5	89.9	90.3	91.2	92.7	93.6	121.0
800	91.0	91.0	91.1	91.2	91.3	91.5	91.7	92.0	92.3	92.6	93.1	93.6	94.6	95.9	96.5	124.1
1000	93.4	93.5	93.6	93.7	93.8	94.0	94.2	94.4	94.7	95.1	95.5	96.1	97.2	98.4	98.7	126.6
1250	95.6	95.6	95.7	95.8	96.0	96.2	96.4	96.6	96.9	97.2	97.6	98.1	99.3	100.3	100.3	128.7
1600	97.6	97.7	97.8	97.9	98.1	98.3	98.5	98.7	98.9	99.2	99.6	100.1	101.3	102.0	101.5	130.6
2000	109.3	107.6	105.2	102.4	100.5	100.0	100.1	100.3	100.5	100.8	101.1	101.6	102.8	103.1	102.3	134.1
2500	115.3	115.3	115.0	114.0	112.0	108.9	105.1	102.6	101.9	102.1	102.3	102.8	103.9	103.9	102.7	141.1
3150	108.1	109.7	111.7	113.5	114.6	114.8	113.6	111.1	107.7	104.8	103.6	103.9	104.8	104.4	102.9	142.4
4000	104.4	103.7	103.5	105.0	108.0	111.1	113.2	113.9	113.0	110.8	108.0	106.1	105.7	104.6	102.8	141.5
5000	109.3	109.2	108.9	107.9	106.6	106.1	108.2	111.1	113.0	113.2	112.2	110.4	108.6	106.5	104.3	141.5
6300	107.3	107.6	108.0	108.6	109.0	108.9	108.2	107.9	109.6	111.7	112.6	112.4	111.4	109.8	108.1	141.3
8000	105.0	105.3	105.9	106.5	107.1	107.8	108.4	108.6	108.4	109.0	110.4	111.4	111.6	110.9	109.9	140.3
10000	104.2	104.4	104.6	104.8	105.3	106.0	106.9	107.7	108.3	108.5	109.0	110.0	110.6	110.5	110.2	139.3
12500	103.4	103.6	103.8	104.1	104.5	105.0	105.5	106.4	107.3	108.1	108.6	109.3	109.8	110.0	109.9	138.6
16000	101.9	102.0	102.3	102.6	103.0	103.4	104.0	104.6	105.3	106.2	107.0	107.9	108.5	108.6	108.7	137.0
20000	100.7	100.9	101.1	101.4	101.8	102.3	102.8	103.3	104.0	104.7	105.6	106.6	107.3	107.5	107.7	135.7
25000	99.5	99.7	99.9	100.2	100.6	101.1	101.6	102.1	102.7	103.4	104.1	105.2	106.0	106.3	106.6	134.5
31500	97.9	98.1	98.4	98.7	99.1	99.6	100.2	100.7	101.3	101.9	102.6	103.6	104.4	104.9	105.2	133.0
40000	95.6	95.8	96.1	96.5	96.9	97.4	98.0	98.6	99.3	99.9	100.6	101.5	102.3	102.8	103.1	130.9
50000	91.3	92.0	92.9	93.7	94.5	95.2	95.8	96.5	97.2	97.9	98.5	99.5	100.2	100.7	101.0	128.7
63000	82.6	83.7	85.3	87.3	89.3	91.1	92.5	93.1	93.9	94.6	95.3	96.5	97.2	97.7	98.1	125.2
80000	74.9	75.6	76.4	77.4	78.6	79.9	81.2	82.5	83.7	84.8	85.6	86.9	87.2	85.6	83.3	114.7
OVERALL	119.0	119.1	119.1	119.2	119.3	119.3	119.4	119.4	119.5	119.5	119.5	119.6	119.7	119.3	118.8	150.8
PNL	132.3	132.3	132.2	131.9	132.6	132.7	132.1	132.2	131.7	131.3	130.6	130.2	129.9	128.9	127.7	
PNLT	135.8	135.5	134.8	134.0	135.6	135.1	133.6	134.1	131.7	131.3	130.6	130.2	129.9	128.9	127.7	

Table B-18. Computational Acoustic Data for Pressure Ratio 4.5 : Total Noise Levels

ANGLE	20	30	40	50	60	70	80	90	100	110	120	130	140	150	160	PWL
FREQ																
50	38.9	38.8	38.8	38.7	38.6	38.6	38.5	38.5	38.6	38.8	39.0	39.3	40.1	41.9	43.7	71.2
63	43.9	43.8	43.8	43.7	43.6	43.6	43.5	43.5	43.6	43.8	44.0	44.3	45.1	46.8	48.7	76.2
80	49.0	49.0	48.9	48.8	48.8	48.7	48.7	48.7	48.8	48.9	49.1	49.5	50.2	52.0	53.8	81.3
100	53.8	53.7	53.7	53.6	53.5	53.5	53.5	53.5	53.5	53.7	53.9	54.3	55.0	56.8	58.5	86.1
125	58.5	58.5	58.4	58.3	58.3	58.2	58.2	58.2	58.3	58.5	58.7	59.0	59.8	61.5	63.2	90.8
160	63.7	63.6	63.6	63.5	63.5	63.4	63.4	63.4	63.5	63.7	63.9	64.2	65.0	66.7	68.4	96.0
200	68.2	68.2	68.2	68.1	68.1	68.0	68.0	68.1	68.2	68.3	68.6	68.9	69.7	71.3	72.9	100.6
250	72.7	72.6	72.6	72.6	72.5	72.5	72.5	72.6	72.7	72.9	73.1	73.4	74.2	75.9	77.4	105.1
315	77.1	77.1	77.0	77.0	77.0	77.0	77.0	77.1	77.2	77.4	77.7	78.0	78.8	80.4	81.8	109.7
400	81.3	81.3	81.3	81.3	81.3	81.3	81.4	81.5	81.7	81.9	82.2	82.5	83.4	84.9	86.2	114.1
500	84.9	84.9	85.0	85.0	85.0	85.1	85.2	85.3	85.5	85.7	86.1	86.5	87.3	88.9	90.0	117.9
630	88.2	88.3	88.3	88.4	88.5	88.6	88.7	88.9	89.1	89.4	89.7	90.2	91.1	92.6	93.5	121.5
800	91.2	91.3	91.4	91.5	91.6	91.7	91.9	92.1	92.3	92.7	93.1	93.5	94.6	95.9	96.5	124.7
1000	93.7	93.8	93.8	93.9	94.1	94.2	94.4	94.6	94.9	95.3	95.7	96.2	97.3	98.5	98.8	127.2
1250	95.8	95.9	96.0	96.1	96.3	96.4	96.6	96.8	97.1	97.4	97.8	98.3	99.5	100.5	100.4	129.4
1600	97.8	97.9	98.0	98.2	98.3	98.5	98.7	98.9	99.2	99.4	99.8	100.3	101.5	102.2	101.7	131.3
2000	99.1	99.3	99.4	99.6	99.8	100.1	100.3	100.5	100.7	101.0	101.3	101.8	103.0	103.3	102.4	132.8
2500	100.1	100.2	100.4	100.7	100.9	101.2	101.5	101.8	102.0	102.2	102.5	103.0	104.1	104.0	102.8	133.9
3150	100.6	100.7	101.0	101.3	101.6	102.0	102.3	102.7	103.0	103.2	103.4	104.0	104.9	104.4	102.8	134.7
4000	100.6	100.9	101.2	101.5	101.9	102.4	102.8	103.2	103.5	103.8	104.0	104.6	105.3	104.4	102.6	135.1
5000	100.4	100.6	101.0	101.4	101.9	102.4	102.8	103.3	103.7	103.9	104.2	104.9	105.4	104.2	102.3	135.2
6300	99.9	100.1	100.5	101.0	101.5	102.0	102.6	103.1	103.5	103.8	104.0	104.8	105.0	103.7	102.0	134.9
8000	99.2	99.5	99.8	100.3	100.8	101.4	102.0	102.6	103.1	103.4	103.6	104.4	104.5	103.2	101.7	134.5
10000	98.5	98.8	99.1	99.6	100.1	100.7	101.3	101.9	102.5	102.8	103.0	103.8	103.9	102.7	101.5	134.0
12500	97.6	97.9	98.3	98.7	99.3	99.9	100.5	101.1	101.7	102.1	102.3	103.1	103.2	102.1	101.1	133.3
16000	96.6	96.8	97.2	97.7	98.2	98.8	99.5	100.1	100.6	101.1	101.3	102.1	102.2	101.2	100.3	132.5
20000	95.7	96.0	96.3	96.7	97.2	97.8	98.4	99.0	99.5	100.0	100.2	101.1	101.1	100.0	99.2	131.7
25000	94.5	94.8	95.2	95.7	96.2	96.8	97.4	97.9	98.4	98.8	99.0	99.9	99.8	98.8	97.8	130.9
31500	92.4	92.7	93.2	93.9	94.5	95.3	96.0	96.7	97.2	97.5	97.7	98.5	98.5	97.4	96.3	130.1
40000	89.4	89.8	90.4	91.1	91.9	92.8	93.7	94.6	95.4	95.9	96.2	97.0	97.0	95.9	94.4	129.0
50000	85.8	86.3	86.9	87.7	88.6	89.6	90.7	91.7	92.7	93.5	94.0	95.0	95.0	93.7	92.0	127.5
63000	81.0	81.5	82.3	83.2	84.3	85.4	86.6	87.8	88.9	89.9	90.6	91.8	91.9	90.4	88.4	125.5
80000	74.5	75.1	76.0	77.1	78.4	79.7	81.2	82.6	83.9	85.0	85.9	87.3	87.5	85.8	83.5	122.9
OVERALL	110.5	110.7	111.0	111.4	111.8	112.2	112.7	113.2	113.6	113.9	114.1	114.8	115.3	114.7	113.5	145.5
PNL	122.4	122.6	122.9	123.2	123.6	123.9	124.3	124.7	125.0	125.3	125.5	126.1	126.9	126.3	125.1	
PNLT	122.4	122.6	122.9	123.2	123.6	123.9	124.3	124.7	125.0	125.3	125.5	126.1	126.9	126.3	125.1	

Table B-19. Computational Acoustic Data for Pressure Ratio 5.0 : Mixing Noise Component

ANGLE	20	30	40	50	60	70	80	90	100	110	120	130	140	150	160	PWL
FREQ																
50	0.0	0.0	0.0	0.0	0.0	0.0	0.0	0.0	0.0	0.0	0.0	0.0	0.0	0.0	0.0	31.9
63	35.8	35.8	35.8	35.8	35.8	35.8	35.8	35.8	35.8	35.8	35.8	35.8	35.8	35.8	35.8	67.7
80	36.5	36.5	36.5	36.5	36.5	36.5	36.5	36.5	36.5	36.5	36.5	36.5	36.5	36.5	36.5	68.4
100	40.6	40.6	40.6	40.6	40.6	40.6	40.6	40.6	40.6	40.6	40.6	40.6	40.6	40.6	40.6	72.4
125	38.9	38.9	38.9	38.9	38.9	38.9	38.9	38.9	38.9	38.9	38.9	38.9	38.9	38.9	38.9	70.8
160	39.5	39.5	39.5	39.5	39.5	39.5	39.5	39.5	39.5	39.5	39.5	39.5	39.5	39.5	39.5	71.4
200	40.5	40.5	40.5	40.5	40.5	40.5	40.5	40.5	40.5	40.5	40.5	40.5	40.5	40.5	40.5	72.3
250	41.6	41.6	41.6	41.6	41.6	41.6	41.6	41.6	41.6	41.6	41.6	41.6	41.6	41.6	41.6	73.5
315	42.8	42.8	42.8	42.8	42.8	42.8	42.8	42.8	42.8	42.8	42.8	42.8	42.8	42.8	42.8	74.6
400	43.5	43.5	43.5	43.5	43.5	43.5	43.5	43.5	43.5	43.5	43.5	43.5	43.5	43.5	43.5	75.4
500	44.6	44.6	44.6	44.6	44.6	44.6	44.6	44.6	44.6	44.6	44.6	44.6	44.6	44.6	44.6	76.5
630	45.8	45.8	45.8	45.8	45.8	45.8	45.8	45.8	45.8	45.8	45.8	45.8	45.8	45.8	45.8	77.7
800	46.5	46.5	46.5	46.5	46.5	46.5	46.5	46.5	46.5	46.5	46.5	46.5	46.5	46.5	46.5	78.4
1000	47.4	47.4	47.4	47.4	47.4	47.4	47.4	47.4	47.4	47.4	47.4	47.4	47.4	47.4	47.4	79.3
1250	49.2	48.9	48.9	48.9	48.9	48.9	48.9	48.9	48.9	48.9	48.9	48.9	48.9	48.9	48.9	80.8
1600	94.1	90.4	84.8	76.9	66.5	54.4	49.5	49.5	49.5	49.5	49.5	49.5	49.5	49.5	49.5	113.6
2000	112.6	111.5	109.6	106.5	101.7	94.9	85.8	74.3	61.0	51.0	50.4	50.4	50.4	50.4	50.4	135.3
2500	112.6	113.5	114.2	114.4	113.7	111.5	107.7	101.9	94.1	84.7	74.0	63.0	54.0	51.6	51.6	141.3
3150	98.8	101.7	105.2	108.8	111.7	113.5	113.7	112.3	109.0	104.1	97.7	90.6	83.3	76.6	71.2	141.2
4000	105.9	104.6	102.5	99.9	100.9	105.7	109.9	112.2	112.6	111.1	108.0	103.8	99.0	94.4	90.6	140.2
5000	107.2	107.7	108.0	107.8	106.7	104.5	103.4	106.9	110.3	111.9	111.6	109.9	107.2	104.4	101.8	140.4
6300	105.2	105.5	105.8	106.2	106.9	107.5	107.1	105.9	106.1	108.7	110.7	111.1	110.3	109.0	107.5	140.1
8000	102.7	102.7	103.0	103.6	104.5	105.3	106.1	106.7	106.5	106.4	107.7	109.2	109.8	109.6	109.0	138.8
10000	101.8	101.9	102.2	102.4	102.7	103.1	104.0	105.1	106.0	106.4	106.7	107.6	108.5	108.9	108.9	137.8
12500	101.1	101.2	101.4	101.7	102.0	102.4	102.9	103.6	104.6	105.7	106.4	107.1	107.7	108.3	108.5	137.1
16000	99.4	99.6	99.8	100.0	100.3	100.7	101.2	101.7	102.4	103.4	104.5	105.5	106.3	106.8	107.1	135.6
20000	98.2	98.4	98.6	98.8	99.1	99.5	99.9	100.5	101.1	101.9	102.9	104.0	105.0	105.7	106.1	134.5
25000	97.0	97.2	97.3	97.6	97.9	98.3	98.7	99.3	99.8	100.6	101.5	102.5	103.6	104.4	105.0	133.6
31500	95.6	95.7	95.9	96.2	96.5	96.9	97.3	97.8	98.4	99.1	99.9	100.9	102.0	102.9	103.6	132.7
40000	93.0	93.3	93.7	94.0	94.4	94.8	95.2	95.7	96.3	97.0	97.8	98.7	99.8	100.7	101.4	131.3
50000	85.6	87.1	88.7	90.3	91.6	92.5	93.2	93.8	94.4	95.0	95.8	96.6	97.7	98.5	99.4	130.1
63000	68.3	71.5	75.5	79.7	83.6	86.9	89.2	90.8	91.1	91.8	92.6	93.4	94.7	95.4	96.6	128.1
80000	0.0	0.0	0.0	0.0	0.0	0.0	0.0	0.0	0.0	0.0	0.0	0.0	0.0	0.0	0.0	31.9
OVERALL	117.6	117.6	117.7	117.7	117.8	117.8	117.7	117.7	117.7	117.6	117.5	117.4	117.2	117.0	116.8	149.7
PNL	129.2	129.7	130.1	130.1	129.7	130.1	130.1	129.1	129.0	127.8	127.0	125.5	124.4	122.9	121.4	
PNLT	133.6	133.7	133.7	133.2	136.3	134.1	133.2	131.5	132.3	130.2	128.5	127.8	126.6	124.1	121.4	

Table B-20. Computational Acoustic Data for Pressure Ratio 5.0 : Shock Noise Component

ANGLE	20	30	40	50	60	70	80	90	100	110	120	130	140	150	160	PWL
FREQ																
50	38.9	38.8	38.8	38.7	38.6	38.6	38.5	38.5	38.6	38.8	39.0	39.3	40.1	41.9	43.7	71.2
63	44.5	44.4	44.4	44.3	44.3	44.2	44.2	44.2	44.3	44.4	44.6	44.9	45.5	47.2	48.9	76.7
80	49.2	49.2	49.1	49.1	49.0	49.0	48.9	48.9	49.0	49.1	49.4	49.7	50.4	52.1	53.9	81.5
100	54.0	53.9	53.9	53.8	53.7	53.7	53.7	53.7	53.8	53.9	54.1	54.4	55.2	56.9	58.6	86.3
125	58.6	58.5	58.5	58.4	58.3	58.3	58.3	58.3	58.4	58.5	58.7	59.1	59.8	61.5	63.2	90.9
160	63.7	63.6	63.6	63.5	63.5	63.4	63.4	63.4	63.5	63.7	63.9	64.3	65.0	66.7	68.4	96.0
200	68.3	68.2	68.2	68.1	68.1	68.0	68.0	68.1	68.2	68.3	68.6	68.9	69.7	71.3	72.9	100.6
250	72.7	72.7	72.6	72.6	72.5	72.5	72.5	72.6	72.7	72.9	73.1	73.5	74.2	75.9	77.4	105.1
315	77.1	77.1	77.0	77.0	77.0	77.0	77.0	77.1	77.2	77.4	77.7	78.0	78.8	80.4	81.8	109.7
400	81.3	81.3	81.3	81.3	81.3	81.3	81.4	81.5	81.7	81.9	82.2	82.5	83.4	84.9	86.2	114.1
500	84.9	84.9	85.0	85.0	85.0	85.1	85.2	85.3	85.5	85.7	86.1	86.5	87.3	88.9	90.0	117.9
630	88.2	88.3	88.3	88.4	88.5	88.6	88.7	88.9	89.1	89.4	89.7	90.2	91.1	92.6	93.5	121.5
800	91.2	91.3	91.4	91.5	91.6	91.7	91.9	92.1	92.3	92.7	93.1	93.5	94.6	95.9	96.5	124.7
1000	93.7	93.8	93.8	93.9	94.1	94.2	94.4	94.6	94.9	95.3	95.7	96.2	97.3	98.5	98.8	127.2
1250	95.8	95.9	96.0	96.1	96.3	96.4	96.6	96.8	97.1	97.4	97.8	98.3	99.5	100.5	100.4	129.3
1600	99.3	98.6	98.2	98.2	98.3	98.5	98.7	98.9	99.2	99.4	99.8	100.3	101.5	102.2	101.7	131.4
2000	112.8	111.8	110.0	107.3	103.9	101.2	100.4	100.5	100.7	101.0	101.3	101.8	103.0	103.3	102.4	137.2
2500	112.8	113.7	114.4	114.6	113.9	111.9	108.6	104.8	102.7	102.3	102.5	103.0	104.1	104.0	102.8	142.0
3150	102.8	104.3	106.6	109.5	112.1	113.8	114.1	112.7	110.0	106.7	104.4	104.2	105.0	104.4	102.8	142.0
4000	107.0	106.1	104.9	103.8	104.5	107.4	110.7	112.8	113.1	111.9	109.5	107.2	106.3	104.8	102.9	141.3
5000	108.1	108.4	108.8	108.7	107.9	106.6	106.2	108.5	111.2	112.5	112.3	111.1	109.4	107.3	105.1	141.4
6300	106.3	106.6	106.9	107.3	108.0	108.6	108.4	107.7	108.0	109.9	111.5	112.0	111.5	110.1	108.6	141.1
8000	104.3	104.4	104.7	105.3	106.0	106.8	107.5	108.1	108.1	108.2	109.1	110.5	111.0	110.5	109.8	140.0
10000	103.4	103.6	103.9	104.3	104.6	105.1	105.9	106.8	107.6	108.0	108.3	109.1	109.8	109.8	109.6	139.0
12500	102.7	102.9	103.2	103.5	103.9	104.3	104.9	105.5	106.4	107.2	107.8	108.5	109.0	109.2	109.2	138.2
16000	101.3	101.4	101.7	102.0	102.4	102.9	103.4	104.0	104.6	105.4	106.2	107.1	107.7	107.8	107.9	136.7
20000	100.2	100.3	100.6	100.9	101.3	101.7	102.2	102.8	103.4	104.0	104.8	105.8	106.5	106.7	106.9	135.5
25000	98.9	99.1	99.4	99.8	100.2	100.6	101.1	101.6	102.2	102.8	103.4	104.4	105.1	105.5	105.7	134.3
31500	97.3	97.5	97.8	98.2	98.6	99.2	99.7	100.3	100.9	101.4	102.0	102.9	103.6	104.0	104.3	132.8
40000	94.6	94.9	95.3	95.8	96.3	96.9	97.5	98.2	98.9	99.5	100.1	100.9	101.6	101.9	102.2	130.7
50000	88.7	89.7	90.9	92.2	93.4	94.3	95.2	95.9	96.6	97.3	98.0	98.9	99.6	99.8	100.1	128.4
63000	81.2	82.0	83.1	84.8	87.0	89.2	91.1	92.6	93.1	94.0	94.7	95.7	96.5	96.6	97.2	124.8
80000	74.5	75.1	76.0	77.1	78.4	79.7	81.2	82.6	83.9	85.0	85.9	87.3	87.5	85.8	83.5	115.3
OVERALL	118.3	118.4	118.5	118.6	118.7	118.8	118.9	119.0	119.1	119.1	119.1	119.3	119.4	119.0	118.4	150.8
PNL	130.8	131.3	131.7	131.8	131.5	132.0	132.2	131.6	131.7	131.1	130.7	130.1	129.9	129.1	127.9	
PNLT	134.9	135.0	135.2	134.8	133.5	134.9	134.5	131.6	133.3	131.1	130.7	130.1	129.9	129.1	127.9	

Table B-21. Computational Acoustic Data for Pressure Ratio 5.0 : Total Noise Levels

REPORT DOCUMENTATION PAGE

Form Approved: OMB No. 0704 - 0188

1. AGENCY USE ONLY	2. REPORT DATE	3. REPORT TYPE AND DATES COVERED
	September, 1996	Contractor's Report

4. TITLE AND SUBTITLE

Computational Noise Study of a Supersonic Short Conical Plug-Nozzle Jet

5. FUNDING NUMBERS

NASA Grant No. NAG3-1708

6. AUTHOR(S)

Indu S. Das, Abbas Khavaran and A. P. Das

7. PERFORMING ORGANIZATION NAME(S) AND ADDRESS(ES)

The Pennsylvania State University
Sharon, PA 16146

8. PERFORMING RGANIZATION REPORT NUMBER

9. SPONSORING/MONITORRING AGENCY NAME(S) AND ADDRESS(ES)

National Aeronautics and Space Organization
Lewis Research Center, Cleveland, OH 44135

10. SPONSORING/MONITORING AGENCY REPORT NUMBER

NASA CR- ?

11. SUPPLEMENTARY NOTES

Indu S. Das (Responsible Person), The Pennsylvania State University, Sharon, PA 16146; Abbas Khavaran, Lewis Research Center Group, NYMA, OH 44142; A. P. Das, Graduate Student, Youngstown State Univ., Ohio.

12a. DISTRIBUTION/AVAILABILITY STATEMENT

Unclassified - Unlimited. Subject Categories: 71 and 07

12b. DISTRIBUTION CODE

13. ABSTARCT (*Maximum 200 words*)

A computational jet noise study of a short conical plug-nozzle (CPN) is presented. The CPN has an exit diameter of 45mm and the geometrical configuration closely approximates that of an ideal contoured plug-nozzle having shockless flow at pressure ratio $\xi_d = 3.62$. The gasdynamics of the jet flows have been predicted using the CFD code, NPARC with k-ε turbulence model; these data are then used for noise computations based on the modified GE/MGB code. The study covers a range of pressure ratio, $2.0 \leq \xi \leq 5.0$. The agreement of the computational results with the available experimental data is favorable. The results indicate consistent noise reduction effectiveness of the CPN as compared to equivalent convergent, convergent-divergent and ideal contoured plug nozzles at all pressure ratios. At design pressure ratio, codes predict noise levels within 4.0dB of the measurements; and at off-design pressure ratios, in general, within 5.0dB except at very high frequencies when deviations up to 10dB are noted. The shock formation mechanism in the CPN jet is noted to be basically different from those in the convergent and CD nozzle jets.

14. SUBJECT TERMS	15. NUMBER OF PAGES	85
Aeroacoustics, Aerodynamic Noise, Jet Noise Prediction, Jet Noise Suppression, Plug-Nozzle	16. PRICE CODE	

17. SECURITY CLASSIFICATION OF REPORT	18. SECURITY CLASSIFICATION OF THIS PAGE	18. SECURITY CLASSIFICATION OF ABSTRACT	20. LIMITATION OF ABSTRACT
Unclassified	Unclassified	Unclassified	